NASA CR-178094

FAULT TOLERANT CONTROL LAWS

Uy-Loi Ly
Boeing Military Airplane Company

and

John K. Ho
Boeing Commercial Airplane Company

Prepared for

NASA Langley Research Center
under contract NAS1-17635 Task No. 10

National Aeronautics and
Space Administration

1986

FAULT TOLERANT CONTROL LAWS

Uy-Loi Ly
Boeing Military Airplane Company
and
John K. Ho
Boeing Commercial Airplane Company

TABLE OF CONTENTS

LIST OF TABLES

LIST OF TABLES (Continued)

LIST OF FIGURES

LIST OF FIGURES (Continued)

LIST OF FIGURES (Continued)

1.0 SUMMARY

This report provides a systematic procedure for the synthesis of fault tolerant control laws to actuator failures at three design conditions: landing approach (Mach .25, h = 5000 ft), low altitude cruise (Mach .60, h = 5000 ft), and high altitude cruise (Mach .90, h = 20,000 ft). The design concept for robustness to control actuator failure evolves around the idea that the redundant surface activities must be balanced properly in accordance to their control effectiveness. Intuitively, one adjusts the control activities (e.g., evaluated from the rms responses to turbulence) in the feedback design such that they are inversely proportional to the controllability indices with respect to a dominant mode. Here the dominant mode for a relaxed static stability aircraft is the unstable real divergent mode.

Two design methods were used to synthesize fault tolerant controllers: the conventional LQ design method and the direct output feedback controller synthesis method SANDY. The LQ approach enables designers to compute design gains rapidly that satisfy the desired stability and performance. The solution involves solving a matrix Riccati equation, which computationally is less extensive than the direct optimization method associated with the second design approach SANDY. Hence, numerous design iterations can be performed initially using the LQ method.

Results of the full-state feedback provide useful information on the design feasibility and its maximum achievable performance when all the system states are available for feedback. The latter design method is used primarily to streamline the full-state feedback design into a practical implementable output feedback controller structure. Design parameters selected in the full-state feedback synthesis can be used to define the initial cost function for the output feedback design. A simple gain schedule structure involving only three gains was designed to handle all the three design conditions.

Fault tolerant control developed in this study provides a good stability augmentation system for the relaxed static stability aircraft. From simulation and covariance analysis to longitudinal and vertical turbulences, the augmented aircraft responses are found to be invariant to the presence of a failure. Imperceptible changes in the aircraft responses are seen during the transition from a nonfailed state to a failed state.

Single-loop stability margins of ± 6 dB in gain and ± 30 deg in phase were achieved along with -40 dB/decade gain attenuation at high frequency.

2.0 INTRODUCTION

The advent of advanced aircraft having multiple control mode functions poses a great challenge in the area of control law development and design integration. Of equal importance are the problems associated with the reconfiguration or restructure of these control laws in the event of actuator or sensor failures (ref. 1). Sometimes, it is necessary to revert totally back to the manual mode for a safe continuation of the flight.

Unfortunately, future aircraft, driven by consideration of improved fuel efficiency and increased maneuverability, will tend to be unstable statically. The relaxed static stability resulting usually from the aft movement of the aircraft center of gravity (cg) puts stringent reliability and integrity requirements on the control effectors, sensors, and automatic flight control system.

In general, for an aircraft with relaxed static stability, minimum flying qualities can be maintained only with stability augmentation. Thus, any failure in either sensor or actuator components would be catastrophic unless rapid recovery via reconfiguration or restructure of the controller is implemented within the flight control system. Extensive research has been conducted in the area of reconfigurable and restructurable controls (refs. 2 and 3). The development of a reconfiguration strategy, which maximizes the capability of the flight control system after actuator or sensor failure, is, however, a complex task.

Schemes used in a reconfiguration strategy involve primarily a fault detection and identification process followed by a process of control law refinement. Each of these events are time consuming. Postfault refinement of the controller gains is designed to maximize the aircraft performance capabilities consistent with the (remaining) feasible force and moment generation capabilities. The time delay involved in the fault identification is found to be critical to the success of the overall reconfiguration/restructure strategy (ref. 4).

A key element that plays a significant role in most reconfiguration and restructurable control strategy is the backup fault tolerant controller. The robust backup controller, a priori designed to cope with a wide class of fault modes, flight conditions, and aircraft configurations, would provide the crucial time period needed for the fault to be isolated and the reconfiguration/restructure completed. Hence, the robust fault tolerant control design concept complements a reconfiguration/restructure strategy and renders it practical to develop both from a design and eventual flight validation standpoints.

The topic of the study concerns the synthesis and evaluation of such fault tolerant control systems in flight control applications. Systematic design approaches leading to the development of fault tolerant control laws are presented. Various controller structures have been investigated: (1) full-state feedback designs at individual flight conditions, (2) output feedback designs at individual flight conditions, and (3) output feedback designs with gain schedule at three flight conditions (the gain schedule is kept simple intentionally for purpose of reliability and ease of implementation).

Analysis of closed-loop eigenvalues, aircraft covariance responses to gust turbulence, and loop stability margins have been performed to assess the general robustness characteristics of each control design in the presence of aerodynamic control surface actuator failures. Limited linear time simulation has been conducted for the final optimized gain scheduled output feedback designs to random vertical and longitudinal gust inputs.

The aircraft considered in the study is a multiple controls AFTI-F16 with three design flight conditions: symmetric horizontal tail surfaces, symmetric vertical canard surfaces, and engine thrust. Redundancy in control effectors and sensor devices are basic prerequisites in the synthesis of robust fault tolerant control laws. The design problem to handle failure in sensors is a dual problem to the one dealing with failure in control actuators. Due to the limited scope and without loss of generality, only the problem associated with actuator failure will be addressed.

Neutral failure in control actuation of an aerodynamic surface is interpreted as a loss of effectiveness of that surface to perform a control task. This translates mathematically into a situation where the respective column of the control input distribution matrix is reduced to zero. Off-neutral failures, such as surface hardover, are not addressed in this study and left for future research.

3.0 SYMBOLS AND ABBREVIATIONS

A	augmented aircraft state matrix
A_c	controller state matrix
ADVC	vertical canard deflection (deg)
ADHT	horizontal tail deflection (deg)
AFTI	Advanced Fighter Technology Integration
ALPHAO	angle of attack perturbation (deg)
A_{nc}	normal acceleration (g)
ANC	normal acceleration (g)
B	control input distribution matrix
B_c	controller input distribution matrix
$B_{.i}$	ith column of the B matrix
C	state to output distribution matrix
C_c	controller output distribution matrix
C_i	ith constraint
$C_{i.}$	ith row of the C matrix
C_{imin}	lower bound on the ith constraint
C_{imax}	upper bound on the ith constraint
cg	center of gravity
dB	decibel
deg	degree
dt	time differential
D	input to output distribution matrix
D_c	direct output feedback gain matrix
DDHT	horizontal tail rate (deg/s)
DDVC	vertical canard rate (deg/s)
ft	feet
g	units of sea level gravitational constant

g_o	sea level gravitational constant
h	altitude (ft)
IBU	independent backup unit
j	$\sqrt{-1}$
J	cost function
K	controller design parameter
$K_{\delta plac}$	gain schedule factor on the δ_{plac} command
$K_{\delta htc}$	gain schedule factor on the δ_{htc} command
$K_{\delta vcc}$	gain schedule factor on the δ_{vcc} command
L	turbulence scale length (ft)
Lim	limit
LQ	Linear Quadratic Regulator
min	minimum
max	maximum
M	Mach number
Max( )	maximum of ( )
Min( )	minimum of ( )
N	order of the augmented aircraft model
N_c	number of design constraints
N_p	number of design plant models
P	Riccati matrix solution
q	pitch rate (deg/s)
q_o	dynamic pressure (lbf/ft^2)
Q	symmetric positive semidefinite output penalty matrix
Q_o	nominal pitch rate (deg/s)
QB	pitch rate (deg/s)
rad	radian
rms	root mean square
R	symmetric positive semidefinite control penalty matrix
s	second

SANDY	a computer program for the synthesis of robust low order controller
t	time (sec)
t_f	terminal time (sec)
T	block diagonal transformation matrix
T_{Idle}	idle thrust (lb)
T_{Max}	maximum thrust (lb)
$T_{Military}$	military thrust (lb)
THETA	pitch attitude perturbation (deg)
u	control input
u_b	aircraft forward speed (ft/s)
u_g	longitudinal gust velocity (ft/s)
u_{min}	minimum bound on the input u
u_{max}	maximum bound on the input u
u_{noise}	zero mean white-noise input for the longitudinal gust
UB	aircraft forward speed (ft/s)
UG	longitudinal gust velocity (ft/s)
U_o	aircraft trim velocity (ft/s)
w_b	aircraft vertical speed (ft/s)
w_g	vertical gust velocity (ft/s)
w_{g1}	vertical gust filter state
w_{g2}	vertical gust filter state
w_{noise}	zero mean white-noise input to the vertical gust
WG1	vertical gust filter state
WG2	vertical gust filter state
W_o^i	power spectral density matrix of the input disturbances for the ith plant model
W_{pi}	design weighting factor for the ith plant model
x	augmented aircraft state vector
X_o	x coordinate of the accelerometer
y	output vector

y_{min}	minimum bound on the output y
y_{max}	maximum bound on the output y
y_s	sensor output vector
z	controller state vector
α	angle of attack perturbation (deg)
α_i	scale factor of the ith control in the controllability matrix calculation
β_i	scale factor of the ith output in the observability matrix calculation
δ_{ht}	horizontal tail (deg)
δ_{htc}	horizontal tail command (deg)
δ_{pla}	power lever angle position (percent)
δ_{plac}	power lever angle command (percent)
δ_{vc}	vertical canard (deg)
δ_{vcc}	vertical canard command (deg)
$\delta(\ )$	Dirac delta function
ΔK_{max}	maximum allowable incremental change in the parameter K
$\Delta\sigma_{jmax}$	maximum allowable change in the real part of the jth closed-loop eigenvalue
γ	turbulence filter lag
Γ	disturbance input distribution matrix
η	disturbance input vector
ζ	damping ratio
ζ_{min}	minimum damping ratio
τ	time variable
ω	frequency
Ω	disturbance to output distribution matrix
θ	pitch attitude (deg)
Θ	observability matrix
Θ_o	nominal pitch attitude (deg)
σ_j	real part of the jth closed-loop eigenvalue
σ_u	power spectral density of the white noise input u_{noise}
σ_w	power spectral density of the white noise input w_{noise}

Σ	summation
χ	controllability matrix
$( )^i$	( ) at the ith iteration
$( )^i$	( ) at the ith plant model
$(\dot{})$	time derivative of ( )
$( )_{ik}$	(i,k)th element of the matrix ( )
$( )^T$	transpose of the matrix ( )
$( )^{½}$	square root of ( )
$( )^{-1}$	inverse of the matrix ( )
$( )^2$	square of ( )
$( )_k$	k-th element of the vector ( )
%	percent
∞	infinity
$\int$	integral
E[ ]	expected value operator

4.0 OPEN-LOOP MODEL DESCRIPTION

At the outset, both the longitudinal and lateral equations of motion of the AFTI-F16 aircraft (fig. 1) have been considered in the design of fault tolerant control laws. Subsequent analysis shows that the longitudinal and lateral modes are well decoupled and, furthermore, the eigenvalues of the lateral perturbation models are stable at the chosen design flight conditions:

- Mach .25, Altitude 5000 ft (A power approach condition with landing gear down and flaps extended.)
- Mach .60, Altitude 5000 ft (A level flight with landing gear up.)
- Mach .90, Altitude 20,000 ft (A level flight with landing gear up.)

Hence, failure in lateral control would not pose severe threat to the flight safety. The longitudinal aircraft models, however, are unstable at these conditions. Detailed description of the open-loop aircraft characteristics are given in Sections 4.5 through 4.7. Full-time stability augmentation definitely must be provided in the longitudinal channel in order to maintain adequate stability and minimum flying qualities. Furthermore, the augmentation system must be tolerant to any failure in the control actuation of the aerodynamic surfaces. The design task concerns the synthesis of a fault tolerant stability augmentation system for the longitudinal axis only.

4.1 Equations of Motion

The longitudinal equations of motion for the AFTI-F16 aircraft are given in the body-axis coordinate system with the following state space description,

$$\dot{x}(t) = Ax(t) + Bu(t) + \Gamma\eta(t) \qquad (4.1.1)$$

$$y(t) = Cx(t) + Du(t) + \Omega\eta(t) \qquad (4.1.2)$$

where the state vector x(t) consists of the motion variables: horizontal speed $u_b(t)$ [ft/s], vertical velocity w_b (t) [ft/s], pitch rate q(t) [deg/s], and pitch angle $\Theta(t)$ [deg]. The input vector u(t) includes the symmetric horizontal tail surface deflection $\delta_{htc}(t)$ [deg], the symmetric vertical canard deflection $\delta_{vcc}(t)$ [deg], and the thrust indicated by the deflection of the power lever angle $\delta_{plac}(t)$[%MAX].

These are the only common control effectors available for feedback purpose across the three design conditions (table 1). For example, the flaperons are extended fully to +20 deg at the landing approach condition, while the leading edge flaps are retracted fully to -2 deg at the Mach .90, altitude 20,000-ft flight condition. Thus, they cannot be used as feedback control surfaces.

The disturbance input vector $\eta(t)$ has two components: a longitudinal gust velocity $u_g(t)$ [ft/s] and a vertical gust velocity $w_g(t)$ [ft/s]. Description of the turbulence models used in the study are given in Section 4.4.

A servoactuator model is defined for each control surface in the state equations (4.1.1) and (4.1.2). A simplified integrated servoactuator (ISA) model of first-order lag filter 13/(s+13) was used. It introduces two additional states $\delta_{ht}(t)$ and $\delta_{vc}(t)$. The thrust model used in the design is described in the following section.

4.2 Thrust Model

A linearized engine thrust dynamic model is generated from a nonlinear thrust dynamic model and the associated thrust performance curves for T_{Idle}, $T_{Military}$, and T_{Max}. Values of these thrust limits at the

three design conditions are tabulated in Table 2. A simple nonlinear model representation of the thrust produced as a function of the power lever angle command $\delta_{plac}(t)$ is depicted in Figure 2. Note that a first-order engine lag model with a one-second time constant was used. This adds another state $\delta_{pla}(t)$ to the synthesis state model. Table 3 lists the nominal power lever angle [%MAX] and the trim thrusts at the flight conditions of interest. At the three design conditions, the operating ranges of the power lever angle are less than 50%MAX. Within these ranges of $\delta_{plac}(t)$, a simplified linear thrust model is obtained as shown in Figure 3.

4.3 Sensor Equations

The design method presented in Section 7.2 allows designers to synthesize output feedback controllers directly from a set of measurement variables. In this study, sensors of the following motion variables are available: normal acceleration $A_{nc}(t)$, pitch rate q(t), and angle of attack $\alpha(t)$. Preliminary design results indicate that adding airspeed sensor $u_b(t)$ and thrust control $\delta_{plac}(t)$ have enabled better control of the neutrally stable speed mode.

Pitch angle sensor $\Theta(t)$ is also added to the output feedback structure to improve the frequency and damping of the short period mode. The pitch angle can be derived, if not available directly, by integrating the pitch rate signal in a manner similar to the analog implementation of the existing independent backup unit (IBU) described in Section 5.0.

The pitch rate q(t), pitch angle $\Theta(t)$, and airspeed $u_b(t)$ are those outputs that are also states of the synthesis model (app. A). The angle of attack output is given by

$$\alpha(t) = w_b(t) / U_o \tag{4.3.1}$$

and the normal acceleration output is derived from the following equation,

$$A_{nc}(t) = -[\dot{w}_b(t) - U_o q(t) + g_o \sin\Theta_o \Theta(t) - X_o \dot{q}(t)] / g_o \tag{4.3.2}$$

where

g_o = sea level gravitational constant [32.174 ft/s^2],

X_o = x coordinate of the accelerometer location in the cg centered body coordinate system [ft], positive forward

U_o = x component of the aircraft trim velocity [ft/s],

Θ_o = aircraft trim pitch angle [deg].

Values for these parameters are shown in Table 4. In summary, the five sensor variables used in the robust fault tolerant output feedback controller described in Sections 9.0 and 10.0 are: $u_b(t)$, q(t), $\Theta(t)$, $\alpha(t)$, and $A_{nc}(t)$.

4.4 Turbulence Model

Spectral characteristics of the wind turbulence are functions of altitude and true airspeed. A first-order Dryden turbulence model commonly is used to model the longitudinal gust $u_g(t)$, while a second-order model is appropriate for the vertical gust $w_g(t)$. Details are given below.

For the longitudinal gust model, we have

$$\dot{u}_g(t) = -\gamma\, u_g(t) + \sqrt{2\gamma}\, u_{noise}(t) \tag{4.4.1}$$

where

$$\gamma = U_o/L \text{ [rad/s]}, \tag{4.4.2}$$

U_o = True airspeed [ft/s], (4.4.3)

L = Turbulence scale length [ft] as a function of altitude, defined by

$$= \begin{cases} 1750 & \text{for } h > 1750 \text{ ft}, \\ 145h^{1/3} & \text{for } h < 1750 \text{ ft}, \end{cases} \tag{4.4.4}$$

The input $u_{noise}(t)$ is a zero-mean white noise process with power spectral density σ_u^2.

The vertical (transverse) gust model is described by

$$\begin{pmatrix} \dot{w}_{g1}(t) \\ \dot{w}_{g2}(t) \end{pmatrix} = \begin{pmatrix} -\gamma & 0.01\gamma \\ -0.01\gamma & -\gamma \end{pmatrix} \begin{pmatrix} w_{g1}(t) \\ w_{g2}(t) \end{pmatrix} + \begin{pmatrix} \sqrt{3\gamma} \\ -42.27\sqrt{3\gamma} \end{pmatrix} w_{noise}(t) \tag{4.4.5}$$

The vertical gust output $w_g(t)$ is given by

$$w_g(t) = \begin{pmatrix} 1 & 0 \end{pmatrix} \begin{pmatrix} w_{g1}(t) \\ w_{g2}(t) \end{pmatrix} \tag{4.4.6}$$

The input $w_{noise}(t)$ is a zero-mean white noise process with power spectral density σ_w^2.

The input noises $u_{noise}(t)$ and $w_{noise}(t)$ are uncorrelated. Gust intensities of 10 ft/s for σ_u and σ_w are used in the evaluation of the design cost function of Sections 9.0 and 10.0 and in the analysis of aircraft covariance responses. Table 4 gives the airspeed U_o and altitude h of the three design conditions. Including states $u_g(t)$, $w_{g1}(t)$, and w_{g2} (t) from the turbulence models, the final state model for control law synthesis is 10th order.

For completeness, the set of state model matrices derived for this study are summarized in Appendix A for the three design flight conditions.

4.5 Stability

Stability of the open-loop aircraft longitudinal models augmented with control actuator and turbulence dynamics is determined from the eigenvalues of the system matrix A of equation (4.1.1). Tables 5, 8, and 11 summarize the open-loop eigenvalues at the three design flight conditions. Note that the actuator model for the two aerodynamic surfaces has a pair of real eigenvalues at -13 rad/s and the

thrust model has an eigenvalue at -1 rad/s. The Dryden turbulence models for the longitudinal and vertical gusts contribute three (uncontrollable) eigenvalues at $-\gamma$ (eq. 4.4.2) that vary with flight conditions. The open-loop aircraft exhibits an unstable real mode (predominantly a short period mode) at all three flight conditions. The instability is less severe at the high altitude condition. The unstable mode has small coupling (observed in its eigenvector) to the phugoid at the Mach .90 altitude 20,000-ft condition. Note further that the complex eigenvalues for the phugoid mode at the two low altitude conditions are poorly damped with damping of 0.13 and 0.17.

The three design flight conditions cover a large range of dynamic pressure. From the landing approach (a low dynamic pressure condition) to the level flight at Mach .90 altitude 20,000 ft, the dynamic pressure changes by a factor greater than seven (table 4). With such a wide variation in dynamic pressure, adequate stability and robustness cannot be achieved using a single-constant gain controller. In fact, it is found that a good stabilizing controller design at the low dynamic pressure condition would result in excessive high gain at the cruise conditions. Hence, in the synthesis of fault tolerant control laws, gain schedule will be needed when going from one flight condition to another in order to satisfy the design requirements outlined in Section 6.0.

However, at a particular design condition, the fault tolerant controller will have constant gains irrespective of the type of actuator failure. To achieve design robustness without reverting to control reconfiguration, redundant control surfaces must exhibit similar effectiveness in generating forces and moments. This can be determined from the controllability matrix of the open-loop system described in the next section.

4.6 Controllability

The controllability analysis yields useful information on the relative effectiveness among selected controls. The controllability matrix is obtained by putting the open-loop aircraft state model into modal form. The computation of the controllability matrix χ proceeds by first transforming the control input distribution matrix B into modal coordinates using a modal transformation matrix T (obtained from the eigenvector matrix) (ref. 5).

The element χ_{ik} of the controllability matrix χ represents the controllability index of the ith control for the kth mode. Depending on whether the kth mode is real or complex, we have

$$\chi_{ik} = \begin{cases} \alpha_i \, (\mathbf{T}^{-1} \, \mathbf{B}_{.i})_k & \text{(real mode)} \\ \alpha_i \, [(\mathbf{T}^{-1}\mathbf{B}_{.i})_k^2 + (\mathbf{T}^{-1}\mathbf{B}_{.i})_{k+1}^2]^{1/2} & \text{(complex mode)} \end{cases} \tag{4.4.7}$$

The factor α_i represents the maximum allowable excursion of the ith control input. Here, the aerodynamic control surfaces have equal ranges of maximum deflections, therefore, we can set α_i=1.0 (i=1,2). The scaling factor α_3 for the thrust control is set to one for 100% power angle deflection. Controllability index for each mode are later normalized for all the control inputs so that the control having the most effectiveness in controlling the kth mode has a controllability index of one.

The controllability matrices evaluated at all three flight conditions are shown in Tables 6, 9, and 12 respectively. All the modes are found to be controllable by the selected control effectors: δ_{htc}, δ_{vcc}, and δ_{plac}. Of particular interest are the results corresponding to the unstable real mode. As expected, the symmetric horizontal tail surface δ_{htc} is the most effective surface in controlling the unstable real mode. The symmetric horizontal tail surfaces are found to be five to eight times more effective in controlling the unstable mode than the symmetric vertical canard surfaces. Hence, it is anticipated that, in a fault tolerant control design, feedback gains to the less effective surface will have to be higher (proportionally) than those going to the more effective surface. Proper balancing of the control usage is a direct intuitive way of achieving robustness to anticipated failure.

The relative controllability of the surfaces provides quantitative measures on how to balance these control gains in anticipation of failure of either controls. Roughly, the control activities of the nonfailed surface must increase to compensate for the loss of effectiveness of the other control surface. The amount of increase is related closely to the ratio of controllability indices as seen in Sections 8.0, 9.0, and 10.0.

One can achieve this in optimal control synthesis by penalizing each control variable with the square of the inverse of its controllability index (associated with the unstable real mode) in the quadratic cost function. These apply to the aerodynamic control surfaces only. Penalty on the engine control variable (not a candidate for possible failure in the fault tolerant control synthesis) is determined iteratively using the root square locus method. Details can be found in Sections 8.0 and 9.0.

4.7 Observability

To select appropriate sensors in the feedback control, observability analysis of the open-loop airplane outputs are performed. Similar to the computation of the controllability matrix χ, the observability matrix Θ is derived by transforming the system into block diagonal form using a transformation T (obtained again from the system eigenvector matrix) (ref. 5). The element Θ_{ik} of the observability matrix is associated with the observability index of the kth mode with the ith output sensor scaled by a factor β_i. The factor β_i gives an indication of the (nonzero) magnitude of the observed ith output. For example, approximate values of β_i can be taken from respective rms output responses of a full-state feedback design to turbulence.

Depending on whether the kth mode is real or complex, we have

$$\Theta_{ik} = \begin{cases} (C_i T)_k / \beta_i & \text{(real mode)} \\ [(C_i T)_k^2 + (C_i T)_{k+1}^2]^{1/2} / \beta_i & \text{(complex mode)} \end{cases} \tag{4.4.8}$$

Values of Θ_{ik} have been normalized for each mode so that the output having the largest observability index has a value of one and the remaining outputs are scaled accordingly by the normalization factor. Tables 7, 10, and 13 show that all the modes are observable from the five sensor outputs in the fault tolerant controller design of Sections 9.0 and 10.0.

5.0 ANALYSIS OF AN EXISTING BACK-UP SYSTEM

An independent backup unit (IBU) was developed for the AFTI-F16 aircraft. It is a single-input, single-output, second-order control system that uses the symmetric horizontal tail as the control surface and aircraft pitch rate output as the sensor. Pitch attitude information was extracted by integrating pitch rate as shown in Figure 4. A gain schedule based on landing gear up/down logic is used in this IBU. No provision is made for redundant control surfaces in this design except possibly the use of redundancy in control actuation and measurement units. Hence, it cannot sustain the loss of the horizontal tail surface as control effectors.

In contrast, the fault tolerant control developed in this study employs three controls: horizontal tail surface $\delta_{htc}(t)$, vertical canard surface $\delta_{vcc}(t)$, and engine thrust $\delta_{plac}(t)$, where $\delta_{htc}(t)$ and $\delta_{vcc}(t)$ serve as redundant aerodynamic control surfaces. The addition of the thrust control is to improve the ability to control speed and, hence indirectly, the stability of the phugoid mode independently from the short-term response associated with the short period mode. Failure of the thrust engine is not considered as part of the fault tolerant system design. Only failure of the aerodynamic control surfaces is addressed. Results of robust fault tolerant designs are shown in Sections 8.0, 9.0, and 10.0 for various controller structures.

This section briefly evaluates the performance and stability provided by the existing backup system. These results will serve as guidelines in our subsequent design of fault tolerant controls. Closed-loop eigenvalues of the aircraft with the IBU system are shown in Table 14. The damping of the short period mode is greater than 0.5. The speed mode is marginally stable with a time constant of at least 50 sec. The covariance responses to simultaneous longitudinal and vertical turbulences of intensity 10 ft/s are summarized in Table 15. Rms responses of the $\delta_{ht}(t)$ surface vary from 0.047 to 1.425 deg while the aircraft normal acceleration $A_{nc}(t)$ ranges from 0.107 to 0.261 g.

Robustness properties are determined in terms of control loop phase and gain margins, and rolloff behavior at high frequencies. Phase margins of at least 40 deg and gain margins of greater than 12 dB are achieved with the IBU system (table 16). However the rolloff characteristics defined by the loop gain at 10 rad/s are unsatisfactory. In particular, at the Mach .90 condition, a loop gain of -4 dB is not adequate to attenuate effects of unmodeled high-frequency structural modes in the feedback path. A requirement of at least -10 dB at 10 rad/s was imposed in our fault tolerant control design.

Notice that the existing IBU uses the landing gear up/down logic to provide gain schedule between the cruise and landing approach conditions. A different and high gain design is necessary at the low dynamic pressure condition as seen in Figure 4. This type of gain schedule (i.e., with respect to the discrete logic of landing gear up/down) will be used also in the synthesis of a practical robust output feedback fault tolerant controllers. It is evident that, without gain schedule, a single-constant gain controller cannot provide both the desired stability and performance over the entire design conditions where the dynamic pressure varies significantly (table 4).

6.0 DESIGN REQUIREMENTS FOR FAULT TOLERANT CONTROL LAWS

The basic requirement for a fault tolerant control system is its ability to maintain minimum safe flight in the event of a loss of effectiveness in one or several of its controls without resorting to control reconfiguration. This statement entails a whole set of requirements to be considered in the control law synthesis.

The following is a set of requirements the fault tolerant control design must satisfy:

(1) Minimum stability: damping of all the closed-loop system modes must exceeds 0.4.

(2) Robustness properties: they are based on criterion for single-loop stability margins. Gain margin of at least 6 dB and phase margin of greater than 60 deg must be met when all controls are effective. In the presence of a failure of one control, the remaining control loops still must have at least 6 dB gain margin and phase margin of 30 deg. For robustness to unmodeled structural dynamics, the loop gain must be down -10 dB at frequency of 10 rad/s and roll off with a slope of -40 dB/decade.

(3) Low control activities and good performance responses: the results are based on covariance responses of the augmented aircraft to longitudinal and vertical turbulences. To a 10 ft/s rms turbulence, the rms surface deflection and rate must be less than 1/3 of the actuator maximum position and rate limits. Rms responses of the aircraft variables should also be invariant to surface failures.

(4) Transient responses of the aircraft incurred during the transition from a nonfailed state to a failed state should not be excessive. Responses of the control surfaces must lie within their maximum limits. These criteria are based on time simulation of the aircraft to longitudinal and vertical turbulence.

7.0 THEORETICAL DESCRIPTION OF THE DESIGN METHOD

This section describes two approaches for the synthesis of robust fault tolerant control laws depending on the controller structures. The controller structures considered in the fault tolerant designs are:

(1) Full-state feedback controller at individual flight conditions.

(2) Output feedback controller at individual flight conditions.

(3) Integrated gain schedule output feedback controller with respect to the landing gear up/down logic.

The first approach is based on the standard LQ design procedure where all the system states are fed back. Details are given in Section 7.1. The second approach involves direct optimization of a modified quadratic cost function for an arbitrary output feedback controller structure and an output feedback controller with a predetermined gain schedule structure. Details of the second design approach are given in Section 7.2.

7.1 Robust Full-State Feedback Controller

To synthesize a robust controller using the LQ design technique, the relative effectiveness of the control surfaces must be taken into account. The penalty of the control variables in the familiar quadratic cost function is selected such that control activities of redundant surfaces with dissimilar control effectiveness are balanced. Precisely, to establish a fault tolerant design, a less effective control surface (e.g., vertical canard) must have higher activities (still within the maximum limits of the surface) so it can handle failure of a more effective surface (e.g., horizontal tail). If the increased activities result in full saturation of the less effective surface, then a fault tolerant control law cannot be synthesized with the chosen set of redundant surfaces.

Of course, static trim capability of the remaining surfaces is an important consideration in the early development of an aircraft configuration that is suitable for fault tolerant and/or reconfiguration strategies. In this case, we found that a full-hardover failure of the horizontal tail surface symmetrically would produce excessive pitching moment beyond the amenable range of the vertical canard surface. Hence, in this study we limit ourselves to neutral failure (i.e., assuming the failed surface returns to its trim point). Small hardover failures in the horizontal tail may be manageable by the vertical canard; however, the design for fault tolerant control to small hardover surface failure is similar to the case of neutral failure from stability consideration.

The basic objective, therefore, is to design a full-time augmentation system that meets the design requirements specified in Section 6.0.

The synthesis of a full-state feedback controller is done by using the conventional linear quadratic LQ regulator design technique. Here the cost function to be minimized is of the form,

$$J = \tfrac{1}{2} \int_o^\infty (y^T Q\, y + u^T R\, u)\, dt \qquad (7.1.1)$$

where y(t) is the criterion vector and u(t) is the control vector. Elements of the criterion vector include aircraft response and performance variables such as pitch rate q, pitch angle Θ, airspeed u_b, angle of attack α, and normal acceleration A_{nc}. The control vector consists of $\delta_{htc}(t)$, $\delta_{vcc}(t)$, and $\delta_{plac}(t)$.

Selection of the symmetric positive semidefinite matrix Q is an iterative process. The design goal is to achieve good stability (i.e., damping greater than $\zeta > 0.4$) and performance (i.e., good disturbance rejection). The control penalty matrix R is a symmetric (often diagonal) positive definite matrix. In this study, we find that by balancing the control surface activities as inversely proportional to the controllability index the resulting full-state feedback design inherently will be robust to the respective control failures. For example, if the kth mode is dominant (e.g., unstable mode) in the system, then the diagonal element of the R matrix should have approximately the following ratio for the ith and jth redundant control surfaces,

$$\frac{R_{ii}}{R_{jj}} \sim \left(\frac{\chi_{ik}}{\chi_{jk}}\right)^2 \qquad (7.1.2)$$

where χ_{ik} is the controllability index of the ith control surface for the kth mode as defined in Section 4.6.

Solution of the full-state feedback control for the system described in equations (4.1.1) and (4.1.2) is given by (when D = 0),

$$u(t) = - R^{-1}B^T P\, x(t) \qquad (7.1.3)$$

where the symmetric positive semidefinite matrix P satisfies the following steady-state Riccati equation (ref. 6).

$$A^T P + PA - PBR^{-1}B^T P + C^T QC = 0 \qquad (7.1.4)$$

Results of the robust full-state feedback controller designs are presented in Section 8.0.

7.2 Robust Output Feedback Controller

Solution of the output feedback controller structures involves direct parameter optimization. The method is based on the design algorithm SANDY for robust low order controller described in Reference 7.

It is a systematic approach to directly determine control law gains and filter parameters that will meet practical design constraints in terms of control law structure, performance objectives, and robustness requirements. The algorithm handles a general class of linear time invariant controller design problems. The output feedback controller structure for the fault tolerant control law is a subset of such a class of controller design. Details of the numerical procedure can be found in Reference 8. The method was later extended to handle nonlinear constrained optimization with improved built-in safeguards for numerical overflow. For completeness, a brief summary of the extended design method is given in this section.

Given a plant model,

$$\dot{x}(t) = A^i x(t) + B^i u(t) + \Gamma^i \eta(t) \tag{7.2.1}$$

$$y(t) = C^i x(t) + D^i u(t) + \Omega^i \eta(t) \tag{7.2.2}$$

for $i=1,N_p$. The superscript $(-)^i$ refers to the ith plant condition, and N_p is the total number of plant conditions.

The design objective is to synthesize a single-constant gain linear time invariant controller of the form,

$$\dot{z}(t) = A_c z(t) + B_c y_s(t) \tag{7.2.3}$$

$$u(t) = C_c z(t) + D_c y_s(t) \tag{7.2.4}$$

that provides satisfactory stability, performance, and robustness over several design conditions ($i=1,N_p$) described in equations (7.2.1) and (7.2.2). Input to the controller in equations (7.2.3) and (7.2.4) is the feedback sensor $y_s(t)$, which is a subset of the output variables y(t) of the plant model.

Equations (7.2.3) and (7.2.4) naturally reduce to an output feedback controller structure when the order of the controller (i.e., order of the controller state vector z(t)) is zero. Thus, we have,

$$u(t) = D_c y_s(t) \tag{7.2.5}$$

Any combination of parameters in the controller state matrices A_c, B_c, C_c, and D_c can be selected to minimize the following modified quadratic cost function,

$$J(t_f) = \tfrac{1}{2} \sum_{i=1}^{N_p} W_{pi} E\left[\int_o^{t_f} (y^T Q^i y + u^T R^i u)\, dt\right] \tag{7.2.6}$$

where W_{pi} is the weighting assigned to the ith plant condition depicting its relative contribution into the design cost function. The matrices Q^i and R^i are the respective design penalty matrices for the ith plant condition. The weighted average cost function over N_p conditions in equation (7.2.6) permits designers to synthesize a constant gain controller that methodically trade off performance and control activities over these conditions simultaneously.

This feature can be used to incorporate control failure states into the design cost function as demonstrated in Section 10.0 for the design of an integrated robust gain schedule output feedback controller. This is done by formulating multiple plant models: a nominal plant model for the no failure case and additional plant models, one for each failure state. Here, for fault tolerant control design to actuator failure, a plant model with a failed control surface will have the entire column corresponding to the failed control in the input distribution matrix B (eq. 4.1.1) equal to zero.

Minimization of the cost function $J(t_f)$ can be performed subject to additional nonlinear constraints,

$$C_{imin} \leq C_i(A_c,B_c,C_c,D_c) \leq C_{imax} \qquad (0 \leq i \leq N_c) \tag{7.2.7}$$

where N_c is the total number of constraints. Minimization of the cost function in equation (7.2.6) subject to the above constraints is carried out numerically using a nonlinear programming technique based on a projected Lagrangian method (ref. 8).

The cost function is evaluated to stochastic input disturbances. The input disturbance vector $\eta(t)$ is modeled as a white noise process of zero mean and covariance $E[\eta(t)\eta^T(\tau)] = W_o^i\delta(t-\tau)$. The integral from 0 to t_f in the cost function is performed explicitly by expressing the combined plant and controller closed-loop system in modal form.

Note that the finite-time cost function shown in equation (7.2.6) does not guarantee closed-loop stability. However, asymptotic stability is achieved when the terminal time t_f approaches "infinity," and the usual conditions of controllability and observability have been satisfied. In practice, "infinity" is usually reached at three or four times the largest time constant of the closed-loop system eigenvalues. There is a significant advantage in using a finite terminal time cost function. In contrast to a steady state cost function (refs. 9 and 10), this approach does not require a stabilizing initial guess to start the optimization process.

In the design algorithm SANDY, the terminal time t_f is stepped up automatically by a multiplicative factor ρ ($\rho > 1$) specified by the designers. Convergence to the steady state solution is assumed reached when the optimal value of the cost function $J(t_f^{i+1})$ (where $t_f^{i+1} = \rho t_f^i$) settles to within 0.1% of its previous value $J(t_f^i)$.

The early version of the SANDY design algorithm (ref. 7) had encountered numerous problems associated with numerical overflow. This occurs at a large value of finite t_f^i time and in the line search procedure. The underlying reason is due to the fact that a "large" step was undertaken in the nonlinear programming algorithm resulting in a highly unstable closed-loop design at an intermediate trial solution. To avoid this, direct constraints have been set up to limit the size of the line search using information of the closed-loop eigenvalue sensitivity to the design parameters.

Let K be a design parameter of the controller, the change of K during the ith iteration of the numerical line search is limited by ΔK^i_{max} given by,

$$K^i - \Delta K^i_{max} \leq K^{i+1} \leq K^i + \Delta K^i_{max} \tag{7.2.8}$$

where

$$\Delta K^i_{max} = \underset{1 \leq j \leq N}{\text{Min}} \left(\Delta \sigma^i_{jmax} \; / \; | \partial \sigma^i_j / \partial K | \right) \tag{7.2.9}$$

$\Delta \sigma^j_{jmax}$ = Maximum allowable incremental change of the jth closed-loop eigenvalues along the real axis (fig. 5) at the ith iteration,

$$= \text{Max} \{ 1 \; , \; -\sigma^i_j/2 \}$$

σ^i_j = Real part of the jth closed-loop eigenvalue at the ith iteration.

$\partial \sigma^i_j / \partial K$ = Real part of the jth row of the vector $(-T^{-1} \, \partial A / \partial K \, t_j)^i$

T = Eigenvector matrix of A

t_j = jth column of T

Hence, using the constraint equation (7.2.9) large changes in the design parameters are avoided, and highly unstable designs will not occur during the search for the optimal solution.

Gradients of the cost function also are determined analytically (ref. 7) and its values are supplied to the nonlinear optimization algorithm (ref. 8). Other typical nonlinear constraints of equation (7.2.7) are:

- Covariance constraints in the control and performance variables,

$$u^2_{min} \leq E[u^2(t_f)] \leq u^2_{max} \tag{7.2.10}$$

$$y^2_{min} \leq E[y^2(t_f)] \leq y^2_{max} \tag{7.2.11}$$

and

- Damping constraints on the closed-loop system eigenvalues,

ζ_j = Damping of the jth mode $\geq \zeta_{min}$ (7.2.12)

for j = 1,N where N is the order of the closed-loop system.

Flexibility in the extended design code SANDY allows designers to implement easily any other types of linear/nonlinear equality and inequality constraints. The constrained optimization code (ref. 8) requires the knowledge of the gradients of the constraints, with respect to the design parameters to improve the convergence of the numerical search.

Capability to perform nonlinear constrained optimization is useful since, in general, design requirements are not always expressible in the form of a quadratic cost function. With direct constraints, numerous iterative adjustments in the cost weighting matrices Q^i and R^i, and parameters W_{pi} to satisfy a given design requirement can be eliminated.

In summary, solution of the robust output feedback controller will depend on the following parameters,

- Criterion penalty matrix Q^i at each plant condition.
- Control penalty matrix R^i at each plant condition.
- Formulation of design constraints.
- Disturbance characteristics W_o^i.

The design process is still iterative. However, some of the above design parameters can be derived from the full-state feedback design procedure discussed in Section 7.1. The design approach discussed in this section is used to reoptimize the cost function for a more practical controller structure (e.g., output feedback).

8.0 ROBUST FULL-STATE FEEDBACK CONTROLLER DESIGNS

Full-state feedback designs (fig. 6) have been developed at each individual flight condition. The design method is described in Section 7.1. The purpose is to determine the maximum achievable performance under the ideal circumstance, where all the system states are available. The results subsequently are used to develop low-order controllers where only measurement outputs are fed back. The control activities associated with the full-state feedback controllers provide a measure of minimum control efforts required for the desired performance and stability. It is anticipated that with a low-order controller structure a good design will exhibit similar control surface activities for an equivalent design performance and stability.

The selection of the parameter weights in the cost function is based partially on the controllability of each surface. It is seen that at every flight condition the open-loop aircraft possesses an unstable real mode. The degree of divergence depends on the altitude and Mach condition. The static instability decreases with increasing altitude and Mach number. The design variables penalized in the cost function include the airplane output responses: the airspeed u_b, pitch rate q, pitch angle θ, normal acceleration A_{nc}, and angle of attack α. These responses are traded off with the activities of the control effectors: symmetric horizontal tail deflection δ_{htc}, symmetric vertical canard deflection ("snow plow") δ_{vcc}, and power lever angle δ_{plac}, which controls the engine thrust.

8.1 Flight Condition Mach .25 and Altitude 5000 ft

The penalty weighting coefficients for the outputs are;

256.0 for the variable u_b,
256.0 for the variable q,
1.0 for the variable θ,
1.0 for the variable A_{nc},
1.0 for the variable α,

and those for the control variables are;

64.0 for the symmetric horizontal tail δ_{htc},
4.0 for the symmetric vertical canard δ_{vcc},
4.0 for the power lever angle δ_{plac}.

The set of optimal full-state feedback gains is listed in Table 17. The eigenvalues of the closed-loop system are shown in Table 20. Damping of the phugoid and short period modes exceeds 0.56. The covariance responses to simultaneous longitudinal u_g and vertical w_g turbulence of intensities 10 ft/s are summarized in Table 23. By properly balancing the activities of the two control surfaces, the resulting full-state feedback design becomes robust under failure of either surface. Robustness properties of the full-state feedback controller are shown in Table 26 in terms of individual loop phase, gain margins, and rolloff behavior at high frequencies. The requirement for gain attenuation at high frequencies defined in terms of loop gain at a frequency of 10 rad/s is satisfied.

Frequency responses of individual control loop are shown in Figures 7 through 13. When all controls are effective each control loop shows a peak in gain amplitude (figs. 7 through 9) near the frequency of the unstable mode ($\sim$0.8 rad/s). When either of the control surfaces fails, the remaining control loop has a "1/s" integrator behavior providing the required gain at the low frequency for stability. The rolloff characteristics of -20 dB/decade typical of a full-state feedback design are evident in these frequency responses. Bandwidths of the δ_{plac} and δ_{htc} control loops are not changed significantly in the presence of a δ_{vcc} control failure. The following bandwidths are obtained in this design: 0.8 to 1.0 rad/s for the engine thrust loop, 3.0 rad/s for the horizontal tail control loop, and 0.5 to 2.0 rad/s for the vertical canard control loop. A significant increase of bandwidth in the vertical canard δ_{vcc} control loop is to account for the loss of a more effective control surface δ_{htc}.

8.2 Flight Condition Mach .60 and Altitude 5000 ft

The penalty weighting coefficients for the outputs are;

64.0 for the variable u_b,
64.0 for the variable q,
1.0 for the variable θ,
1.0 for the variable A_{nc},
1.0 for the variable α,

and those for the control variables are;

640.0 for the symmetric horizontal tail δ_{htc},
18.0 for the symmetric vertical canard δ_{vcc},
2.0 for the power lever angle δ_{plac}.

The set of optimal full-state feedback gains are listed in Table 18. The eigenvalues of the closed-loop system are shown in Table 21. Damping of the phugoid and short period modes exceeds 0.62. The covariance responses to simultaneous longitudinal u_g and vertical w_g turbulence of intensities 10 ft/s are summarized in Table 24. By properly balancing the activities of the two control surfaces, the resulting full-state feedback design remains robust under failure of either surface. Robustness properties of the full-state feedback controller are shown in Table 27 in terms of individual loop phase, gain margins, and rolloff behavior at high frequencies. The design meets the requirement for gain attenuation at high frequencies defined in Section 6.0.

Frequency responses of individual control loop are shown in Figures 14 through 20. When all controls are effective each control loop shows high gain amplitude (figs. 14 through 16) near the frequency of the unstable mode (~ 0.9 rad/s). When either of the control surfaces fails, the remaining control loop has a "1/s" behavior providing the required gain at the low frequency for stability. The rolloff characteristics of -20 dB/decade typical of a full-state feedback design are evident in these frequency responses. Bandwidths of the δ_{plac} and δ_{htc} control loops are not changed significantly in the presence of a δ_{vcc} control failure. The following bandwidths are obtained in this design: 0.9 to 1.1 rad/s for the engine thrust loop, 3.0 rad/s for the horizontal tail control loop, and 1.2 to 2.0 rad/s for the vertical canard control loop. An increase of bandwidth in the vertical canard δ_{vcc} control loop is to account for the loss of a more effective control surface δ_{htc}.

8.3 Flight Condition Mach .90 and Altitude 20,000 ft

The penalty weighting coefficients for the outputs are;

16.0 for the variable u_b,
16.0 for the variable q,
1.0 for the variable θ,
1.0 for the variable A_{nc},
1.0 for the variable α,

and those for the control variables are;

512.0 for the symmetric horizontal tail δ_{htc},
12.0 for the symmetric vertical canard δ_{vcc},
1.0 for the power lever angle δ_{plac}.

The set of optimal full-state feedback gains are listed in Table 19. The eigenvalues of the closed-loop system are shown in Table 22. Damping of the phugoid and short period modes exceeds 0.74. The covariance responses to simultaneous longitudinal u_g and vertical w_g turbulence of intensities 10 ft/s are summarized in Table 25. By properly balancing the activities of the two control surfaces, the resulting full-state feedback design remains robust under failure of either surface. Robustness properties of the full-state feedback controller are shown in Table 28 in terms of individual loop phase and gain margins and rolloff behavior at high frequencies. The requirement for gain attenuation at high frequencies is satisfied.

Frequency responses of individual control loop are shown in Figures 21 through 27. When all controls are effective, Figures 21 through 23 show that at this condition of high dynamic pressure the design has much lower gain than the previous two conditions. The rolloff characteristics of -20 dB/decade typical of a full-state feedback design are evident in these frequency responses. Bandwidths (defined as the ~ 0 dB gain crossover frequency) of the δ_{plac} and δ_{htc} control loops are not changed significantly in the presence of a δ_{vcc} control failure. The following bandwidths are obtained in this design: the engine thrust loop has gain less than 0 dB, 2.0 rad/s for the horizontal tail control loop, and 2.2 rad/s for the vertical canard control loop. A large increase in the vertical canard δ_{vcc} control loop gain is to account for the loss of a more effective control surface δ_{htc}.

Robustness of the full-state feedback controller designs described in Sections 8.1 through 8.3 (at each individual flight condition) to failures in either the aerodynamic surfaces δ_{htc} or δ_{vcc} gives a strong indication that design of a fault tolerant control system to actuator failure is feasible. Recognition that feedback of all the system states is required for these designs. Notice further that no simple gain schedule can be developed from these three designs (tables 17, 18, and 19). A total of 30 gains needs to be adjusted from one flight condition to the other. Section 9.0 will demonstrate that it is still possible to synthesize robust control laws at each individual flight condition in the presence of actuator failures using output feedback.

The design philosophy in Section 9.0 is again to develop feedback systems that use each control effector in accordance to their controllability. That is, a surface with low effectiveness will have higher activities in comparison with one having higher effectiveness; hence, when either surface fails, the other would have appropriate authority to withstand the additional moments and forces for trim and stability.

9.0 ROBUST OUTPUT FEEDBACK CONTROLLER DESIGNS

The previous Section 8.0 presents fault tolerant control designs at individual flight conditions using a full-state feedback structure. In general, not all the states are measurable and available for feedback. This section addresses the problem of synthesizing output feedback controllers directly, which are fault tolerant to actuator failure in either the δ_{htc} or the δ_{vcc} aerodynamic surfaces. A block diagram of the output feedback controller at each flight condition is shown in Figure 28. The five output sensors used in feedback are: $u_b(t)$, $q(t)$, $\theta(t)$, $\alpha(t)$ and $A_{nc}(t)$. Hence, a total of 15 gains are designed, using the method described in Section 7.2, in contrast to the full-state feedback case that involves 30 feedback gains.

The fault tolerant output feedback gains are designed at individual flight conditions. An integrated gain schedule design is later developed from these designs, and results are discussed in Section 10.0.

9.1 Flight Condition Mach .25 and Altitude 5000 ft

Using a quadratic cost function as in the full-state feedback design, the following penalty weighting coefficients for the outputs have been selected;

256.0 for the variable u_b,
256.0 for the variable q,
1.0 for the variable θ,
1.0 for the variable A_{nc},
4.0 for the variable α,

and no penalty is put on the control variables (i.e., R=0). Instead, constraints on the control covariances were used to restrict the surface and engine thrust activities. They are,

$$\lim_{t_f \to \infty} E[\delta_{htc}^2] \leq 0.0063 \tag{9.1.1}$$

$$\lim_{t_f \to \infty} E[\dot{\delta}_{htc}^2] \leq 0.0250 \tag{9.1.2}$$

$$\lim_{t_f \to \infty} E[\delta_{vcc}^2] \leq 0.0614 \tag{9.1.3}$$

$$\lim_{t_f \to \infty} E[\dot{\delta}_{vcc}^2] \leq 0.3600 \tag{9.1.4}$$

$$\lim_{t_f \to \infty} E[\delta_{plac}^2] \leq 0.0100 \tag{9.1.5}$$

These bounds on the control deflection and rate covariances are obtained from the previous full-state feedback design to a 10 ft/s turbulence inputs u_g and w_g (table 23). The covariance responses defined in the above constraints (eqs. (9.1.1) through (9.1.5)) are evaluated to longitudinal and vertical turbulences of intensities 1.0 ft/s. By lowering the upper limit on the rate δ_{htc}, we are able to improve the rolloff characteristics of this control loop.

The optimal gains are determined using the design algorithm SANDY for this output feedback controller structure. The set of the optimal output feedback gains are listed in Table 29. The eigenvalues of the closed-loop system are shown in Table 32. Damping of the phugoid and short period modes exceeds 0.64 even in the presence of an actuator failure. The covariance responses to simultaneous longitudinal u_g and vertical w_g turbulence of intensities 10 ft/s are summarized in Table 35.

Notice that these responses are similar to those achieved using full-state feedback. The augmented aircraft responses are not affected significantly by the loss of a control surface; in particular, the normal acceleration A_{nc} response is almost invariant ($\sim 0.105'$g) to failure of either δ_{htc} or δ_{vcc} control surface.

Increased control activities of the remaining controls are expected in a fault tolerant system. The robust fault tolerant feature of the design is obtained by simply balancing the activities of the two control surfaces as described in Section 7.1. Thus the design capability for multiple plant conditions discussed in Section 7.2 was not needed.

Robustness properties of the output feedback controller are shown in Table 38 in terms of individual loop phase, gain margins, and rolloff behavior at high frequencies. The requirements defined in Section 6.0 have been satisfied.

Frequency responses of individual control loop are shown in Figures 29 throught 35. The engine thrust control loop is not affected by the loss of any of the other two controls. When all controls are effective, the δ_{htc} and δ_{vcc} control loops have a maximum gain amplitude (figs. 30 through 31) near the frequency of the unstable mode (~ 1.0 rad/s). When either of the controls fail, the remaining control loop has an increase in loop gain.

Rolloff characteristics of -40 dB/decade was achieved due to the covariance constraints (eqs. 9.1.2 and 9.1.4) in the actuator rates. Bandwidths of the control loops are not affected by either control actuator failure. The following bandwidths are obtained in the design: the engine thrust loop has loop gain less than 0 dB, 3.0 to 4.0 rad/s for the horizontal tail control loop, and 2.0 rad/s for the vertical canard control loop.

9.2 Flight Condition Mach .60 and Altitude 5000 ft

Using a quadratic cost function as in the full-state feedback design, the following penalty weighting coefficients for the outputs have been selected;

66.0 for the variable u_b,

160.0 for the variable q,

85.0 for the variable θ,

2.0 for the variable A_{nc},

1.0 for the variable α,

and those for the control variables are;

980.0 for the symmetric horizontal tail δ_{htc},

20.0 for the symmetric vertical canard δ_{vcc},

12.0 for the power lever angle δ_{plac}.

The optimal gains are determined using the design algorithm SANDY for this output feedback controller structure. The set of the optimal output feedback gains is listed in Table 30. The eigenvalues of the closed-loop system are shown in Table 33. Damping of the phugoid and short period modes exceeds 0.41 even in the presence of an actuator failure. The covariance responses to simultaneous longitudinal u_g and vertical w_g turbulence of intensities 10 ft/s are summarized in Table 36.

Notice that these responses also are similar to those achieved using full-state feedback. The augmented aircraft responses are not sensitive to the loss of a control surface; in particular, the normal acceleration A_{nc} response is almost invariant (~ 0.237'g) to failure of either δ_{htc} or δ_{vcc} control surface.

Increased control activities of the remaining controls are expected in a fault tolerant system. The robust fault tolerant feature of the design is obtained by properly balancing the activities of the two control surfaces as described in Section 7.1. Thus, the design capability for multiple plant conditions discussed in Section 7.2 was not needed.

Robustness properties of the output feedback controller are shown in Table 39 in terms of individual loop phase, gain margins, and rolloff behavior at high frequencies. The requirements defined in Section 6.0 have been satisfied.

Frequency responses of individual control loop are shown in Figures 36 through 42. The engine thrust control loop is not affected by the loss of any of the other two controls. When all controls are effective, the δ_{htc} and δ_{vcc} control loops have a maximum gain amplitude (figs. 37 and 38) near the frequency of the unstable mode (~ 1.0 rad/s). When either of the controls fail, the remaining control loop has an increase in loop gain.

Rolloff characteristics of -40 dB/decade was achieved. Bandwidths of the control loops are not affected by either control actuator failure. The following bandwidths are obtained in the design: 0.25 to 0.40 rad/s for the engine thrust loop, 3.5 to 4.8 rad/s for the horizontal tail control loop, and 3.2 to 5.0 rad/s for the vertical canard control loop.

9.3 Flight Condition Mach .90 and Altitude 20,000 ft

Using a quadratic cost function as in the full-state feedback design, the following penalty weighting coefficients for the outputs have been selected;

203.0 for the variable u_b,

1.0 for the variable q,

11.0 for the variable θ,

0.0 for the variable A_{nc},

0.0 for the variable α,

and those for the control variables are;

576.5 for the symmetric horizontal tail δ_{htc},

10.0 for the symmetric vertical canard δ_{vcc},

12.0 for the power lever angle δ_{plac}.

The optimal gains are determined using the design algorithm SANDY for this output feedback controller structure. The set of the optimal output feedback gains is listed in Table 31. The eigenvalues of the closed-loop system are shown in Table 34. Damping of the phugoid and short period modes exceeds 0.67 even in the presence of an actuator failure. The covariance responses to simultaneous longitudinal u_g and vertical w_g turbulence of intensities 10 ft/s are summarized in Table 37.

Notice that these responses are similar to those achieved using full-state feedback. The augmented aircraft responses are not sensitive to the loss of a control surface; in particular, the normal acceleration A_{nc} response is almost invariant (~ 0.291 'g) to the failure of either δ_{htc} or δ_{vcc} control surface.

Increased control activities of the remaining controls are expected in a fault tolerant system. Robust fault tolerant feature of the design is obtained by adjusting the activities of the two control surfaces as described in Section 7.1. Thus the design capability for multiple plant conditions discussed in Section 7.2 was not needed.

Robustness properties of the output feedback controller are shown in Table 40 in terms of individual loop phase, gain margins, and rolloff behavior at high frequencies. The requirements defined in Section 6.0 have been satisfied.

Frequency responses of individual control loop are shown in Figures 43 through 49. The engine thrust control loop is not affected by the loss of any of the other two controls. When either of the control fails, the remaining control loop has an increase in loop gain.

Rolloff characteristics of -40 dB/decade was achieved. Bandwidths of the control loops are not affected by either control actuator failure. The following bandwidths are obtained in the design: the engine thrust loop has loop gain less than 0 dB, 2.0 rad/s for the horizontal tail control loop, and 1.5 rad/s for the vertical canard control loop. These bandwidths are smaller than previous design conditions because the open-loop divergence mode at a frequency of 0.17 rad/s is mild.

10.0 ROBUST GAIN SCHEDULE OUTPUT FEEDBACK CONTROLLER DESIGNS

Fault tolerant control laws developed in Section 9.0 has proved to be robust to either control actuator failure of δ_{htc} or δ_{vcc}. However, design gains obtained at the three flight conditions (tables 29 through 31) are fairly different and do not lend themselves easily to a simple gain schedule. To be complete, a practical implementation of this fault tolerant control laws needs to be developed, which will involve only a few gain change in going from one flight condition to the other. Here, we adopt the same gain schedule logic as the existing IBU described in Section 5.0.

The gain schedule is based on the discrete switch using the landing gear up/down logic. Thus, in this design case, only two set of gains are needed for the three flight conditions under consideration. The landing approach condition (Mach .25 and altitude 5000 ft) corresponds to the landing gear down case, while the other two are cruise conditions where the landing gears are up.

The gain schedule is kept simple intentionally for purpose of reliability and ease of implementation. A diagonal structure for the controller gain schedule matrix was used with diagonal elements K_{plac}, K_{htc}, and K_{vcc}. For convenience, the design at the landing approach condition was selected as a baseline design for the development of the gain schedule at the other two conditions. The block diagram of the fault tolerant output feedback controller with gain schedule is shown in Figure 50. Notice that three gains are applied to the controller outputs that vary according to the landing gear up/down logic. Since the landing approach condition was used as baseline, the gain factors K_{plac}, K_{htc}, and K_{vcc} are, therefore, unity for the landing gear down conditions. For the cruise conditions, values of the gain factors are determined using the design method described in Section 7.2 for multiple plant models.

There are a total of six plant models for the design of the integrated gain schedule factors K_{plac}, K_{htc}, and K_{vcc}. Models are derived from two cruise conditions along with two possibilities of control surface actuator failures, namely;

Model 1: Flight condition Mach .60 altitude 5000 ft with no failure

Model 2: Flight condition Mach .60 altitude 5000 ft with δ_{htc} failed

Model 3: Flight condition Mach .60 altitude 5000 ft with δ_{vcc} failed

Model 4: Flight condition Mach .90 altitude 20,000 ft with no failure

Model 5: Flight condition Mach .90 altitude 20,000 ft with δ_{htc} failed

Model 6: Flight condition Mach .90 altitude 20,000 ft with δ_{vcc} failed

The design objective is to determine the three gain factors to go with the feedback gains shown in Table 29 so that desired stability and performance are achieved across the above six plant conditions. The unique design capability offered by the method (ref. 7) described in Section 7.2 enables us to optimize these three gains while maintaining fault tolerant robustness. The cost function given in equation (7.2.6) incorporates all six design conditions into a single-design cost function where $N_p=6$, as follows;

$$J(t_f) = 1/2 \sum_{i=1}^{6} W_{pi} E[\int_o^{tf} (y^T Q^i y + u^T R^i u)\, dt] \qquad (10.1)$$

Selection of the design parameters in the above cost function is an iterative process. Design parameters Wp_i, Q_i, and R_i between the two flight conditions are kept identical, and they are summarized in Table 41. Note here the matrices Q_i and R_i are diagonal. Three outputs are penalized at each plant condition: u_b, α, and A_{nc}. The nominal (no failure) conditions are given the highest weighting factor $W_{pi} = 16$. This ensures that the performance of the fault tolerant controller is not degraded significantly at these nominal conditions. Again, equation (10.1) is evaluated with respect to longitudinal and vertical turbulences of intensities 1 ft/s. The optimization converges to the following set of gains,

$$K_{plac} = 1.80400 \tag{10.2}$$

$$K_{htc} = 0.08531 \tag{10.3}$$

$$K_{vcc} = 0.20640 \tag{10.4}$$

The final integrated set of fault tolerant output feedback controller designs with gain schedule are shown in Tables 42 through 44. All three flight conditions share the same basic set of 15 feedback gains on the output sensors. The schedules shown in equations (10.2) through (10.4) remains constant at the cruise conditions, while at the landing approach condition they are equal to unity.

The integrated gain schedule design only affects the cruise conditions. The design at the landing approach condition was unchanged since it was used as baseline in the integrated design. Hence, stability, performance, and robustness are identical to those results described in Section 9.1. Discussion of these results, therefore, are omitted.

Discussion of the design results at the cruise conditions follows. The eigenvalues of the closed-loop system are shown in Tables 45 and 46. Damping of the phugoid and short period modes exceeds 0.50 even in the presence of an actuator failure. The damping is better than those individual designs of Sections 9.2 and 9.3. This happens by coincidence since the designs in Sections 9.2 and 9.3 were finalized, and no further design iteration was conducted when the basic damping requirement of 0.4 defined in Section 6.0 had been satisfied.

Covariance responses to simultaneous longitudinal u_g and vertical w_g turbulence of intensities 10 ft/s are summarized in Tables 47 and 48. Notice that these responses are similar to those achieved using full-state feedback. The augmented aircraft responses are insensitive to the loss of a control surface; in particular, the normal acceleration A_{nc} response is almost invariant ($\sim 0.23'$g and $\sim 0.29'$g) to either failure of δ_{htc} or δ_{vcc} control surface. Increased control activities of the remaining controls are expected in a fault tolerant system.

Robustness properties of the output feedback controller are shown in Tables 49 and 50 in terms of individual loop phase, gain margins, and rolloff behavior at high frequencies. Requirements defined in Section 6.0 have been satisfied. Frequency responses of individual control loop are shown in Figures 51 through 64. The engine thrust control loop is not affected by the loss of any of the other two controls.

When either of the controls fail, the remaining control loop has an increase in loop gain. Rolloff characteristics of -40 dB/decade was achieved. Bandwidths of the control loops are not affected by either control actuator failure. The following bandwidths are obtained in the design: 0.1 to 0.2 rad/s for the engine thrust loop, 2.0 to 3.0 rad/s (Mach .60 condition), and 4.0 to 4.5 rad/s (Mach .90 condition) for the horizontal tail control loop, 2.2 to 3.0 rad/s (Mach .60 condition), and 4.0 to 5.0 rad/s (Mach .90 condition) for the vertical canard control loop.

Finally, aircraft responses are simulated to simultaneous longitudinal and vertical turbulences of intensities 10 ft/s. Results are shown in Figures 65 through 70. Duration of the simulation is two minutes. The first minute corresponds to the "no-failure" case, while in the last 60 seconds of simulation, a failure occurs in either the horizontal tail δ_{htc} or the vertical canard δ_{vcc} control actuators. Notice that at failure the failed surface returns to its trim ("null") position. The random gust inputs are shown in the variables u_g and w_{g1}, respectively, for the longitudinal and vertical components of turbulences. These are outputs of the Dryden filters described in Section 4.4 excited by white noises. The simulated aircraft variables are: thrust, normal acceleration A_{nc}, airspeed u_b, angle of attack α, pitch rate q, and pitch attitude θ. No large transient responses are observed in the aircraft variables in the transition from a nonfailed state to a failed state.

Generally, one observes an increase in activities of the remaining controls in the presence of a failure. The variables ADHT and DDHT are the deflection and rate of the δ_{ht} surface, respectively, while ADVC and DDVC are the deflection and rate of δ_{vc} surface. Activity of the engine thrust, however, is not affected since its function primarily is in the stabilization of the speed mode in the low-frequency region (less than 0.2 rad/s). Peak δ_{ht} surface activity increases by about a factor of two in the case of failure of the δ_{vc} surface. On the other hand, the loss of the δ_{ht} surface results in a nearly three to four time increase in peak activity of the δ_{vc} control surface. Even with these large increases, all surface activities are still within their maximum allowable limits.

11.0 CONCLUSION

A fault tolerant control system has been developed for an advanced fighter with relaxed static stability. The design procedure employed in the control law synthesis involves both the conventional LQ method and the new SANDY technique for robust output feedback controllers. The main feature of a fault tolerant design is its simple control structure, which does not involve fault detection and isolation schemes.

Three types of controller designs have been developed and proved to be fault tolerant to failure in the control actuators of the aerodynamic surfaces. Minimum stability of 0.4 has been achieved throughout all three flight conditions without the need for control reconfiguration/restructure. The concept of balancing the redundant control surface activities to accommodate failures according to their controllability indices seems to produce robust designs for the flight conditions considered in this study.

The method for synthesizing an optimal output feedback controller (ref. 7) provides a means to simplify design complexity associated with full-state feedback while maintaining good performance and robustness. This capability was demonstrated in Sections 9.1, 9.2, and 10.0. Direct constraints on the covariances of the surface activities allow designers to make use of results from full-state feedback in the synthesis of output feedback controller as demonstrated in Section 9.1. An integrated fault tolerant design with minimal gain schedule was achieved using the multiple plant design capability.

Numerical optimization in the SANDY design technique (ref. 7) has been improved significantly by putting additional bounds on the design parameters to constrain the step size of the line search. Details are given in Section 7.2.

The method presented herein can also be applied to the synthesis of fault tolerant control for failure in the sensors. In the synthesis, the observability of the dominant mode by the redundant sensors plays a similar role as the controllability of the dominant mode by the redundant control surfaces.

It is recommended that a complete full nonlinear aircraft simulation of the fault tolerant control system in Section 10.0 be conducted to examine in details the robustness characteristics of these designs to nonlinearities in control actuation and aerodynamics. Due to the limited scope of this study, these aspects will be left for future research.

Table 1. Availability of Controls at Different Flight Conditions

CONTROL EFFECTORS	FLIGHT CONDITION MACH .25 Altitude 5000 ft	MACH .60 Altitude 5000 ft	MACH .90 Altitude 20,000 ft
Leading Edge Flaps	✓	✓	Not Available
Horizontal Tails	✓	✓	✓
Flaperons	Not Available	✓	✓
Vertical Canards	✓	✓	✓
Thrust	✓	✓	✓

Table 2. Thrust Limits at Different Flight Conditions

THRUST LIMITS		FLIGHT CONDITION MACH .25 Altitude 5000 ft	MACH .60 Altitude 5000 ft	MACH .90 Altitude 20,000 ft
T_{Idle}	(lbs)	500.0	220.0	130.0
$T_{Military}$	(lbs)	9200.0	10600.0	7750.0
T_{Max}	(lbs)	17000.0	22000.0	17000.0

Table 3. Nominal Power Lever Angle and Trim Thrust at Different Flight Conditions

	FLIGHT CONDITION MACH .25 Altitude 5000 ft	MACH .60 Altitude 5000 ft	MACH .90 Altitude 20,000 ft
Power Lever Angle [%MAX]	28.25	22.30	41.13
Trim Thrust (lbs)	3715.0	3070.0	3898.0

Table 4. Aircraft Trim Parameters at Different Flight Conditions

Variables	MACH .25 5000 ft Altitude	MACH .6 5000 ft Altitude	MACH .9 20,000 ft Altitude
U_o [ft/s]	274.9	652.8	928.2
θ_o [deg]	10.2	1.9	1.8
X_o [ft]	13.63	13.63	13.63
q_o [lb/ft^2]	77.0	436.4	545.8

Table 5. Eigenvalues of Open-Loop Airplane, Mach .25, Altitude 5000 ft

Mode	Eigenvalues
1	0.845
2	- 0.157
3	- 0.157 + j 0.002
4	(ζ=1.000, ω=0.157)
5	- 0.030 + j 0.171
6	(ζ=0.173, ω=0.174)
7	- 1.000
8	- 1.715
9	-13.000
10	-13.000

Table 6. Controllability Matrix, Mach .25, Altitude 5000 ft

Mode	δhtc	δvcc	δplac
1	1.000	0.1999	5.6169E-03
2	0.000	0.0000	0.0000
3&4	0.000	0.0000	0.0000
5&6	1.000	0.1871	8.1534E-02
7	0.000	0.0000	1.0000
8	1.000	0.2163	1.4823E-03
9	1.000	0.0000	0.0000
10	0.000	1.0000	0.0000

Table 7. Observability Matrix, Mach .25, Altitude 5000 ft

	System modes							
Sensors	1	2	3&4	5&6	7	8	9	10
U	1.0000	1.0000	1.0000	1.0000	1.0000	0.4551	5.8190E-02	6.2163E-02
Q	-0.6804	-5.7477E-02	5.7142E-02	5.4749E-02	1.4157E-02	1.0000	1.0000	1.0000
θ	-0.8057	0.3668	0.3646	0.3151	-1.4157E-02	-0.5830	-7.6923E-02	-7.6923E-02
Anc	-3.8232E-02	-1.1084E-02	6.6256E-03	8.5907E-03	7.1102E-03	-6.3932E-02	-3.3292E-02	-9.4808E-02
α	-0.5153	-6.2493E-02	0.6946	5.2075E-02	3.4040E-02	-0.7909	-4.4568E-02	-7.6374E-02

Table 8. Eigenvalues of Open-Loop Airplane, Mach .60, Altitude 5000 ft

Mode	Eigenvalues
1	0.930
2	- 0.009 + j 0.071
3	(ζ=0.126, ω=0.071)
4	- 0.373
5	- 0.373 + j 0.004
6	(ζ=1.000, ω=0.373)
7	- 1.000
8	- 2.910
9	-13.000
10	-13.000

Table 9. Controllability Matrix, Mach .60, Altitude 5000 ft

Mode	δhtc	δvcc	δplac
1	1.000	0.1426	9.6901E-05
2&3	1.000	0.1403	3.7961E-03
4	0.000	0.0000	0.0000
5&6	0.000	0.0000	0.0000
7	0.000	0.0000	1.0000
8	1.000	0.1502	-1.7003E-05
9	1.000	0.0000	0.0000
10	0.000	1.0000	0.0000

Table 10. Observability Matrix, Mach .60, Altitude 5000 ft

	System modes							
Sensors	1	2&3	4	5&6	7	8	9	10
U	-0.7540	1.0000	-0.6903	1.0000	1.0000	0.1620	1.9345E-02	2.9944E-02
Q	0.9304	9.0508E-03	-0.3730	0.3069	5.9765E-03	1.0000	1.0000	1.0000
θ	1.0000	0.1268	1.0000	0.8226	-5.9765E-03	-0.3437	-7.6923E-02	-7.6923E-02
Anc	0.1946	3.2257E-03	-0.1419	1.0812E-02	2.2417E-03	-0.2835	-8.1057E-02	-0.1439
α	0.4270	2.5914E-03	-7.7640E-02	0.7380	4.6902E-04	-0.5982	-7.3661E-02	-8.7310E-02

Table 11. Eigenvalues of Open-Loop Airplane, Mach .90, Altitude 20,000 ft

Mode	Eigenvalues
1	0.170
2	- 0.175
3	- 0.530
4	- 0.530 + j 0.005
5	(ζ=1.000, ω=0.530)
6	- 1.000
7	- 1.07 + j 1.076
8	(ζ=0.707, ω=1.520)
9	-13.000
10	-13.000

Table 12. Controllability Matrix, Mach .90, Altitude 20,000 ft

Mode	δhtc	δvcc	δplac
1	1.0000	0.1318	2.7941E-03
2	1.0000	0.1319	-4.3140E-03
3	0.0000	0.0000	0.0000
4&5	1.0000	0.0000	0.0000
6	0.0000	0.0000	1.0000
7&8	1.0000	0.1313	3.3947E-04
9	1.0000	0.0000	0.0000
10	0.0000	1.0000	0.0000

Table 13. Observability Matrix, Mach .90, Altitude 20,000 ft

	System Modes							
Sensors	1	2	3	4&5	6	7&8	9	10
U	1.0000	1.0000	1.0000	0.4667	1.0000	0.1127	3.8952E-02	4.0437E-02
Q	-5.1209E-02	-5.4484E-02	-0.4356	0.4823	-2.9987E-02	1.0000	1.0000	1.0000
θ	-0.3006	0.3108	0.8214	0.9095	2.9987E-02	0.6578	-7.6923E-02	-7.6923E-02
Anc	-2.2824E-02	-3.1554E-02	-0.3530	2.5540E-02	-5.2534E-02	0.6258	-0.1107	-0.1634
α	-3.3253E-02	-4.5497E-02	-0.5051	1.0000	-7.4761E-02	0.8782	-7.9153E-02	-8.7208E-02

Table 14. Eigenvalues of Existing Backup Controller Design

No.	FLIGHT CONDITIONS Mach .25	Mach .6	Mach .9
1.	- 0.020	- 0.016	- 0.011
2.	- 0.728	- 1.000	- 1.000
3.	- 1.000	- 1.709	- 1.349
4.	- 1.167 + j 1.866	- 2.056 + j 3.531	- 3.386 + j 5.264
5.	(ζ=0.530, ω=2.201)	(ζ=0.503, ω=4.086)	(ζ=0.541, ω=6.259)
6.	-11.420 + j 5.369	-11.490	-10.550
7.	(ζ=0.905, ω=12.620)	-13.000	-13.000
8.	-13.000	-47.670	-46.470

Table 15. Covariance Responses of Existing Backup Controller Design, σ_u, σ_w = 10 ft/s

Variables (Units)	FLIGHT CONDITIONS Mach .25	Mach .6	Mach .9
Horizontal Tail Position (deg)	1.425	0.151	0.047
Horizontal Tail Rate (deg/s)	1.923	0.454	0.134
Normal Acceleration (g)	0.107	0.245	0.261
Speed (ft/s)	3.383	2.008	1.409
Angle of Attack (deg)	1.894	0.749	0.489
Pitch Rate (deg/s)	0.394	0.261	0.068
Pitch Attitude (deg)	0.366	0.105	0.034

Table 16. Stability Margins of Existing Backup Controller Design

	FLIGHT CONDITIONS Mach .25	Mach .6	Mach .9
Gain Margin (dB)	-32, -12	-54, -14	∞
Phase Margin (deg)	46	40	47
Loop Gain (dB) at 10 r/s	-12	-8	-4

Table 17. Control Gains of Full-State Feedback Design, Mach .25, Altitude 5000 ft

Controls	U	W	Q	θ	δht	δvc	Thrust	Ug	Wg1	Wg2
δhtc	-1.137	.09142	1.849	0.7814	-.1130	-.02325	-9.656E-4	8.044E-3	-.09539	1.859E-5
δvcc	-3.831	.27670	6.098	2.6780	-.3719	-.07656	-3.298E-3	0.014230	-.30000	1.046E-4
δplac	-5.276	-.28460	1.298	2.6550	-.0672	-.01435	-5.015E-3	-0.087750	.25390	4.223E-4

Table 18. Control Gains of Full-State Feedback Design, Mach .60, Altitude 5000 ft

Controls	U	W	Q	θ	δht	δvc	Thrust	Ug	Wg1	Wg2
δhtc	-0.1426	.01262	0.2645	0.1539	-.1232	-.01773	-1.468E-4	-2.151E-3	-.01303	-2.191E-6
δvcc	-0.6608	.06535	1.3540	0.7678	-.6304	-.09080	-7.043E-4	-0.010500	-.06759	-1.203E-5
δplac	-4.5050	-.10120	0.5902	2.8120	-.2439	-.03290	-4.565E-3	-0.067360	.06315	3.293E-4

Table 19. Control Gains of Full-State Feedback Design, Mach .90, Altitude 20,000 ft

Controls	U	W	Q	θ	δht	δvc	Thrust	Ug	Wg1	Wg2
δhtc	-0.1175	-3.677E-3	.1390	0.1103	-.09874	-.01296	-1.213E-4	1.445E-3	.02790	5.843E-6
δvcc	-0.6580	-0.020640	.7781	0.6187	-.55280	-.07253	-6.809E-4	8.111E-3	.01558	3.282E-5
δplac	-1.9500	-0.032840	.3776	1.1510	-.23670	-.03113	-2.057E-3	-0.016590	.01991	8.882E-5

Table 20. Eigenvalues of Full-State Feedback Design, Mach .25, Altitude 5000 ft

No.	Open Loop	Effective Controls		
		δhtc, δvcc, δplac	δvcc, δplac	δhtc, δplac
1.	0.845	- 0.389 + j 0.176	- 0.228 + j 0.337	- 0.334 + j 0.271
2.	- 0.030 + j 0.171	(ζ=0.911, ω=0.427)	(ζ=0.560, ω=0.407)	(ζ=0.776, ω=0.430)
3.	(ζ=0.173, ω=0.174)	- 1.090 + j 0.581	- 0.939 + j 0.710	- 1.103 + j 0.678
4.	- 1.000	(ζ=0.883, ω=1.235)	(ζ=0.798, ω=1.177)	(ζ=0.834, ω=1.229)
5.	- 1.715	- 5.645	- 2.473	- 3.232
6.	-13.000	-11.820	-12.680	-12.490
7.	-13.000	-13.000	-13.000	-13.000

Table 21. Eigenvalues of Full-State Feedback Design, Mach .60, Altitude 5000 ft

No.	Open Loop	Effective Controls		
		δhtc, δvcc, δplac	δvcc, δplac	δhtc, δplac
1.	0.930	- 0.523	- 0.459 + j 0.582	- 0.760 + j 0.368
2.	- 0.009 + j 0.071	- 0.813 + j 0.567	(ζ=0.619, ω=0.742)	(ζ=0.900, ω=0.844)
3.	(ζ=0.126, ω=0.071)	(ζ=0.820, ω=0.991)	- 0.783 + j 0.494	- 0.701 + j 0.588
4.	- 1.000	- 1.298	(ζ=0.846, ω=0.925)	(ζ=0.766, ω=0.915)
5.	- 2.910	- 8.565	- 4.050	- 4.719
6.	-13.000	-10.170	-12.440	-12.180
7.	-13.000	-13.000	-13.000	-13.000

Table 22. Eigenvalues of Full-State Feedback Design, Mach .90, Altitude 20,000 ft

No.	Open Loop	Effective Controls		
		δhtc, δvcc, δplac	δvcc, δplac	δhtc, δplac
1.	0.170	- 0.589 + j 0.483	- 0.487 + j 0.436	- 0.527 + j 0.457
2.	- 0.175	(ζ=0.773, ω=0.762)	(ζ=0.745, ω=0.654)	(ζ=0.756, ω=0.697)
3.	- 1.000	- 0.871	- 0.868	- 0.869
4.	- 1.074 + j 1.076	- 1.747	- 1.879 + j 1.142	- 2.266 + j 0.867
5.	(ζ=0.707, ω=1.520)	- 5.246	(ζ=0.855, ω=2.198)	(ζ=0.934, ω=2.426)
6.	-13.000	-11.770	-12.640	-12.470
7.	-13.000	-13.000	-13.000	-13.000

Table 23. Covariance Responses of Full-State Feedback Design, Mach .25, Altitude 5000 ft, σ_u, σ_w = 10 ft/s

Variables (Units)	Open Loop*	Effective Controls		
		δhtc, δvcc, δplac	δvcc, δplac	δhtc, δplac
Horizontal Tail Position (deg)	-	0.795	0	1.379
Vertical Canard Position (deg)	-	2.478	8.061	0
Horizontal Tail Rate (deg/s)	-	1.630	0	1.935
Vertical Canard Rate (deg/s)	-	5.155	7.433	0
Thrust (lb)	-	137.300	347.700	133.400
Normal Acceleration (g)	-	0.102	0.125	0.113
Speed (ft/s)	-	0.160	0.537	0.158
Angle of Attack (deg)	-	1.828	2.040	1.879
Pitch Rate (deg/s)	-	0.167	0.610	0.339
Pitch Attitude (deg)	-	0.424	1.580	0.823

* Unstable

Table 24. Covariance Responses of Full-State Feedback Design, Mach .60, Altitude 5000 ft, σ_u, σ_w = 10 ft/s

Variables (Units)	Open Loop*	Effective Controls		
		δhtc, δvcc, δplac	δvcc, δplac	δhtc, δplac
Horizontal Tail Position (deg)	-	0.070	0	0.124
Vertical Canard Position (deg)	-	0.365	0.912	0
Horizontal Tail Rate (deg/s)	-	0.315	0	0.365
Vertical Canard Rate (deg/s)	-	1.633	2.042	0
Thrust (lb)	-	72.560	135.400	84.740
Normal Acceleration (g)	-	0.235	0.276	0.260
Speed (ft/s)	-	0.155	0.115	0.114
Angle of Attack (deg)	-	0.715	0.719	0.717
Pitch Rate (deg/s)	-	0.123	0.408	0.334
Pitch Attitude (deg)	-	0.181	0.509	0.124

* Unstable

Table 25. Covariance Responses of Full-State Feedback Design, Mach .90, Altitude 20,000 ft, σ_u, σ_w = 10 ft/s

Variables (Units)	Open Loop*	Effective Controls: δhtc, δvcc, δplac	Effective Controls: δvcc, δplac	Effective Controls: δhtc, δplac
Horizontal Tail Position (deg)	-	0.025	0	0.040
Vertical Canard Position (deg)	-	0.138	0.291	0
Horizontal Tail Rate (deg/s)	-	0.083	0	0.094
Vertical Canard Rate (deg/s)	-	0.465	0.562	0
Thrust (lb)	-	14.240	34.730	21.620
Normal Acceleration (g)	-	0.268	0.265	0.264
Speed (ft/s)	-	0.128	0.188	0.145
Angle of Attack (deg)	-	0.490	0.503	0.495
Pitch Rate (deg/s)	-	0.094	0.192	0.150
Pitch Attitude (deg)	-	0.167	0.297	0.236

* Unstable

Table 26. Stability Margins of Full-State Feedback Design, Mach .25, Altitude 5000 ft

	Effective Controls: δhtc, δvcc, δplac			δvcc, δplac		δhtc, δplac	
	δhtc loop	δvcc loop	δplac loop	δvcc loop	δplac loop	δhtc loop	δplac loop
Gain Margin (dB)	∞	∞	∞	-6	∞	-10	∞
Phase Margin (deg)	115	180	-159, 128	68	-130, 110	75	-157, 122
Loop Gain (dB)*	-10	-13	-25	-13	-25	-10	-25

Table 27. Stability Margins of Full-State Feedback Design, Mach .60, Altitude 5000 ft

	Effective Controls: δhtc, δvcc, δplac			δvcc, δplac		δhtc, δplac	
	δhtc loop	δvcc loop	δplac loop	δvcc loop	δplac loop	δhtc loop	δplac loop
Gain Margin (dB)	∞	∞	∞	-7	∞	-10	∞
Phase Margin (deg)	118	-174, 150	-168, 106	65	-171, 96	75	-170, 104
Loop Gain (dB)*	-9	-12	-24	-12	-24	-9	-24

Table 28. Stability Margins of Full-State Feedback Design, Mach .90, Altitude 20,000 ft

	Effective Controls: δhtc, δvcc, δplac			δvcc, δplac		δhtc, δplac	
	δhtc loop	δvcc loop	δplac loop	δvcc loop	δplac loop	δhtc loop	δplac loop
Gain Margin (dB)	∞	∞	∞	∞	∞	∞	∞
Phase Margin (deg)	142	180	180	92	180	89	180
Loop Gain (dB)*	-11	-14	-34	-14	-34	-11	-34

* evaluated at 10 rad/s

Table 29. Control Gains of Optimal Output Feedback Design, Mach .25, Altitude 5000 ft

Controls	U	Q	θ	α	Anc
δhtc	-0.6526	1.6400	2.841	0.5875	2.0510
δvcc	-1.9740	5.3400	7.491	1.5020	9.8150
δplac	-0.4207	-0.1626	-1.072	-0.5150	0.3276

Table 30. Control Gains of Optimal Output Feedback Design, Mach .60, Altitude 5000 ft

Controls	U	Q	θ	α	Anc
δhtc	-0.3864	0.2184	0.5845	-0.06012	0.2234
δvcc	-2.3160	1.5600	3.7050	-0.36560	1.5980
δplac	-5.5090	-1.3890	4.9320	-1.05000	0.2767

Table 31. Control Gains of Optimal Output Feedback Design, Mach .90, Altitude 20,000 ft

Controls	U	Q	θ	α	Anc
δhtc	-0.1875	0.07889	0.1044	-0.011120	-.08694
δvcc	-0.9650	0.58910	0.7898	-0.047500	-.72170
δplac	0.2106	-0.08320	-0.1483	1.558E-3	-.07616

Table 32. Eigenvalues of Optimal Output Feedback Design, Mach .25, Altitude 5000 ft

		Effective Controls		
No.	Open Loop	δhtc, δvcc, δplac	δvcc, δplac	δhtc, δplac
1.	0.845	- 0.322 + j 0.159	- 0.297	- 0.376 + j 0.086
2.	- 0.030 + j 0.171	(ζ=0.897, ω=0.359)	- 0.682 + j 0.242	(ζ=0.975, ω=0.386)
3.	(ζ=0.173, ω=0.174)	- 0.837	(ζ=0.942, ω=0.724)	- 0.811
4.	- 1.000	- 5.162	- 1.155 + j 1.185	- 1.818 + j 2.154
5.	- 1.715	- 4.358 + j 2.826	(ζ=0.698, ω=1.654)	(ζ=0.645, ω=2.819)
6.	-13.000	(ζ=0.839, ω=5.194)	-11.310	- 9.850
7.	-13.000	-13.040	-13.000	-13.000

Table 33. Eigenvalues of Optimal Output Feedback Design, Mach .60, Altitude 5000 ft

No.	Open Loop	Effective Controls		
		δhtc, δvcc, δplac	δvcc, δplac	δhtc, δplac
1.	0.930	- 0.849	- 0.657 + j 0.413	- 0.675 + j 0.405
2.	- 0.009 + j 0.071	- 1.131 + j 0.414	(ζ=0.847, ω=0.776)	(ζ=0.858, ω=0.787)
3.	(ζ=0.126, ω=0.071)	(ζ=0.939, ω=1.204)	- 1.146 + j 2.313	- 1.174 + j 2.587
4.	- 1.000	- 4.386 + j 4.550	(ζ=0.444, ω=2.581)	(ζ=0.413, ω=2.841)
5.	- 2.910	(ζ=0.694, ω=6.320)	- 2.680	- 2.375
6.	-13.000	- 4.640	-10.080	-10.070
7.	-13.000	-12.990	-13.000	-13.000

Table 34. Eigenvalues of Optimal Output Feedback Design, Mach .90, Altitude 20,000 ft

No.	Open Loop	Effective Controls		
		δhtc, δvcc, δplac	δvcc, δplac	δhtc, δplac
1.	0.170	- 1.009 + j 0.929	- 0.815 + j 0.686	- 0.744 + j 0.815
2.	- 0.175	(ζ=0.736, ω=1.372)	(ζ=0.765, ω=1.065)	(ζ=0.674, ω=1.103)
3.	- 1.000	- 0.833	- 0.910	- 0.961
4.	- 1.074 + j 1.076	- 1.467	- 1.260 + j 0.957	- 1.270 + j 1.285
5.	(ζ=0.707, ω=1.520)	- 4.272	(ζ=0.797, ω=1.582)	(ζ=0.703, ω=1.807)
6.	-13.000	- 7.258	-10.880	-11.060
7.	-13.000	-13.000	-13.000	-13.000

Table 35. Covariance Responses of Optimal Output Feedback Design, Mach .25, Altitude 5000 ft, σ_u, σ_w = 10 ft/s

Variables (Units)	Open Loop*	Effective Controls		
		δhtc, δvcc, δplac	δvcc, δplac	δhtc, δplac
Horizontal Tail Position (deg)	-	0.788	0	1.348
Vertical Canard Position (deg)	-	2.451	7.483	0
Horizontal Tail Rate (deg/s)	-	1.203	0	1.734
Vertical Canard Rate (deg/s)	-	4.611	7.422	0
Thrust (lb)	-	111.100	126.300	111.700
Normal Acceleration (g)	-	0.105	0.105	0.102
Speed (ft/s)	-	0.869	0.381	0.633
Angle of Attack (deg)	-	1.778	2.870	1.808
Pitch Rate (deg/s)	-	0.201	0.513	0.320
Pitch Attitude (deg)	-	0.443	0.729	0.502

* Unstable

Table 36. Covariance Responses of Optimal Output Feedback Design, Mach .60, Altitude 5000 ft, σ_u, σ_w = 10 ft/s

Variables (Units)	Open Loop*	Effective Controls		
		δhtc, δvcc, δplac	δvcc, δplac	δhtc, δplac
Horizontal Tail Position (deg)	-	0.062	0	0.138
Vertical Canard Position (deg)	-	0.452	0.952	0
Horizontal Tail Rate (deg/s)	-	0.284	0	0.363
Vertical Canard Rate (deg/s)	-	2.033	2.508	0
Thrust (lb)	-	50.000	59.740	54.270
Normal Acceleration (g)	-	0.230	0.240	0.237
Speed (ft/s)	-	0.244	0.256	0.261
Angle of Attack (deg)	-	0.727	0.736	0.740
Pitch Rate (deg/s)	-	0.100	0.252	0.257
Pitch Attitude (deg)	-	0.130	0.192	0.196

* Unstable

Table 37. Covariance Responses of Optimal Output Feedback Design, Mach .90, Altitude 20,000 ft, σ_u, σ_w = 10 ft/s

Variables (Units)	Open Loop*	Effective Controls: δhtc, δvcc, δplac	Effective Controls: δvcc, δplac	Effective Controls: δhtc, δplac
Horizontal Tail Position (deg)	-	0.027	0	0.049
Vertical Canard Position (deg)	-	0.215	0.361	0
Horizontal Tail Rate (deg/s)	-	0.125	0	0.128
Vertical Canard Rate (deg/s)	-	1.016	1.024	0
Thrust (lb)	-	3.366	5.392	4.902
Normal Acceleration (g)	-	0.298	0.289	0.291
Speed (ft/s)	-	0.053	0.155	0.130
Angle of Attack (deg)	-	0.495	0.496	0.495
Pitch Rate (deg/s)	-	0.243	0.273	0.285
Pitch Attitude (deg)	-	0.236	0.300	0.291

* Unstable

Table 38. Stability Margins of Optimal Output Feedback Design, Mach .25, Altitude 5000 ft

	Effective Controls: δhtc, δvcc, δplac			Effective Controls: δvcc, δplac		Effective Controls: δhtc, δplac	
	δhtc loop	δvcc loop	δplac loop	δvcc loop	δplac loop	δhtc loop	δplac loop
Gain Margin (dB)	∞	∞	43, 59	-21, -9	∞	-27, -13	38, 51
Phase Margin (deg)	76	180	180	44	180	45	180
Loop Gain (dB)*	-11	-14	-64	-16	-63	-12	-63

Table 39. Stability Margins of Optimal Output Feedback Design, Mach .60, Altitude 5000 ft

	Effective Controls: δhtc, δvcc, δplac			Effective Controls: δvcc, δplac		Effective Controls: δhtc, δplac	
	δhtc loop	δvcc loop	δplac loop	δvcc loop	δplac loop	δhtc loop	δplac loop
Gain Margin (dB)	∞	∞	29, 54	-16	28, 44	-17	26, 46
Phase Margin (deg)	80	-176, 83	136	37	135	33	146
Loop Gain (dB)*	-10	-10	-38	-12	-39	-12	-39

Table 40. Stability Margins of Optimal Output Feedback Design, Mach .90, Altitude 20,000 ft

	Effective Controls: δhtc, δvcc, δplac			Effective Controls: δvcc, δplac		Effective Controls: δhtc, δplac	
	δhtc loop	δvcc loop	δplac loop	δvcc loop	δplac loop	δhtc loop	δplac loop
Gain Margin (dB)	42	36	39	36	45, 40	42	35
Phase Margin (deg)	111	177, 135	180	64	180	58	180
Loop Gain (dB)*	-16	-17	-69	-17	-70	-17	-69

* evaluated at 10 rad/s

Table 41. Design Parameters in the Cost Function for Optimal Gain Schedule at the Landing Gear Up Conditions

Plant condition	i	W_{pi}	Q: u_b	Q: α	Q: A_{nc}	R: δ_{htc}	R: δ_{vcc}	R: δ_{plac}
Mach .6 no failure	1	16.0	9.6	12.0	14.4	1.20	0.04	0.96
Mach .6 δ_{htc} failed	2	1.0	19.2	28.8	38.4	0.00	0.01	0.18
Mach .6 δ_{vcc} failed	3	1.0	2.4	3.6	4.8	0.24	0.00	0.36
Mach .9 no failure	4	16.0	9.6	12.0	14.4	1.20	0.04	0.96
Mach .9 δ_{htc} failed	5	1.0	19.2	28.8	38.4	0.00	0.01	0.18
Mach .9 δ_{vcc} failed	6	1.0	2.4	3.6	4.8	0.24	0.00	0.36

Table 42. Control Gains of Optimal Gain Schedule Output Feedback Design, Mach .25, Altitude 5000 ft, (Same as Table 29.)

Controls	U	Q	θ	α	Anc	Schedule Factor
δhtc	-0.6526	1.6400	2.841	0.5875	2.0510	1.0
δvcc	-1.9740	5.3400	7.491	1.5020	9.8150	1.0
δplac	-0.4207	-0.1626	-1.072	-0.5150	0.3276	1.0

Table 43. Control Gains of Optimal Gain Schedule Output Feedback Design, Mach .60, Altitude 5000 ft

Controls	U	Q	θ	α	Anc	Schedule Factor
δhtc	-0.6526	1.6400	2.841	0.5875	2.0510	0.08531
δvcc	-1.9740	5.3400	7.491	1.5020	9.8150	0.20640
δplac	-0.4207	-0.1626	-1.072	-0.5150	0.3276	1.80400

Table 44. Control Gains of Optimal Gain Schedule Output Feedback Design, Mach .90, Altitude 20,000 ft, (Same as Table 43.)

Controls	U	Q	θ	α	Anc	Schedule Factor
δhtc	-0.6526	1.6400	2.841	0.5875	2.0510	0.08531
δvcc	-1.9740	5.3400	7.491	1.5020	9.8150	0.20640
δplac	-0.4207	-0.1626	-1.072	-0.5150	0.3276	1.80400

Table 45. Eigenvalues of Optimal Gain Schedule Output Feedback Design, Mach .60, Altitude 5000 ft

No.	Open Loop	Effective Controls		
		δhtc, δvcc, δplac	δvcc, δplac	δhtc, δplac
1.	0.930	- 0.944	- 0.665 + j 0.422	- 0.647 + j 0.216
2.	- 0.009 + j 0.071	- 0.462 + j 0.387	(ζ=0.845, ω=0.788)	(ζ=0.948, ω=0.682)
3.	(ζ=0.126, ω=0.714)	(ζ=0.767, ω=0.603)	- 1.053 + j 0.809	- 0.686 + j 1.195
4.	- 1.000	- 3.151 + j 2.364	(ζ=0.793, ω=1.328)	(ζ=0.498, ω=1.378)
5.	- 2.910	(ζ=0.800, ω=3.939)	- 1.776	- 2.288
6.	-13.000	- 8.361	-11.250	-11.160
7.	-13.000	-13.050	-13.000	-13.000

Table 46. Eigenvalues of Optimal Gain Schedule Output Feedback Design, Mach .90, Altitude 20,000 ft

No.	Open Loop	Effective Controls		
		δhtc, δvcc, δplac	δvcc, δplac	δhtc, δplac
1.	0.170	- 0.341 + j 0.786	- 0.296 + j 0.273	- 0.354 + j 0.251
2.	- 0.175	(ζ=0.786, ω=0.434)	(ζ=0.736, ω=0.403)	(ζ=0.816, ω=0.434)
3.	- 1.000	- 0.911	- 0.902	- 0.913
4.	- 1.074 + j 1.076	- 3.808 + j 5.448	- 2.163 + j 3.517	- 2.125 + j 3.467
5.	(ζ=0.707, ω=1.520)	(ζ=0.573, ω=6.647)	(ζ=0.524, ω=4.129)	(ζ=0.523, ω=4.066)
6.	-13.000	- 7.676	-10.920	-10.480
7.	-13.000	-13.060	-13.000	-13.000

Table 47. Covariance Responses of Optimal Gain Schedule Output Feedback Design, Mach .60, Altitude 5000 ft, σ_u, σ_w = 10 ft/s

Variables (Units)	Open Loop*	Effective Controls		
		δhtc, δvcc, δplac	δvcc, δplac	δhtc, δplac
Horizontal Tail Position (deg)	-	0.047	0	0.147
Vertical Canard Position (deg)	-	0.513	0.885	0
Horizontal Tail Rate (deg/s)	-	0.206	0	0.270
Vertical Canard Rate (deg/s)	-	2.246	2.373	0
Thrust (lb)	-	62.450	76.260	94.410
Normal Acceleration (g)	-	0.233	0.252	0.266
Speed (ft/s)	-	0.357	0.252	0.281
Angle of Attack (deg)	-	0.698	0.714	0.744
Pitch Rate (deg/s)	-	0.122	0.293	0.462
Pitch Attitude (deg)	-	0.188	0.278	0.379

* Unstable

Table 48. Covariance Responses of Optimal Gain Schedule Output Feedback Design, Mach .90, Altitude 20,000 ft, σ_u, σ_w = 10 ft/s

Variables (Units)	Open Loop*	Effective Controls		
		δhtc, δvcc, δplac	δvcc, δplac	δhtc, δplac
Horizontal Tail Position (deg)	-	0.046	0	0.060
Vertical Canard Position (deg)	-	0.303	0.520	0
Horizontal Tail Rate (deg/s)	-	0.287	0	0.274
Vertical Canard Rate (deg/s)	-	2.712	2.923	0
Thrust (lb)	-	42.330	49.900	42.600
Normal Acceleration (g)	-	0.230	0.230	0.293
Speed (ft/s)	-	0.318	0.371	0.293
Angle of Attack (deg)	-	0.472	0.489	0.477
Pitch Rate (deg/s)	-	0.337	0.380	0.308
Pitch Attitude (deg)	-	0.202	0.261	0.222

* Unstable

Table 49. Stability Margins of Optimal Gain Schedule Output Feedback Design, Mach .60, Altitude 5000 ft

	Effective Controls						
	δhtc, δvcc, δplac			δvcc, δplac		δhtc, δplac	
	δhtc loop	δvcc loop	δplac loop	δvcc loop	δplac loop	δhtc loop	δplac loop
Gain Margin (dB)	∞	∞	33, 50	-7	27, 36	-6	23, 37
Phase Margin (deg)	95	-160, 88	113	42	116	35	115
Loop Gain (dB)*	-15	-14	-57	-15	-57	-16	-57

Table 50. Stability Margins of Optimal Gain Schedule Output Feedback Design, Mach .90, Altitude 20,000 ft

	Effective Controls						
	δhtc, δvcc, δplac			δvcc, δplac		δhtc, δplac	
	δhtc loop	δvcc loop	δplac loop	δvcc loop	δplac loop	δhtc loop	δplac loop
Gain Margin (dB)	∞	∞	45, 59	∞	∞	∞	42, 49
Phase Margin (deg)	164, 104	-174, 99	133	53	131	51	129
Loop Gain (dB)*	-10	-10	-60	-12	-59	-12	-60

* evaluated at 10 rad/s

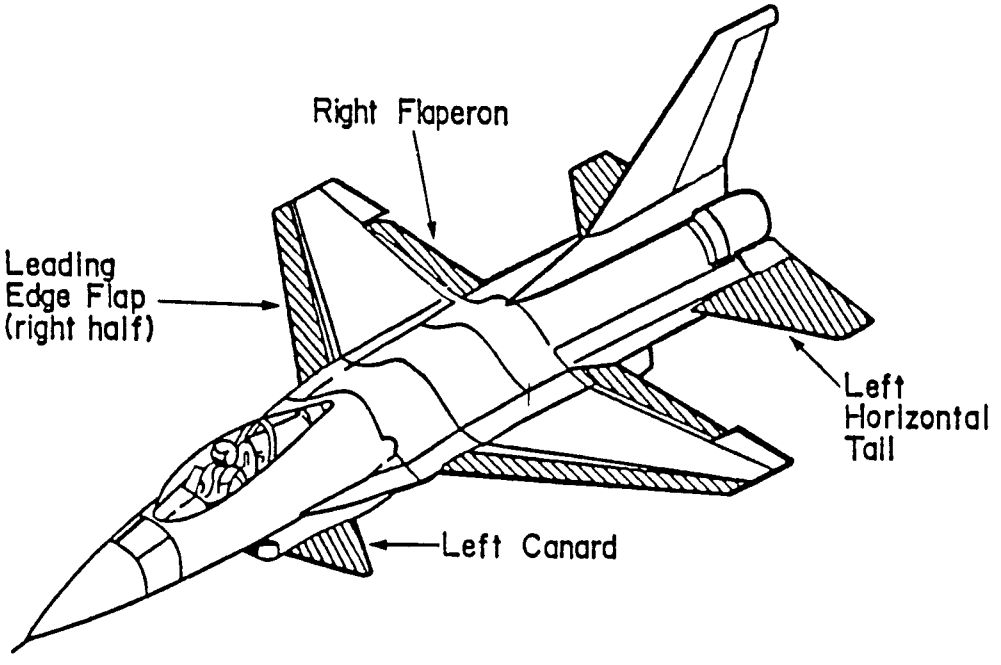

Figure 1. Location of Control Surfaces

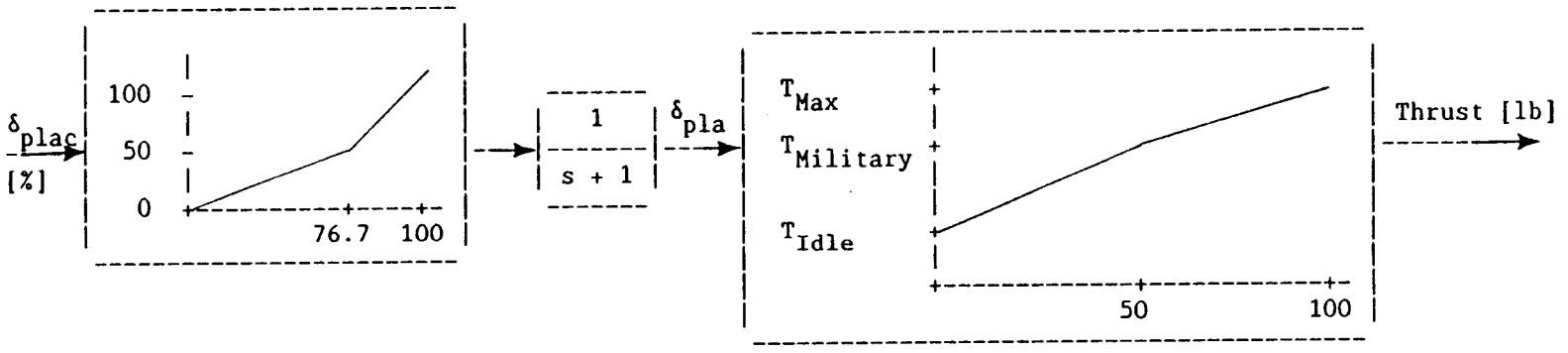

Figure 2. Thrust Dynamic Model

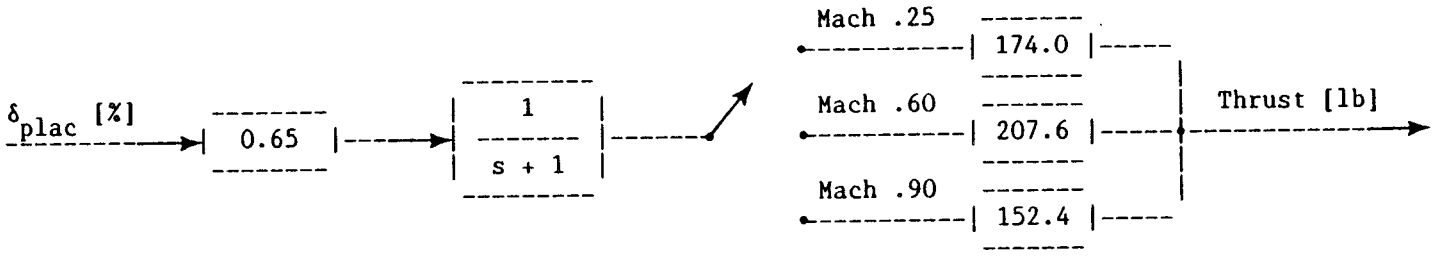

Figure 3. Simplified Thrust Model

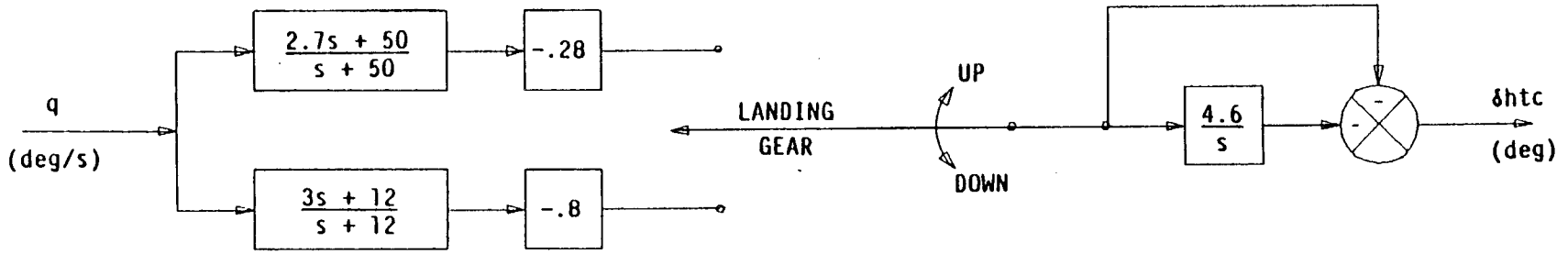

Figure 4. Block Diagram of Existing Backup System

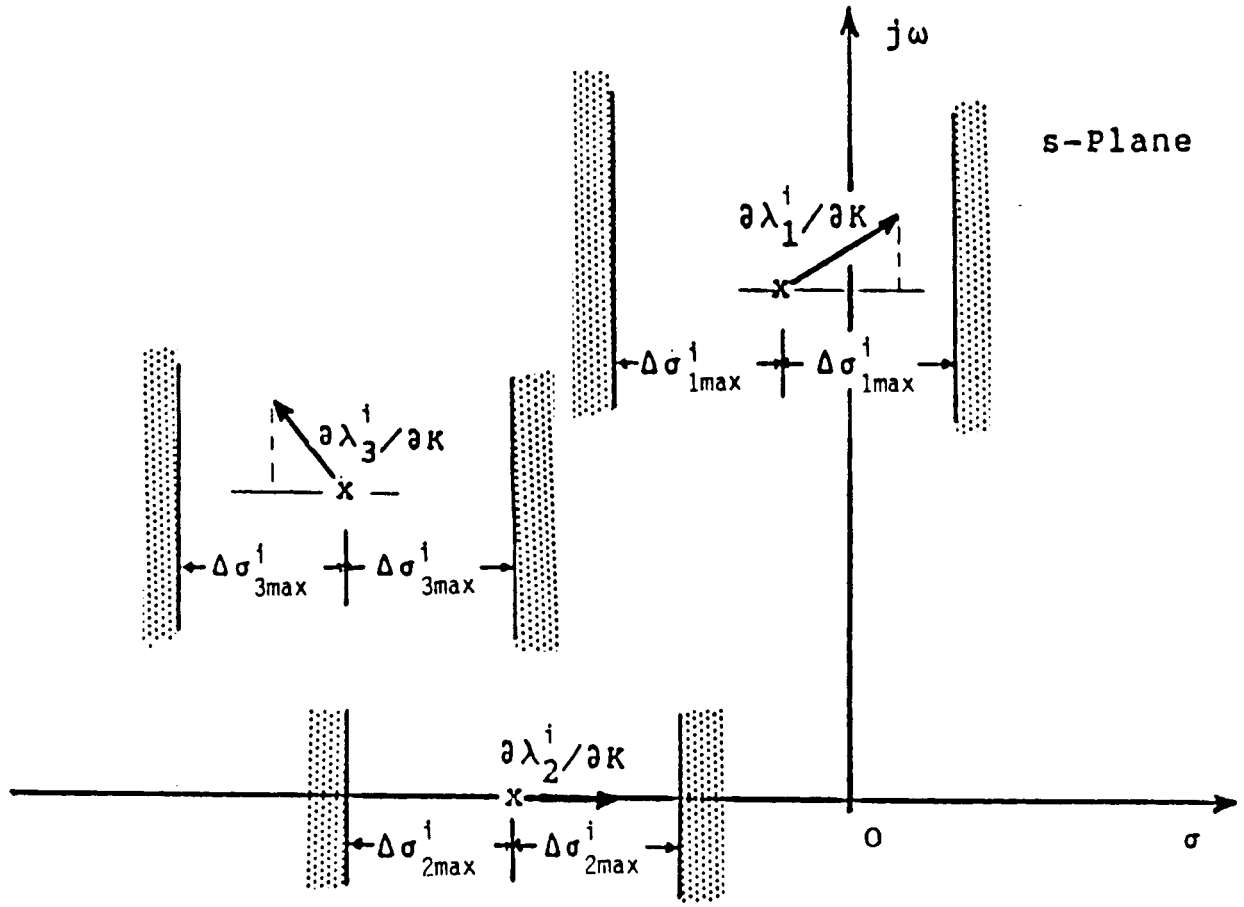

Figure 5. Bounds on the Incremental Change in the Parameter K During the Numerical Line Search

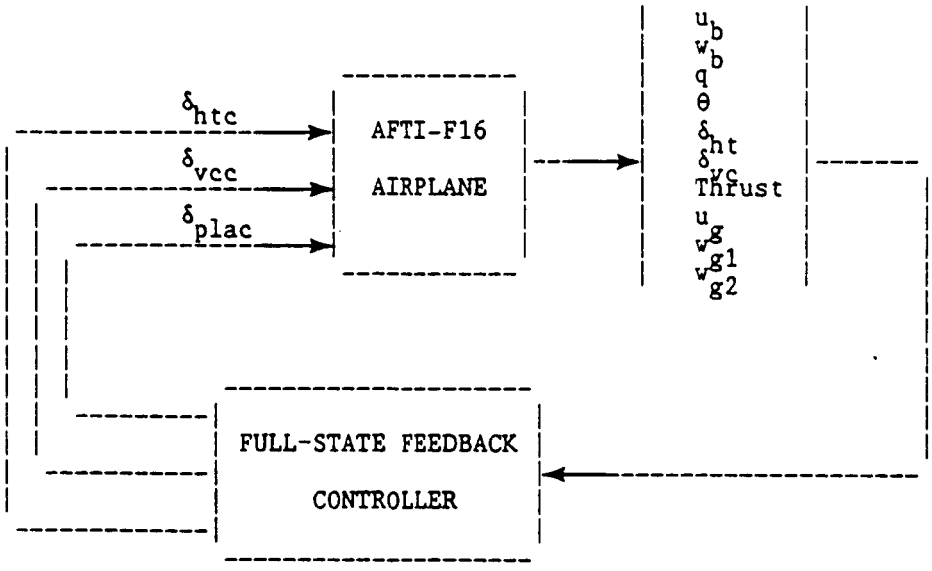

Figure 6. Full-State Feedback Controller Structure

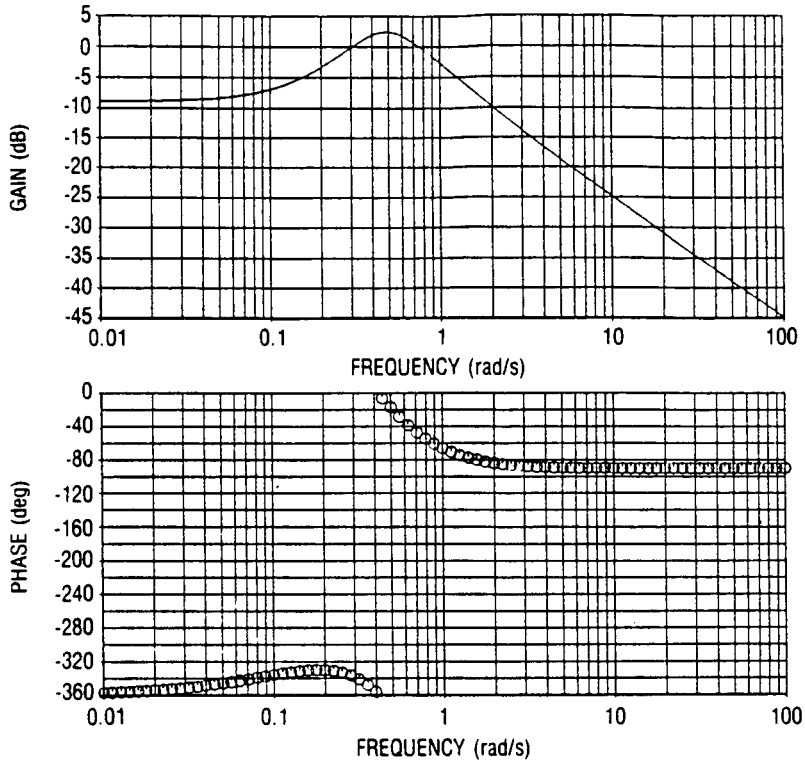

Figure 7. δ_{plac} Control Loop Frequency Response Full-State Feedback Design, Mach .25, Altitude 5000 ft

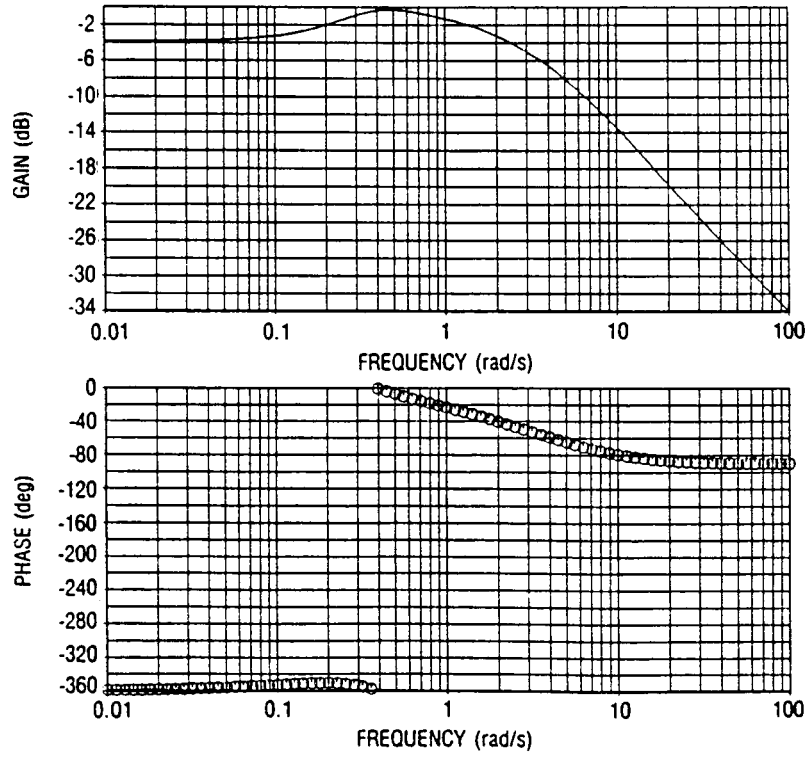

Figure 8. δ_{vcc} Control Loop Frequency Response Full-State Feedback Design, Mach .25, Altitude 5000 ft

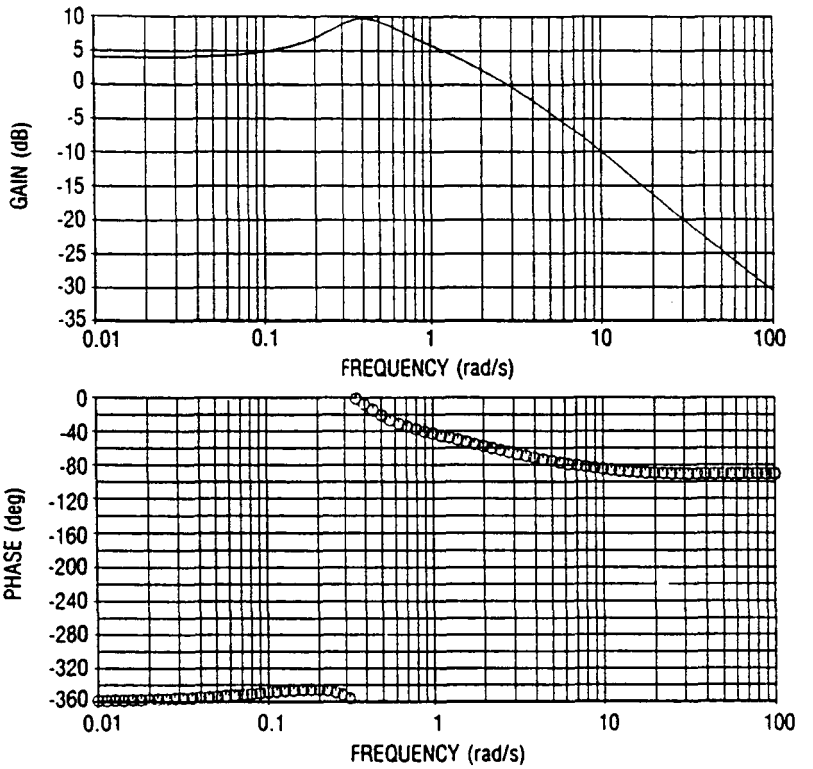

Figure 9. δ_{htc} Control Loop Frequency Response Full-State Feedback Design, Mach .25, Altitude 5000 ft

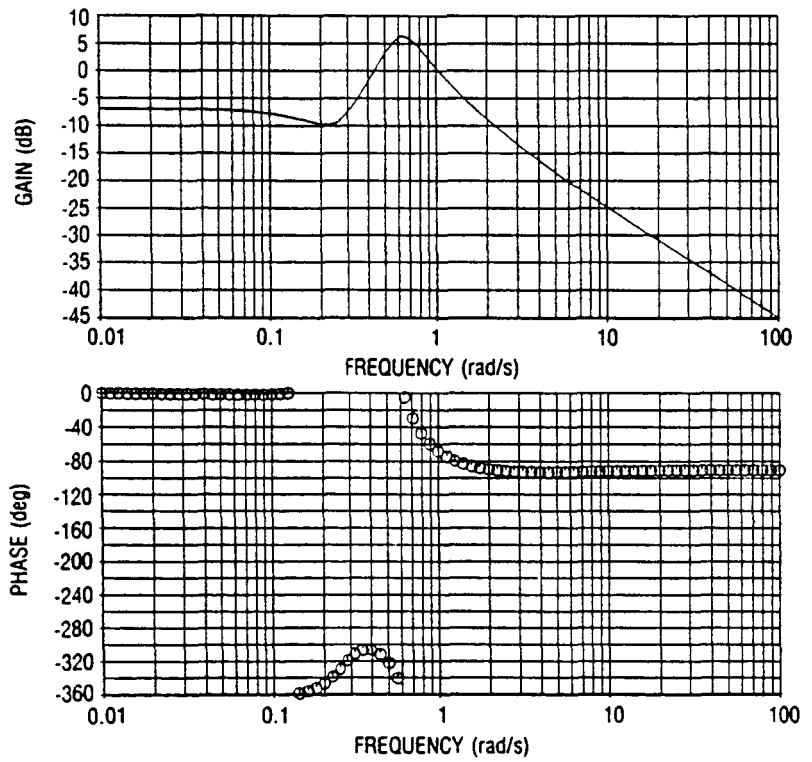

Figure 10. δ_{plac} Control Loop Frequency Response With δ_{ht} Failed Full-State Feedback Design, Mach .25, Altitude 5000 ft

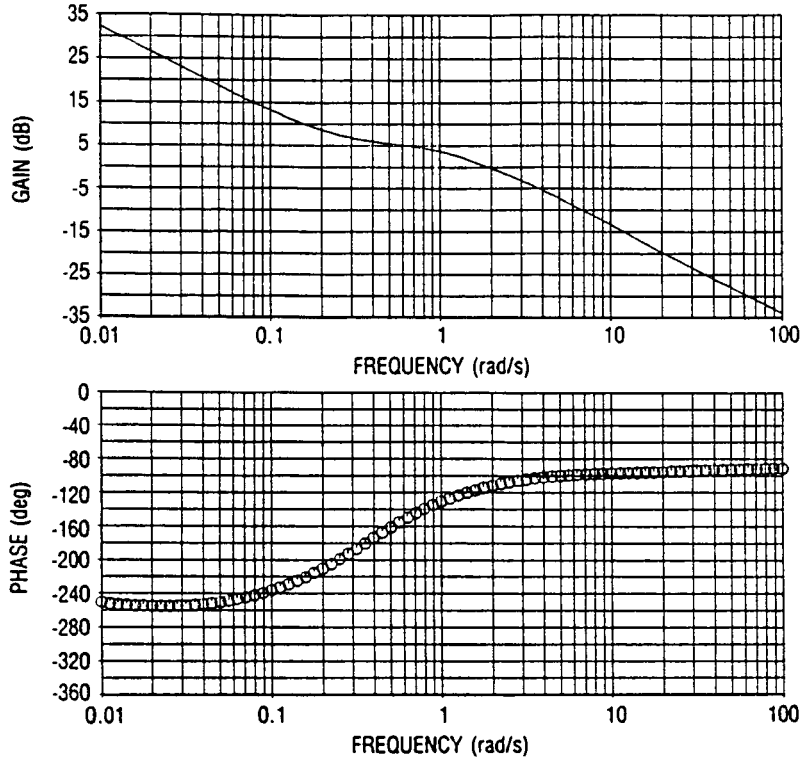

Figure 11. δ_{vcc} Control Loop Frequency Response With δ_{ht} Failed Full-State Feedback Design, Mach .25, Altitude 5000 ft

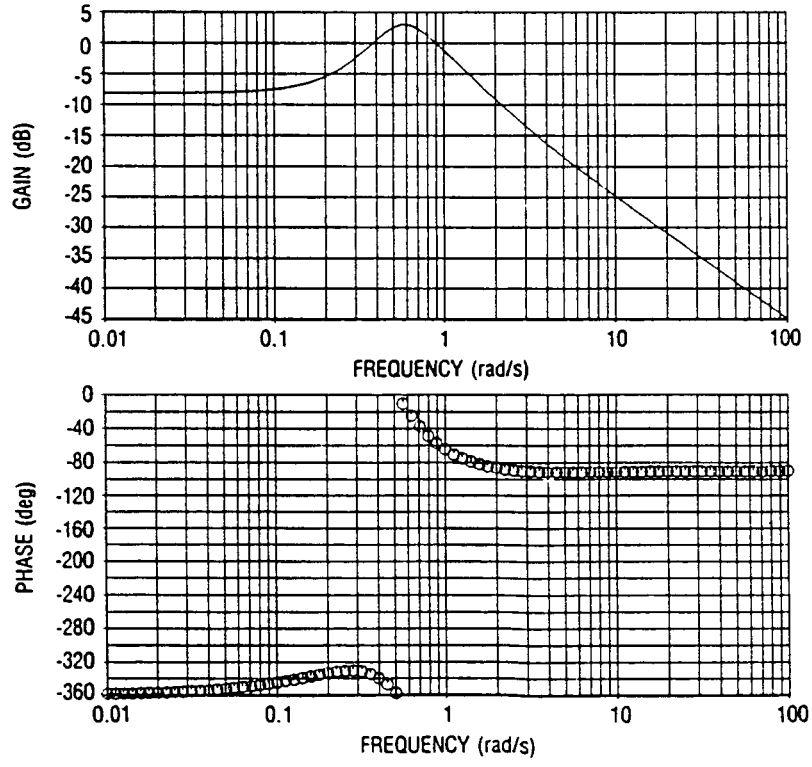

Figure 12. δ_{plac} Control Loop Frequency Response With δ_{vc} Failed Full-State Feedback Design, Mach .25, Altitude 5000 ft

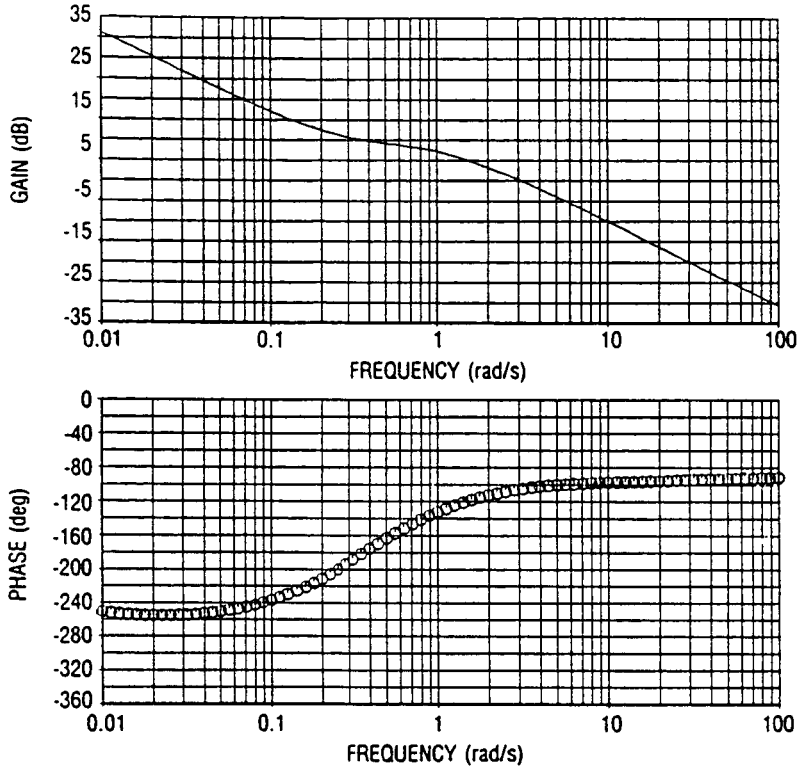

Figure 13. δ_{htc} Control Loop Frequency Response With δ_{vc} Failed Full-State Feedback Design, Mach .25, Altitude 5000 ft

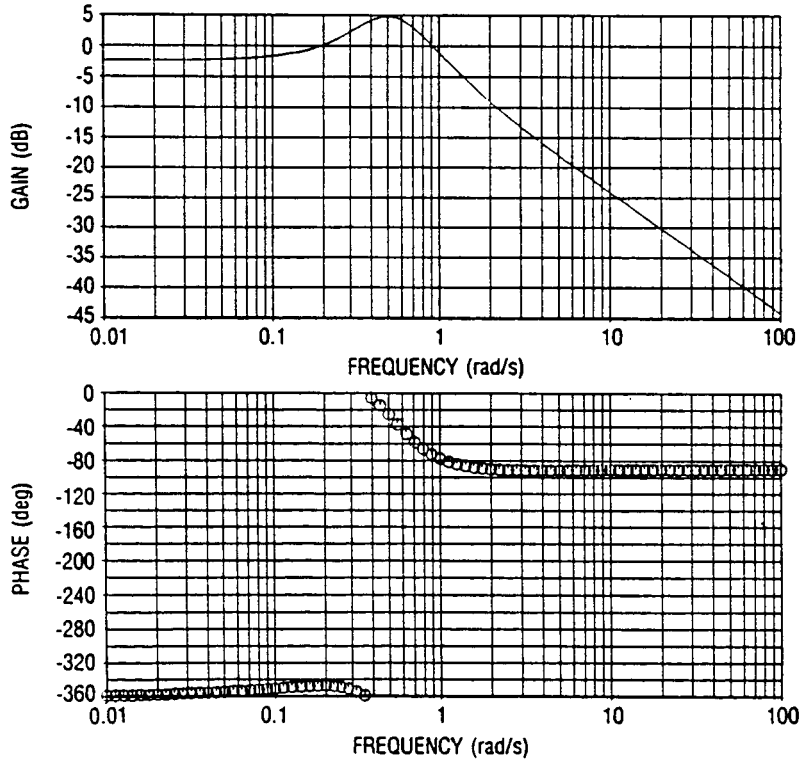

Figure 14. δ_{plac} Control Loop Frequency Response Full-State Feedback Design, Mach .60, Altitude 5000 ft

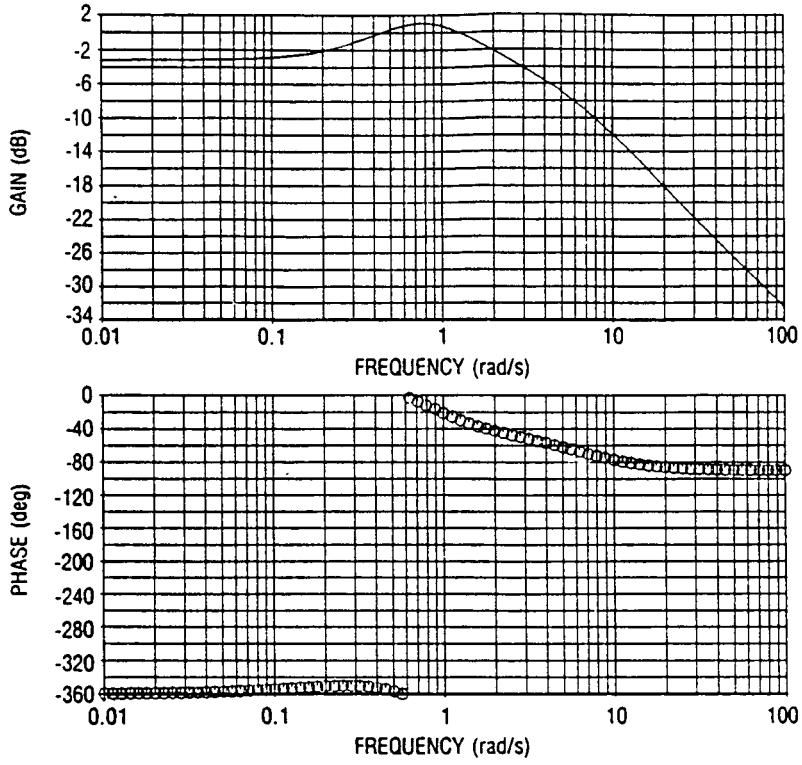

Figure 15. δ_{vcc} Control Loop Frequency Response Full-State Feedback Design, Mach .60, Altitude 5000 ft

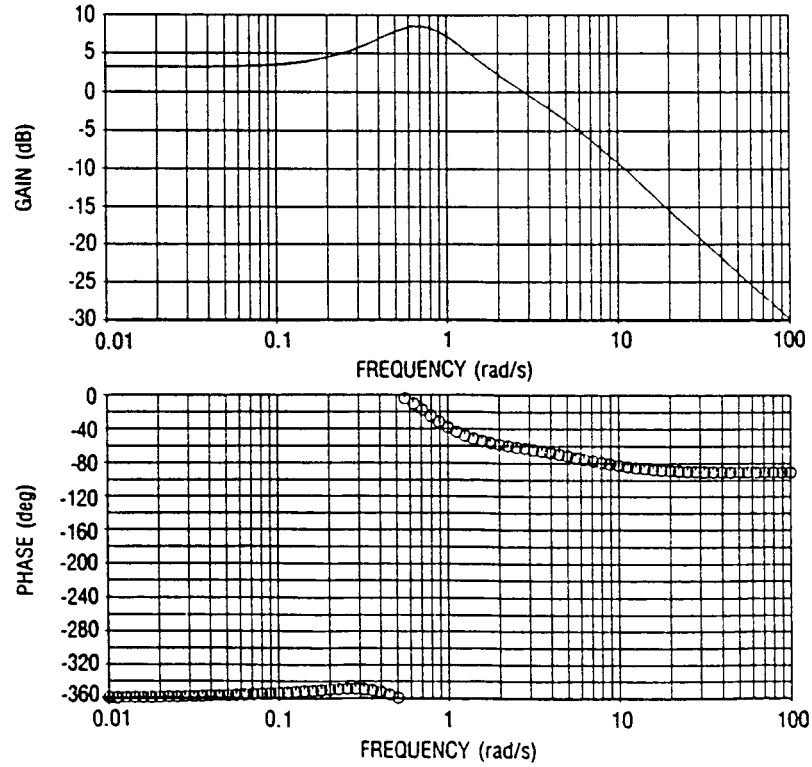

Figure 16. δ_{htc} Control Loop Frequency Response Full-State Feedback Design, Mach .60, Altitude 5000 ft

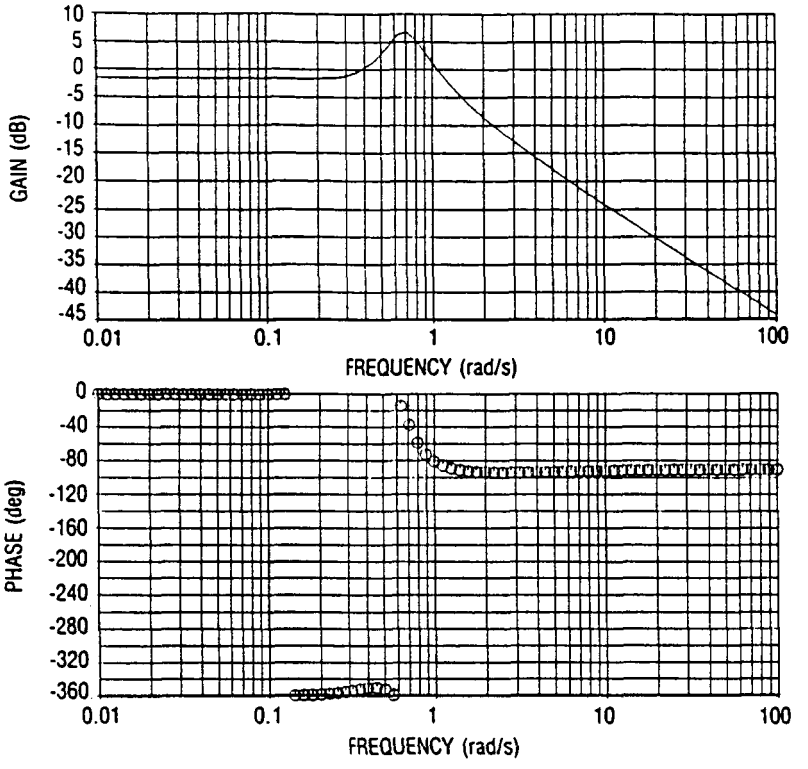

Figure 17. δ_{plac} Control Loop Frequency Response With δ_{ht} Failed Full-State Feedback Design, Mach .60, Altitude 5000 ft

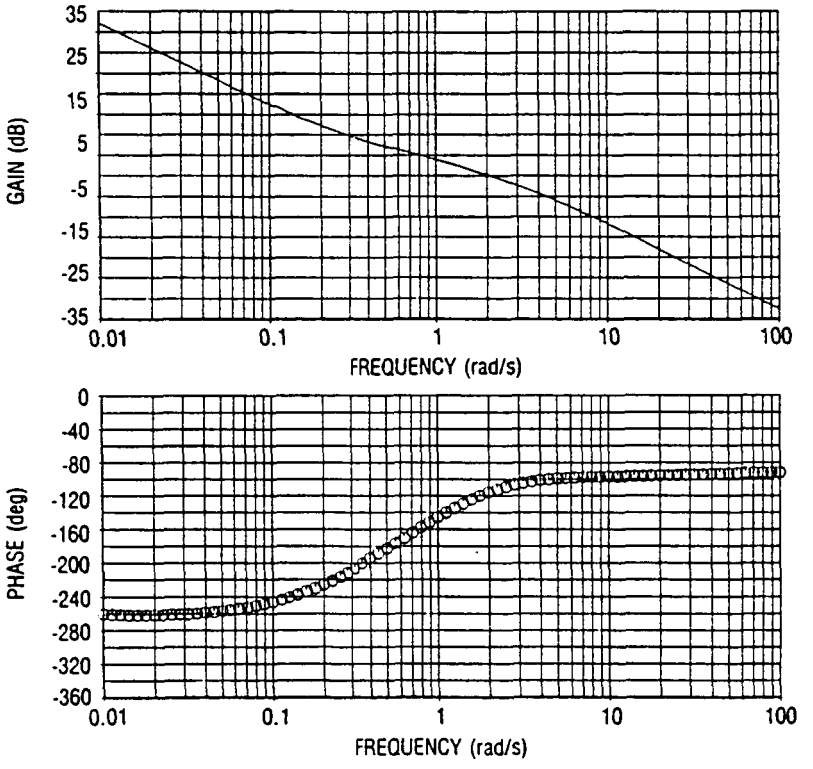

Figure 18. δ_{vcc} Control Loop Frequency Response With δ_{ht} Failed Full-State Feedback Design, Mach .60, Altitude 5000 ft

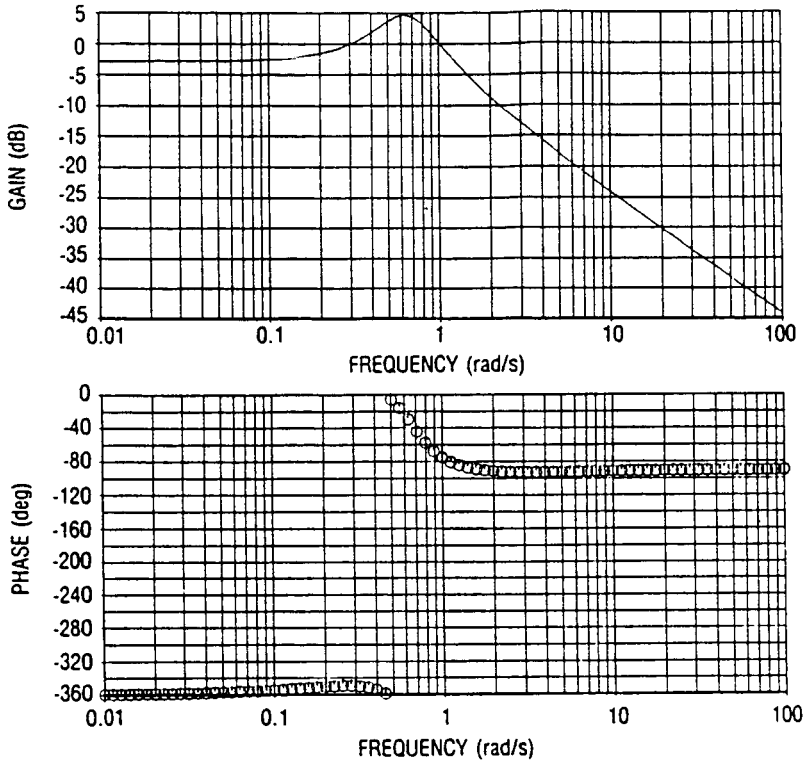

Figure 19. δ_{plac} Control Loop Frequency Response With δ_{vc} Failed Full-State Feedback Design, Mach .60, Altitude 5000 ft

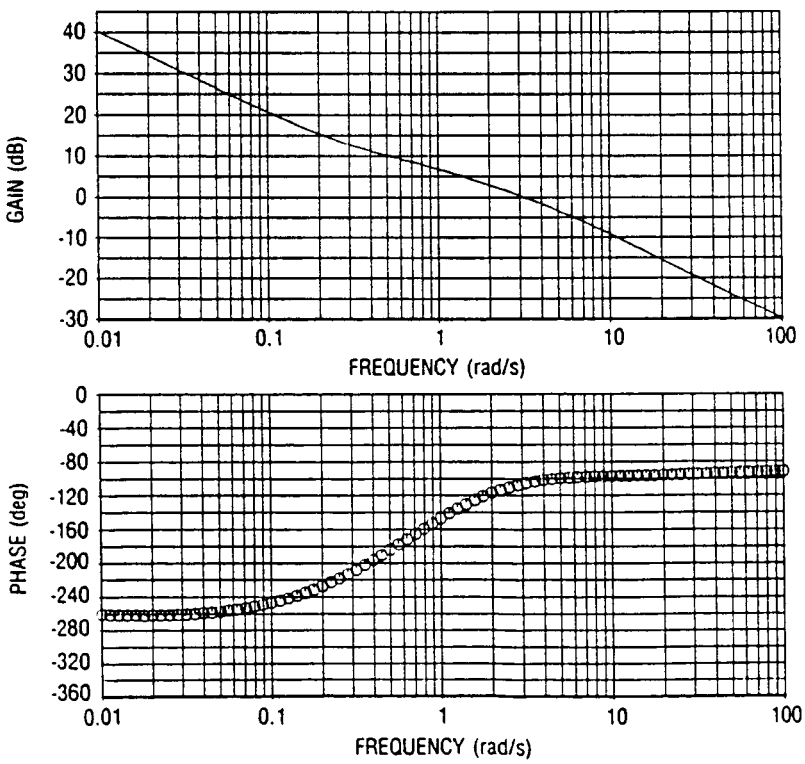

Figure 20. δ_{htc} Control Loop Frequency Response With δ_{vc} Failed Full-State Feedback Design, Mach .60, Altitude 5000 ft

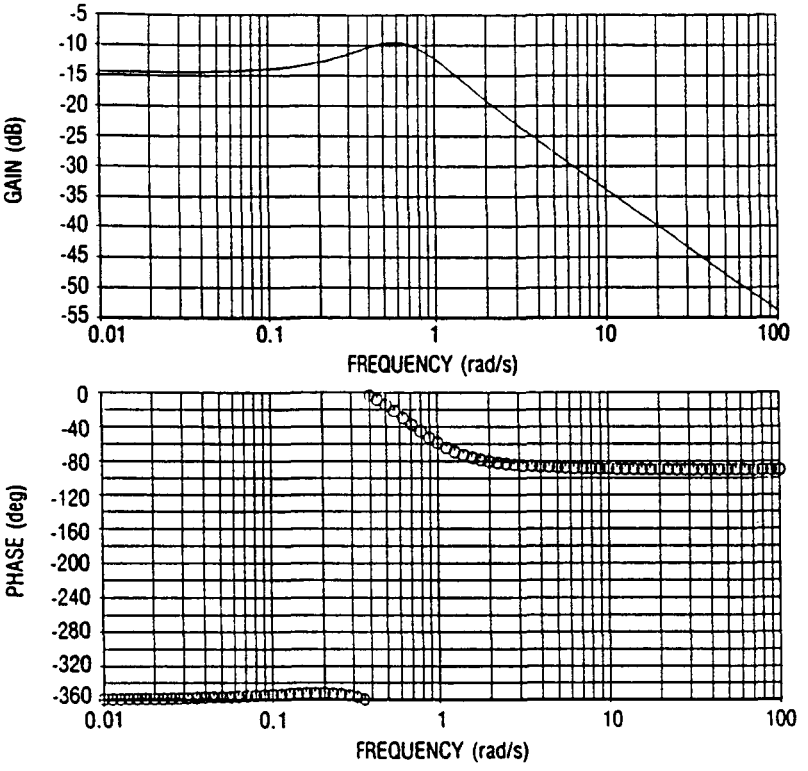

Figure 21. δ_{plac} Control Loop Frequency Response Full-State Feedback Design, Mach .90, Altitude 20,000 ft

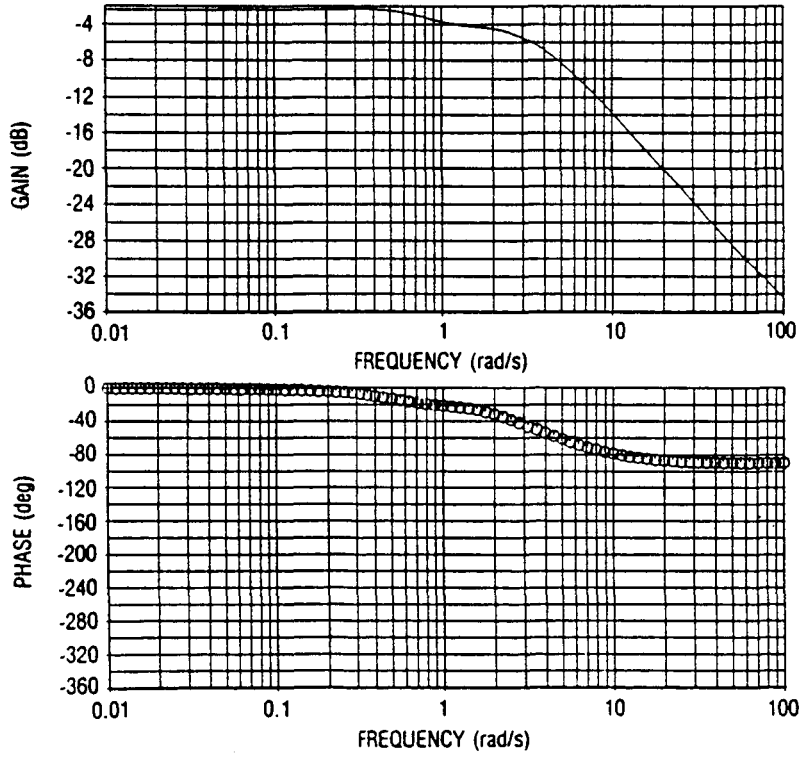

Figure 22. δ_{vcc} Control Loop Frequency Response Full-State Feedback Design, Mach .90, Altitude 20,000 ft

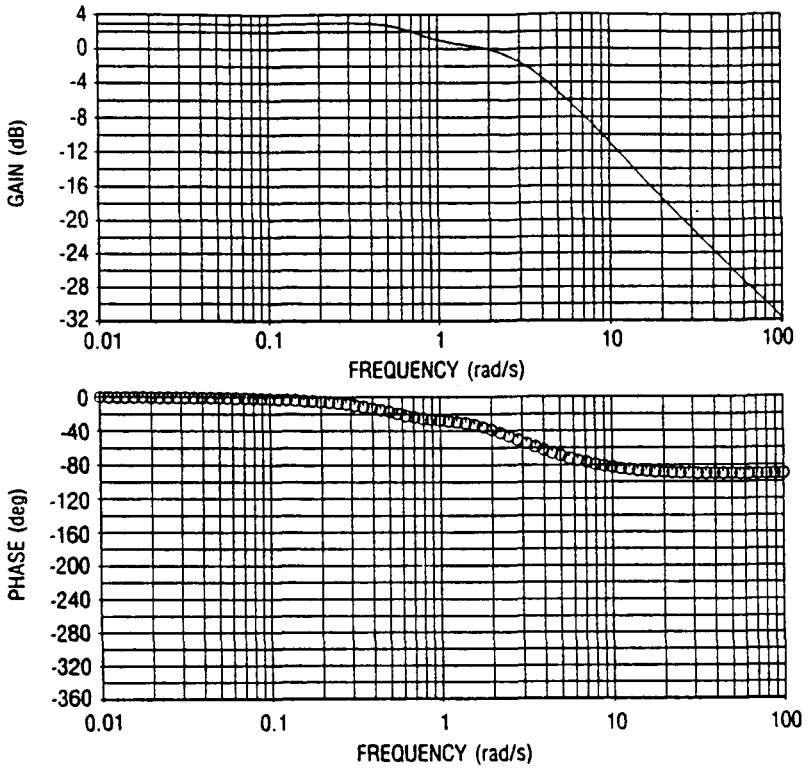

Figure 23. δ_{htc} Control Loop Frequency Response Full-State Feedback Design, Mach .90, Altitude 20,000 ft

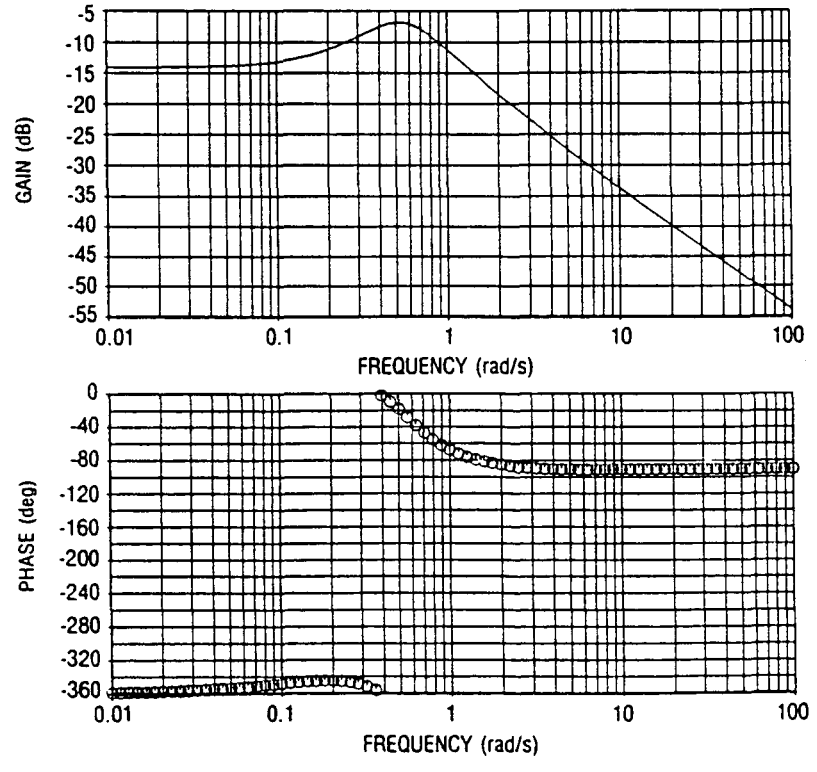

Figure 24. δ_{plac} Control Loop Frequency Response With δ_{ht} Failed Full-State Feedback Design, Mach .90, Altitude 20,000 ft

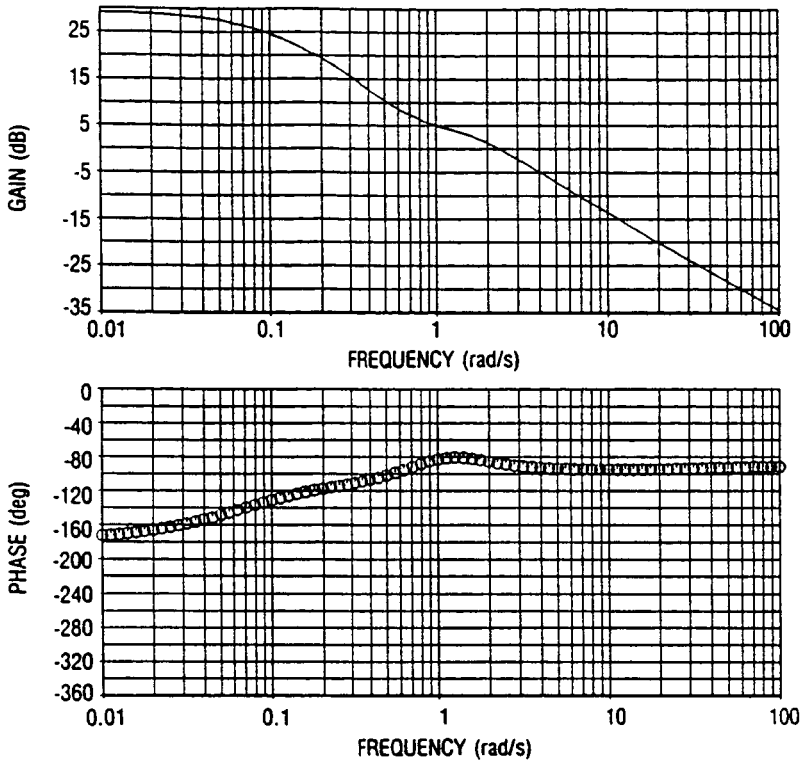

Figure 25. δ_{vcc} Control Loop Frequency Response With δ_{ht} Failed Full-State Feedback Design, Mach .90, Altitude 20,000 ft

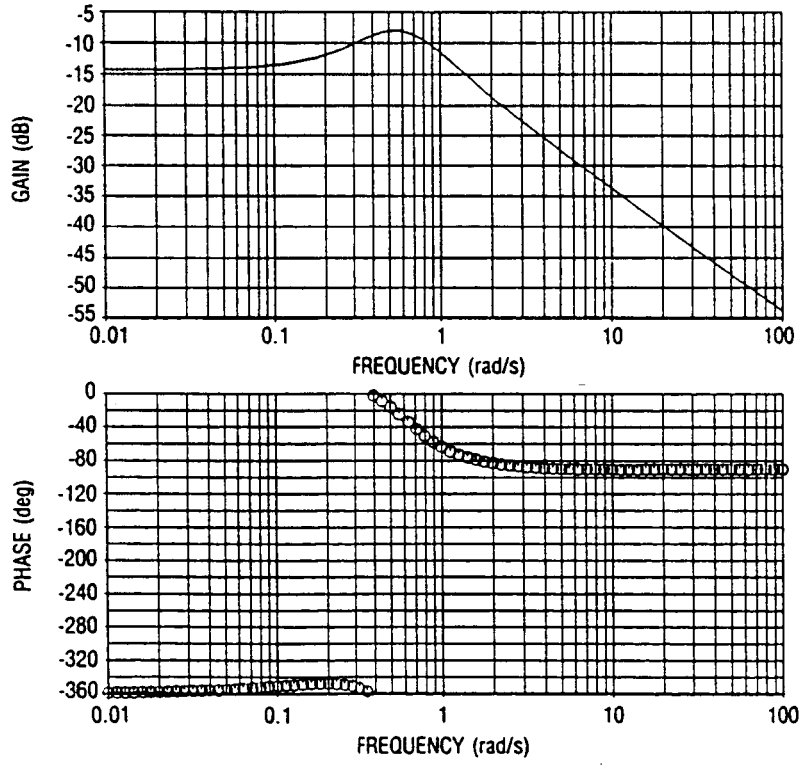

Figure 26. δ_{plac} Control Loop Frequency Response With δ_{vc} Failed Full-State Feedback Design, Mach .90, Altitude 20,000 ft

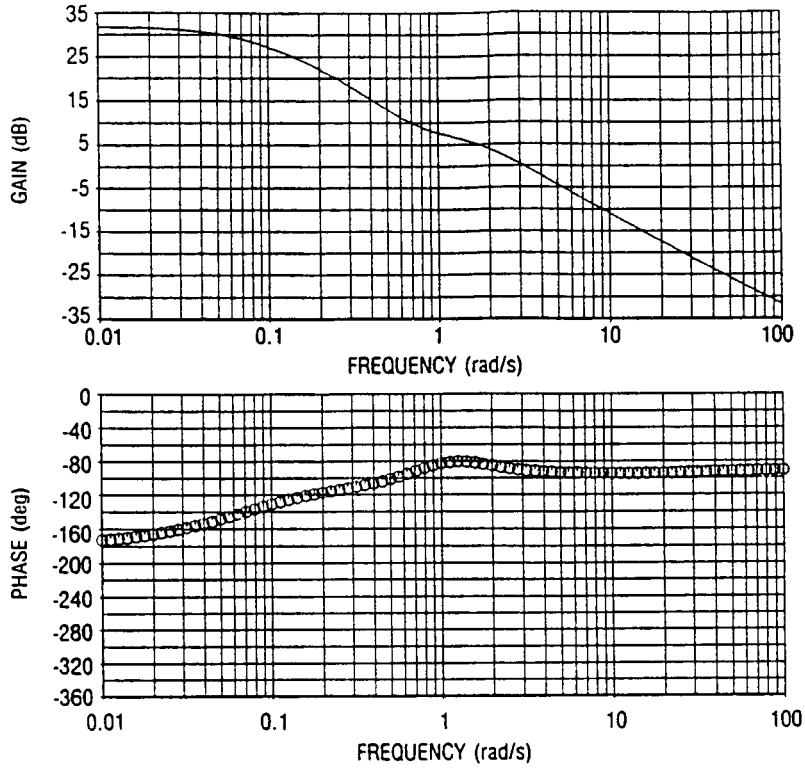

Figure 27. δ_{htc} Control Loop Frequency Response With δ_{vc} Failed Full-State Feedback Design, Mach .90, Altitude 20,000 ft

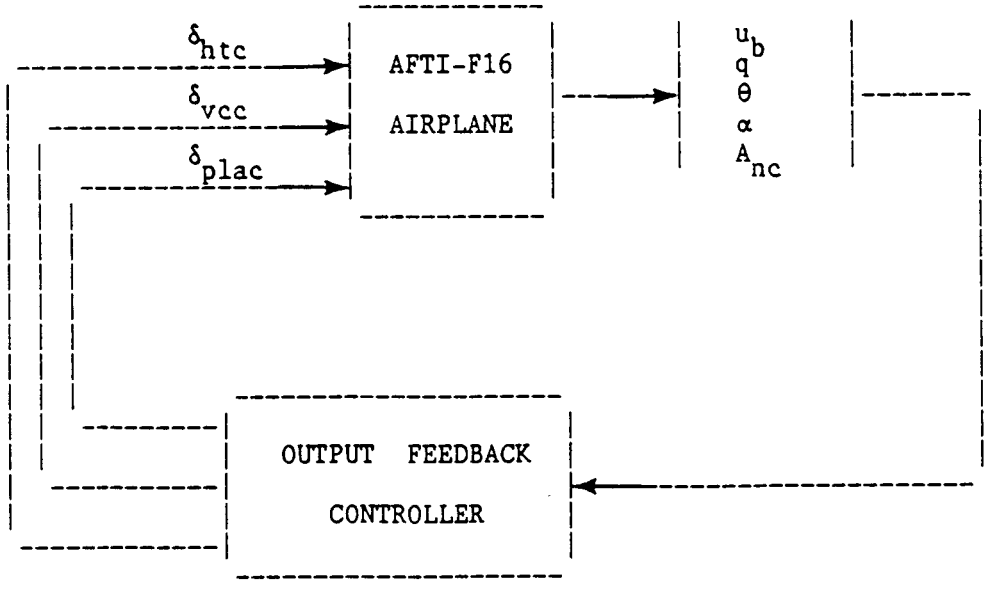

Figure 28. Output Feedback Controller Structure

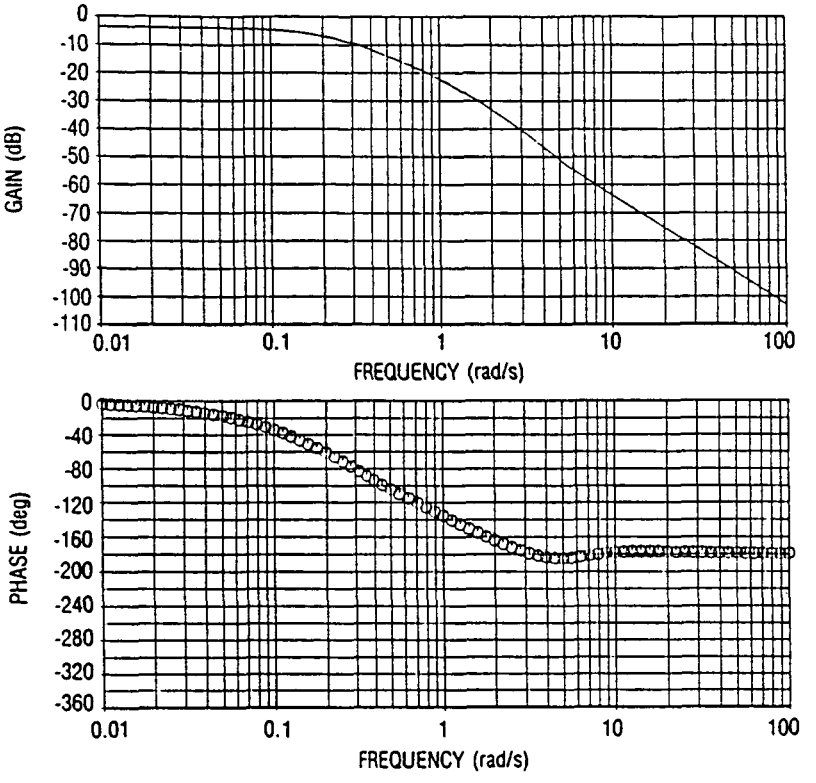

Figure 29. δ_{plac} Control Loop Frequency Response Optimal Output Feedback Design, Mach .25, Altitude 5000 ft

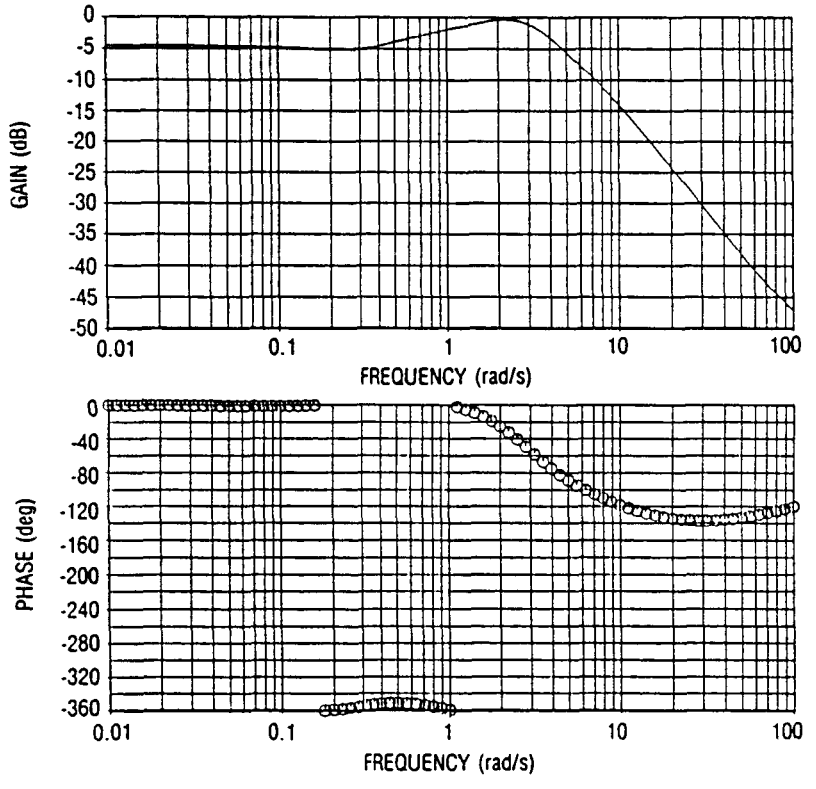

Figure 30. δ_{vcc} Control Loop Frequency Response Optimal Output Feedback Design, Mach .25, Altitude 5000 ft

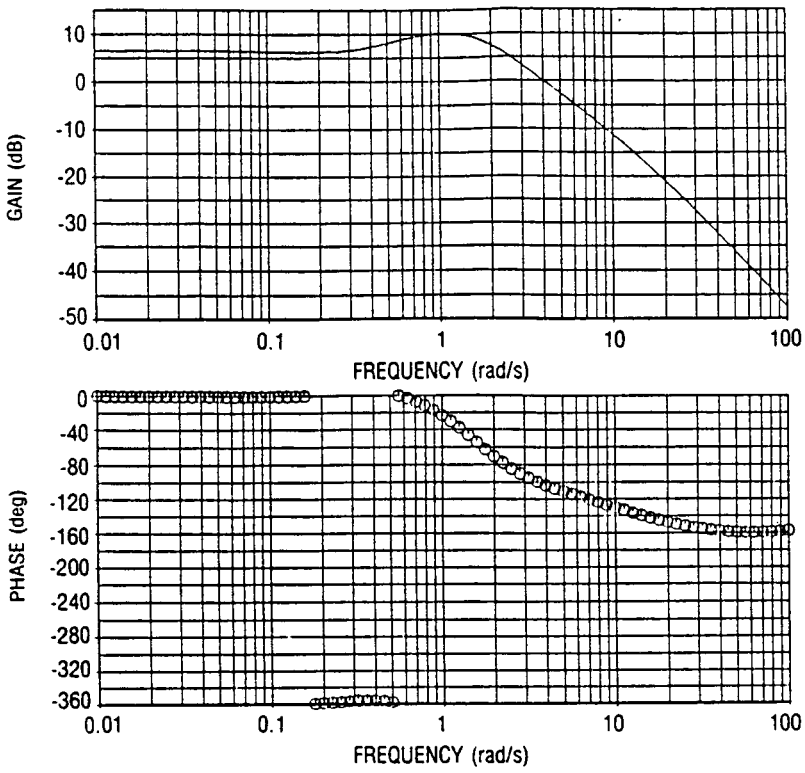

Figure 31. δ_{htc} Control Loop Frequency Response Optimal Output Feedback Design, Mach .25, Altitude 5000 ft

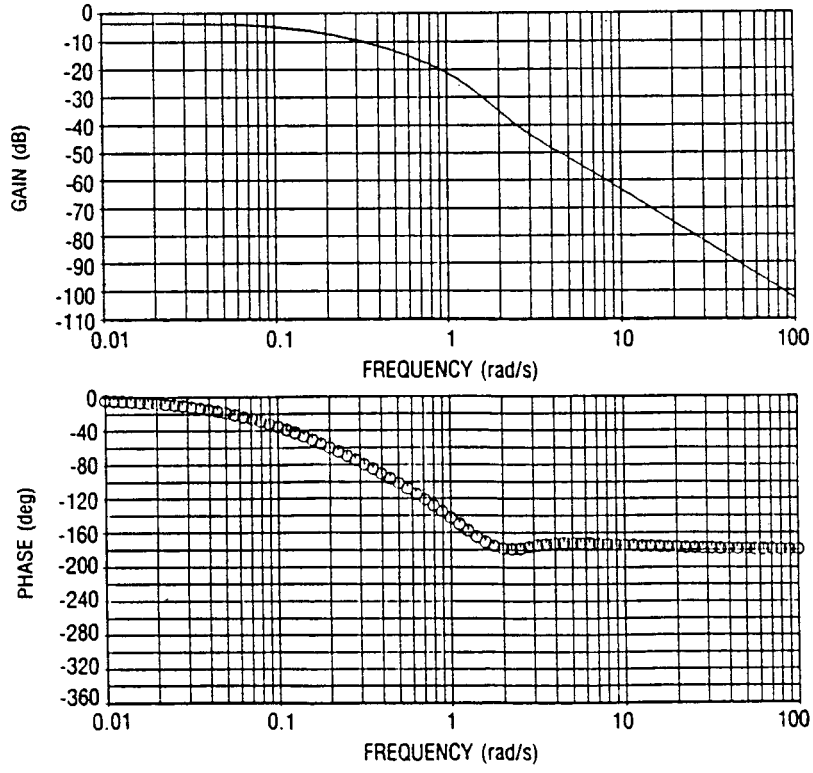

Figure 32. δ_{plac} Control Loop Frequency Response With δ_{ht} Failed Optimal Output Feedback Design, Mach .25, Altitude 5000 ft

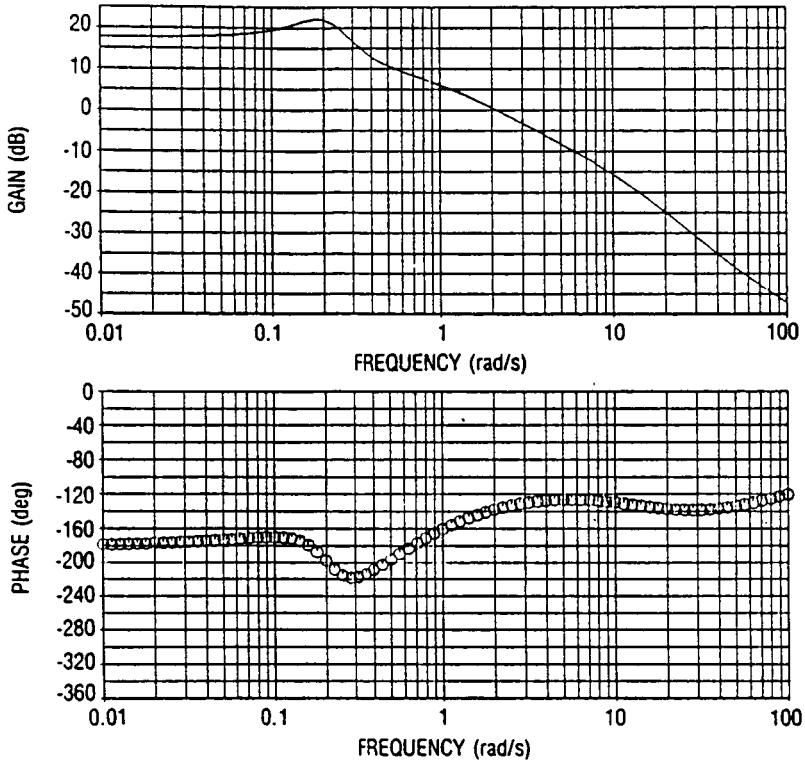

Figure 33. δ_{vcc} Control Loop Frequency Response With δ_{ht} Failed Optimal Output Feedback Design, Mach .25, Altitude 5000 ft

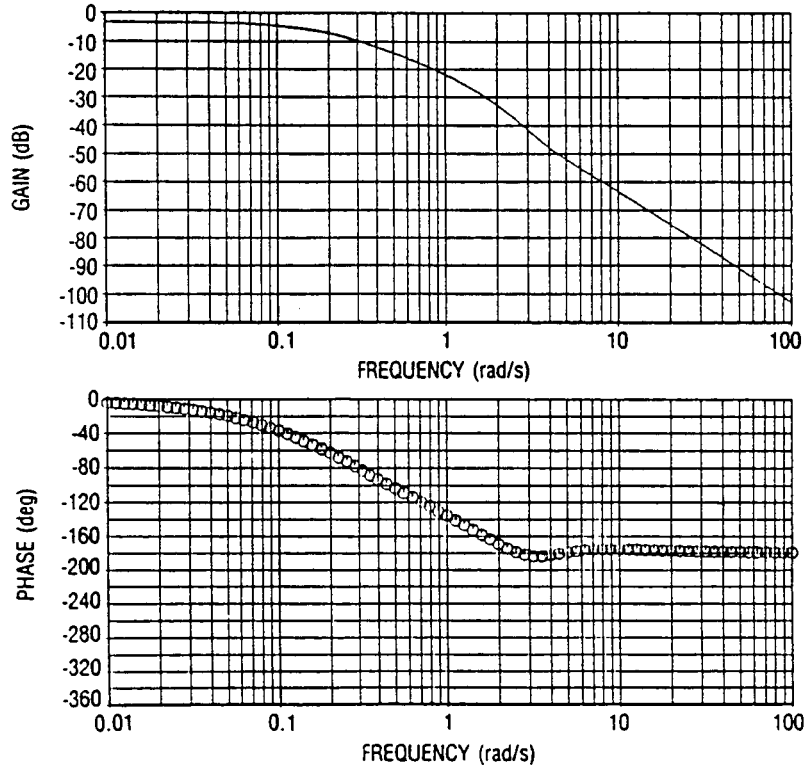

Figure 34. δ_{plac} Control Loop Frequency Response With δ_{vc} Failed Optimal Output Feedback Design, Mach .25, Altitude 5000 ft

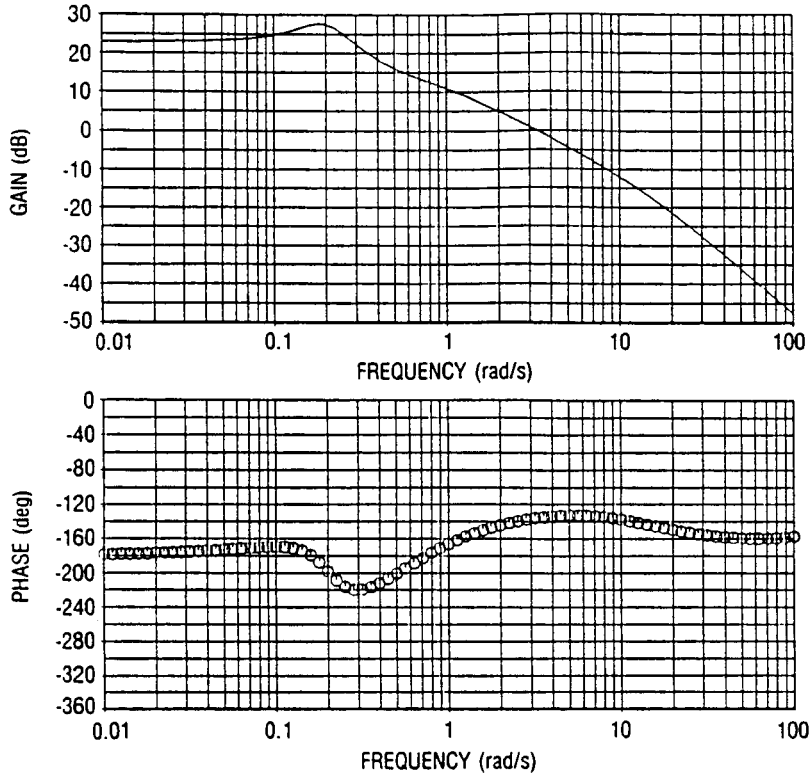

Figure 35. δ_{htc} Control Loop Frequency Response With δ_{vc} Failed Optimal Output Feedback Design, Mach .25, Altitude 5000 ft

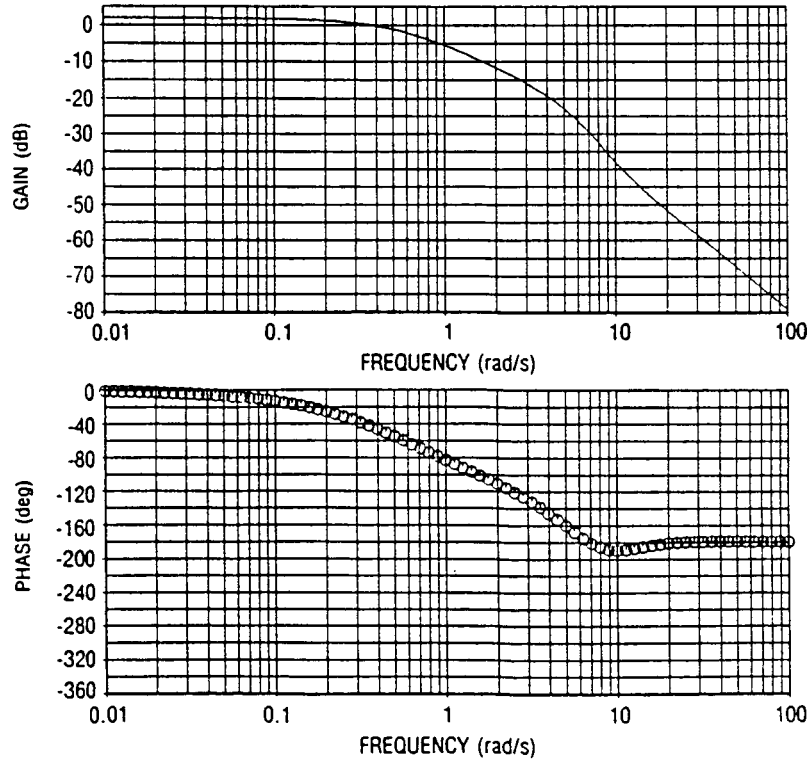

Figure 36. δ_{plac} Control Loop Frequency Response Optimal Output Feedback Design, Mach .60, Altitude 5000 ft

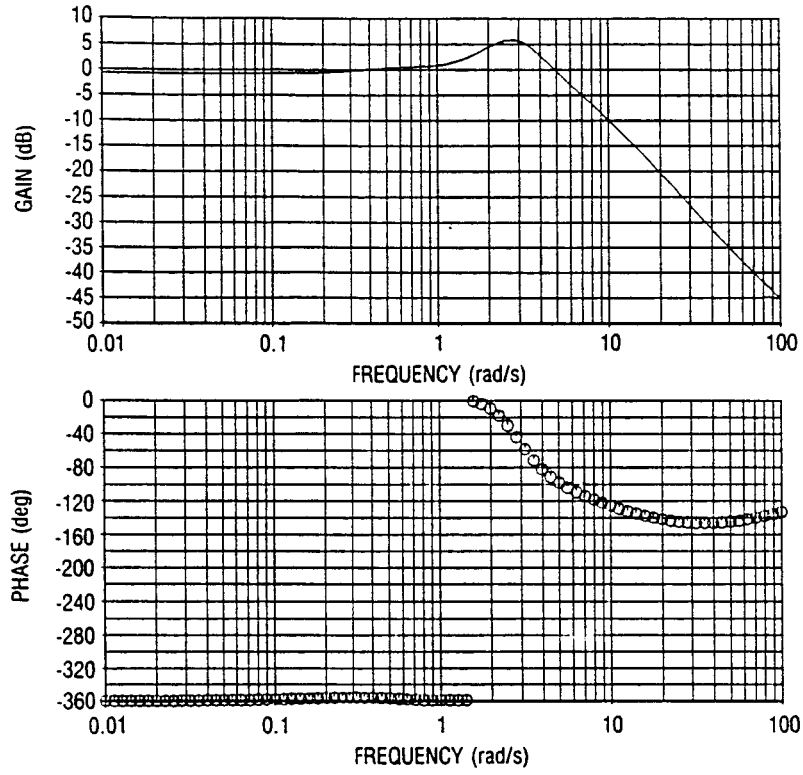

Figure 37. δ_{vcc} Control Loop Frequency Response Optimal Output Feedback Design, Mach .60, Altitude 5000 ft

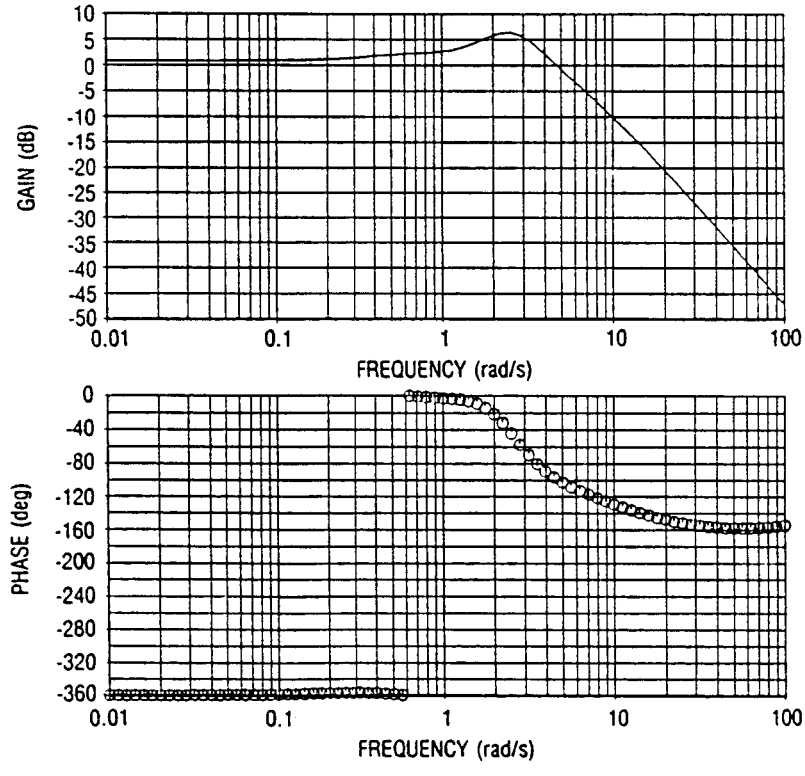

Figure 38. δ_{htc} Control Loop Frequency Response Optimal Output Feedback Design, Mach .60, Altitude 5000 ft

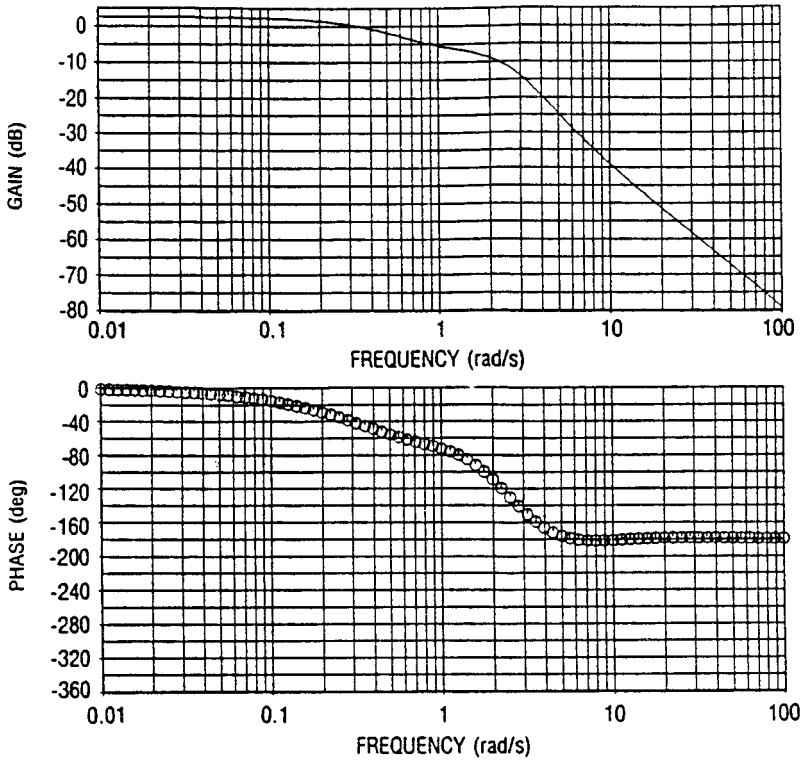

Figure 39. δ_{plac} Control Loop Frequency Response With δ_{ht} Failed Optimal Output Feedback Design, Mach .60, Altitude 5000 ft

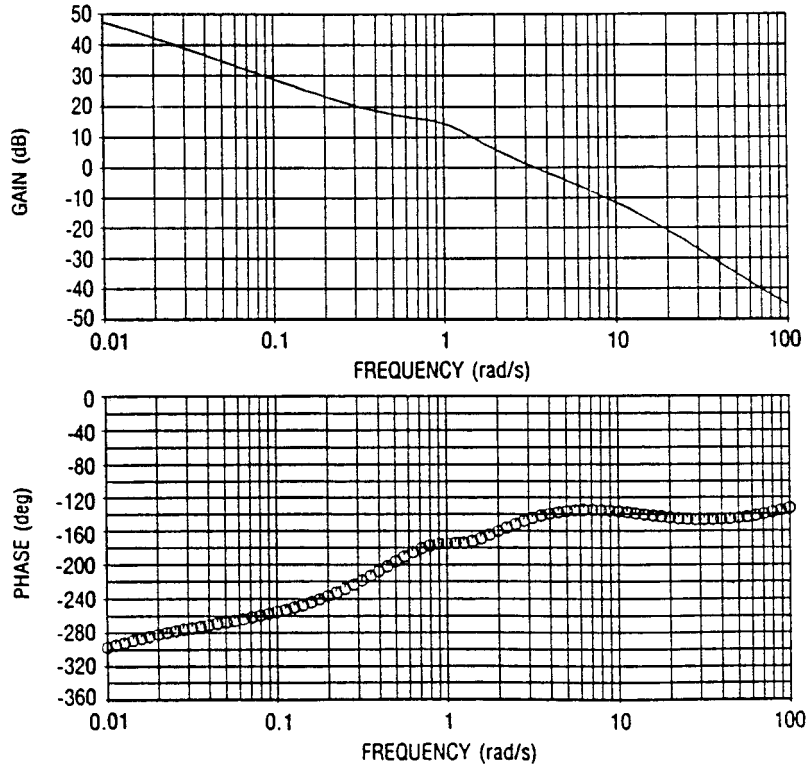

Figure 40. δ_{vcc} Control Loop Frequency Response With δ_{ht} Failed Optimal Output Feedback Design, Mach .60, Altitude 5000 ft

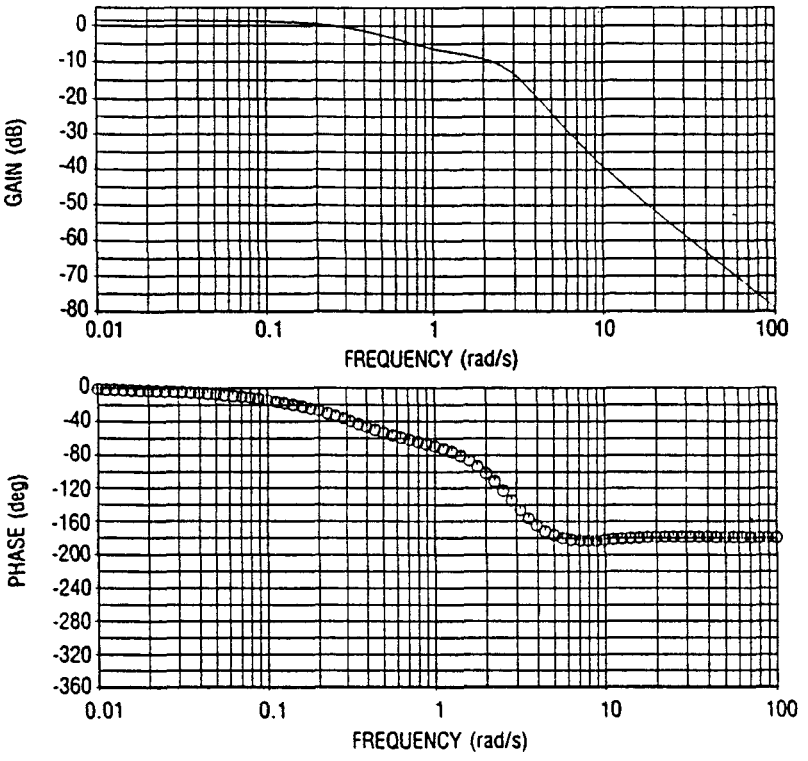

Figure 41. δ_{plac} Control Loop Frequency Response With δ_{vc} Failed Optimal Output Feedback Design, Mach .60, Altitude 5000 ft

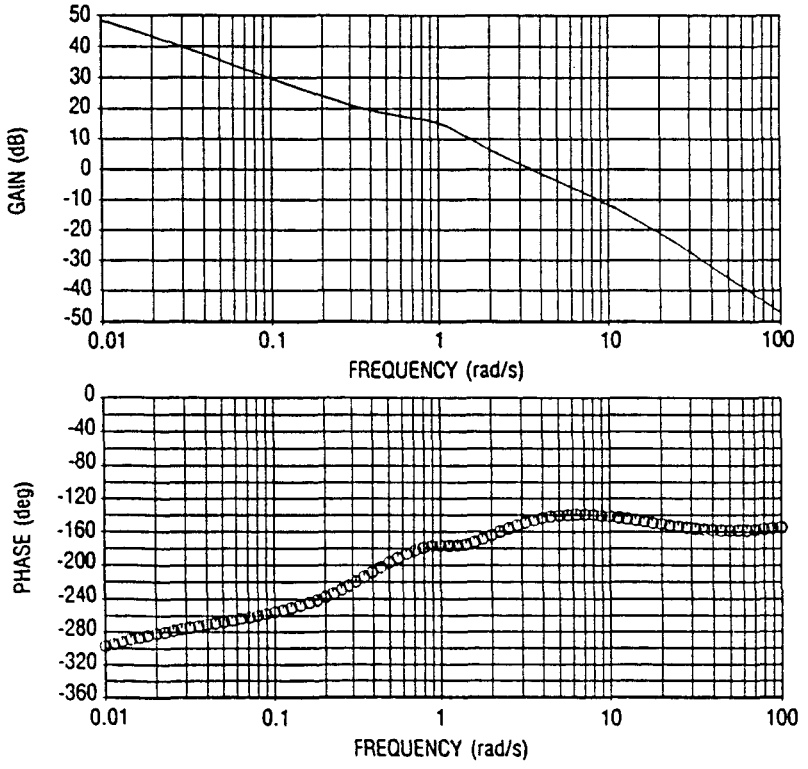

Figure 42. δ_{htc} Control Loop Frequency Response With δ_{vc} Failed Optimal Output Feedback Design, Mach .60, Altitude 5000 ft

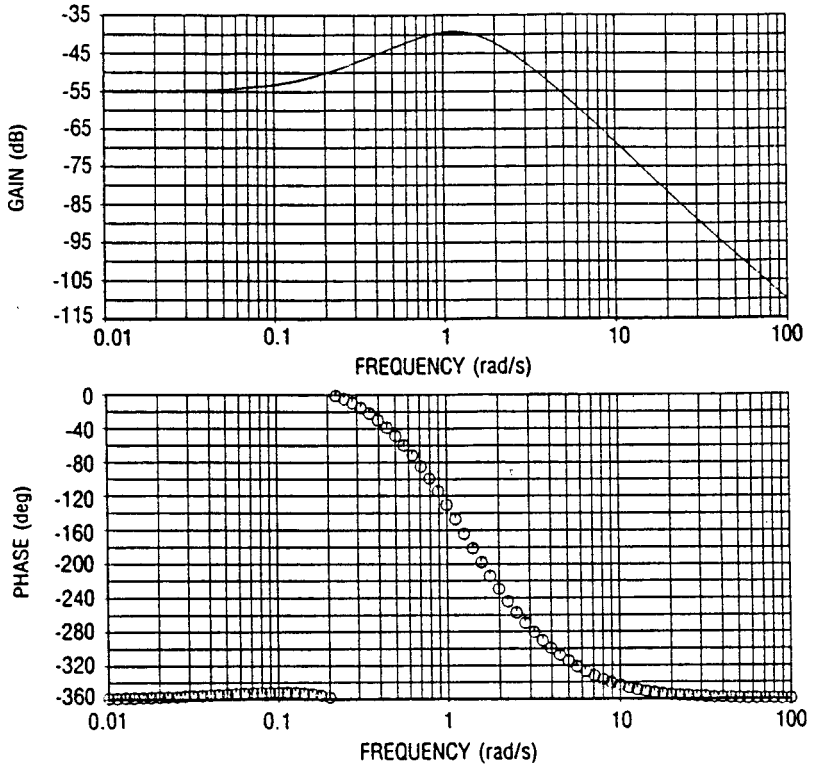

Figure 43. δ_{plac} Control Loop Frequency Response Optimal Output Feedback Design, Mach .90, Altitude 20,000 ft

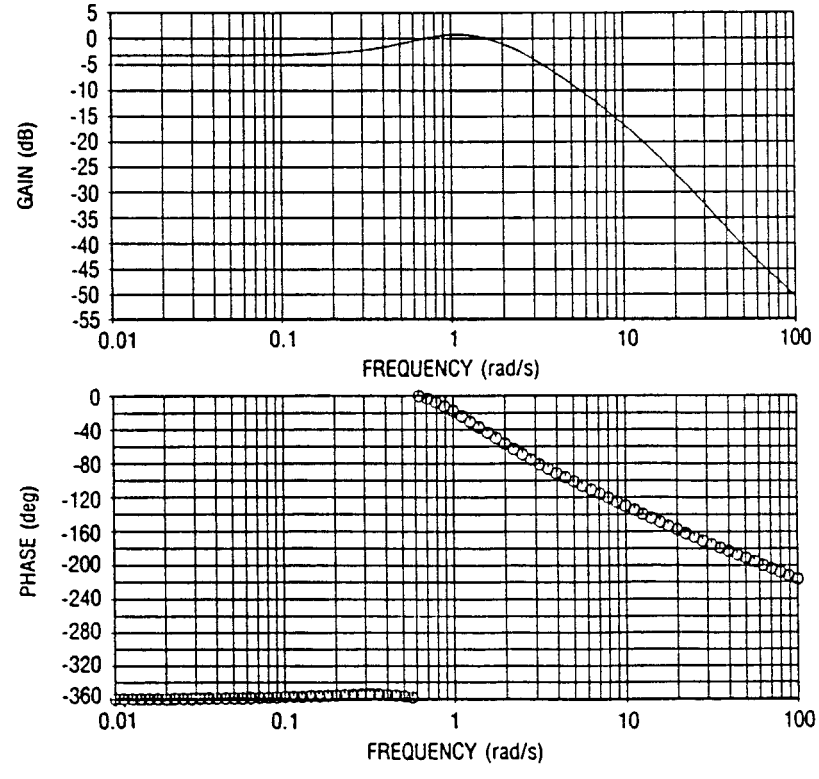

Figure 44. δ_{vcc} Control Loop Frequency Response Optimal Output Feedback Design, Mach .90, Altitude 20,000 ft

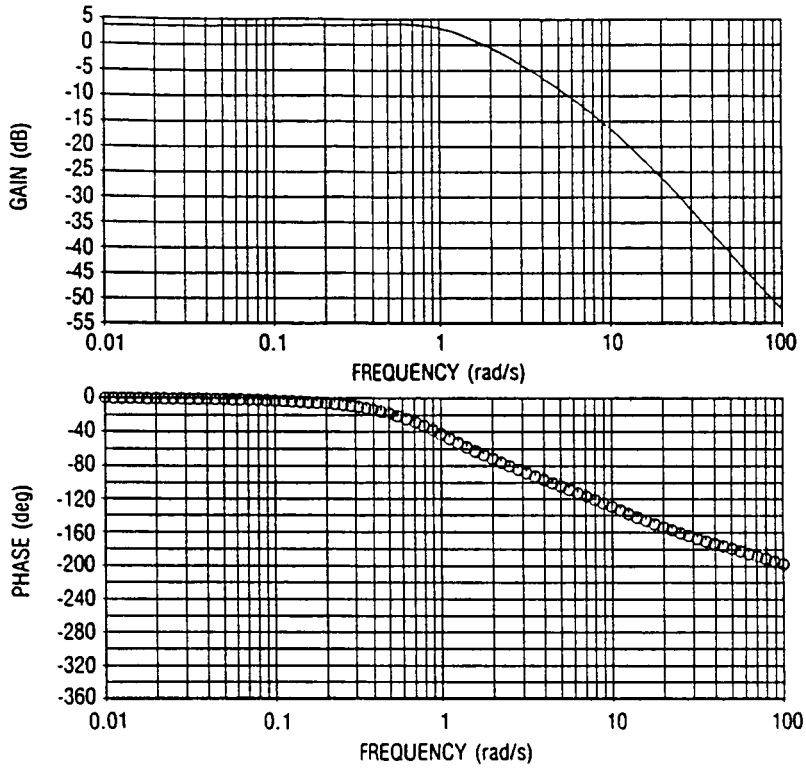

Figure 45. δ_{htc} Control Loop Frequency Response Optimal Output Feedback Design, Mach .90, Altitude 20,000 ft

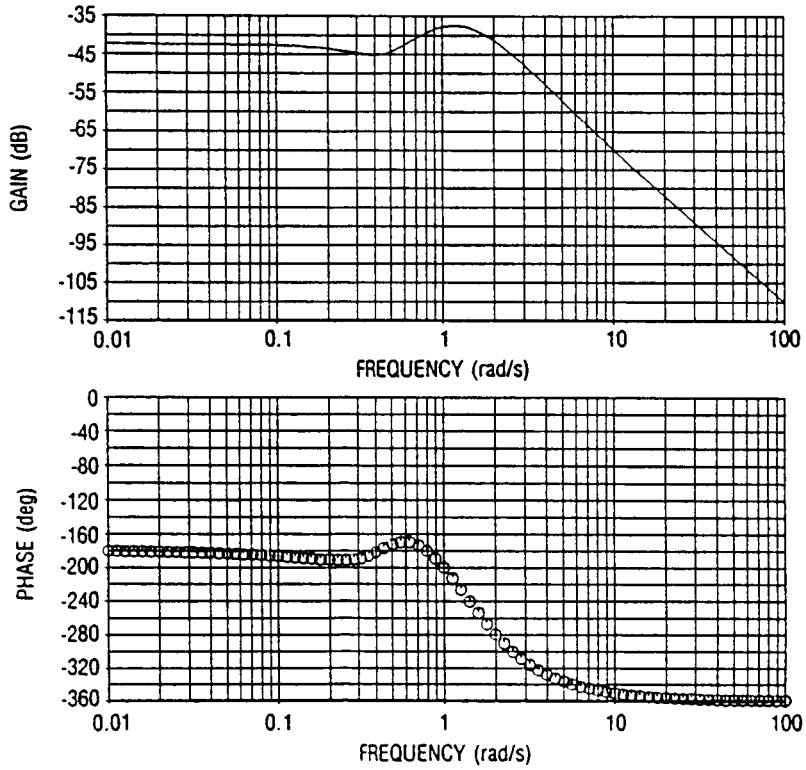

Figure 46. δ_{plac} Control Loop Frequency Response With δ_{ht} Failed Optimal Output Feedback Design, Mach .90, Altitude 20,000 ft

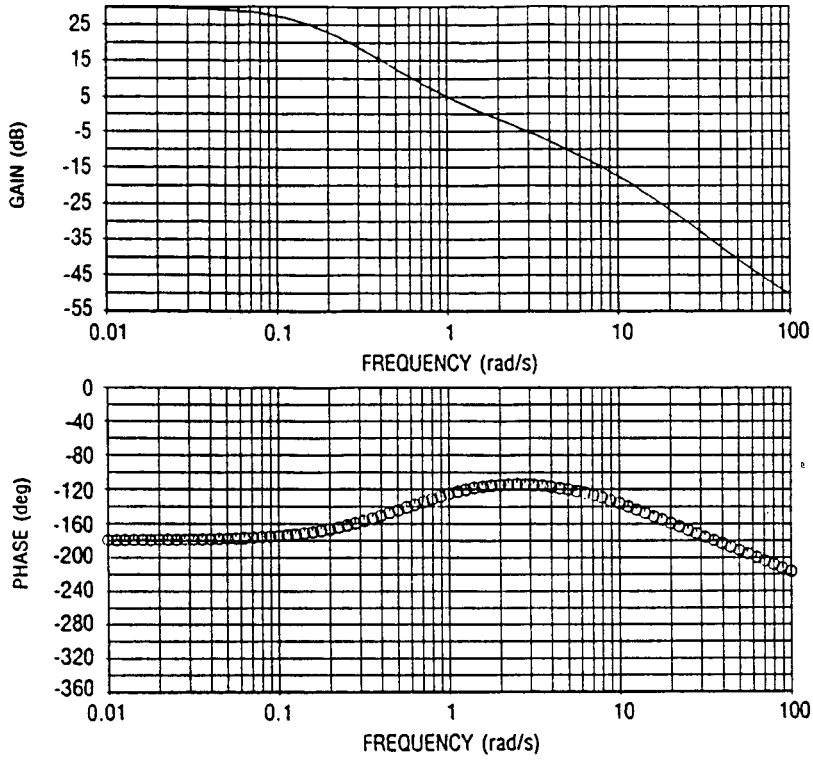

Figure 47. δ_{vcc} Control Loop Frequency Response With δ_{ht} Failed Optimal Output Feedback Design, Mach .90, Altitude 20,000 ft

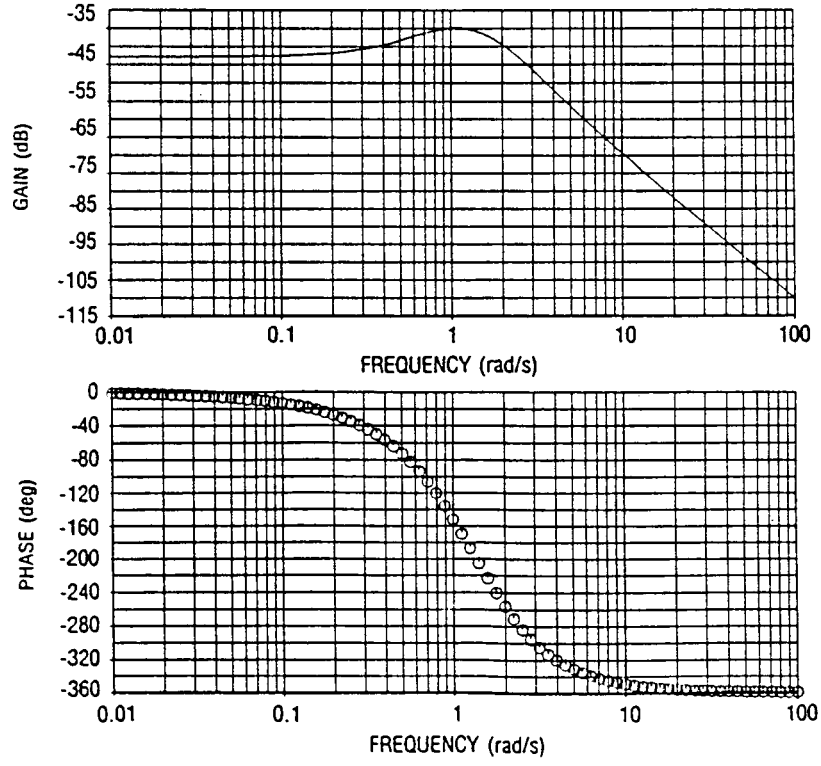

Figure 48. δ_{plac} Control Loop Frequency With δ_{vc} Failed Optimal Output Feedback Design, Mach .90, Altitude 20,000 ft

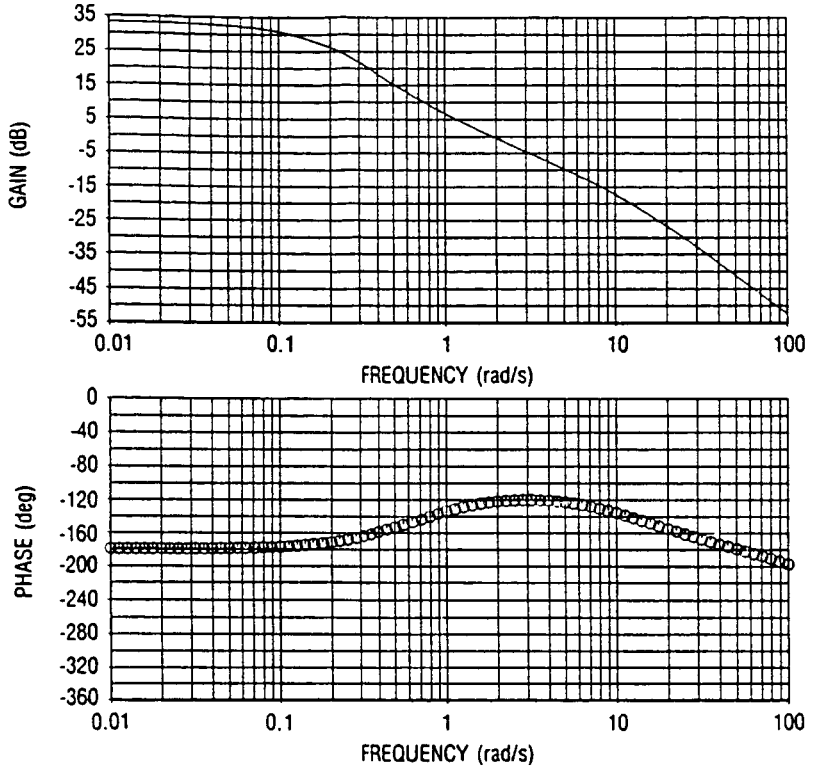

Figure 49. δ_{htc} Control Loop Frequency Response With δ_{vc} Failed Optimal Output Feedback Design, Mach .90, Altitude 20,000 ft

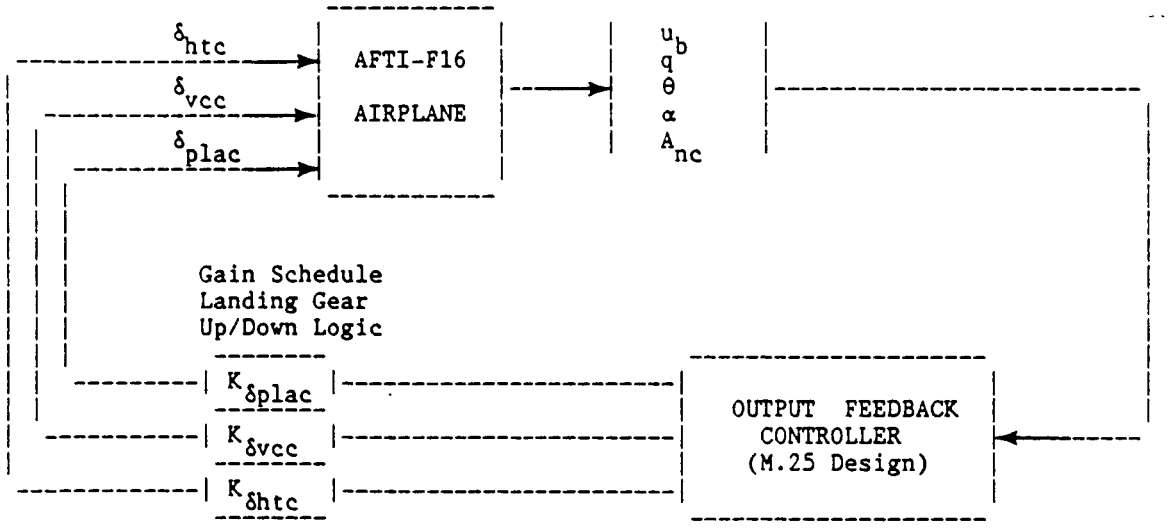

Figure 50. Output Feedback Controller Structure With Gain Schedule

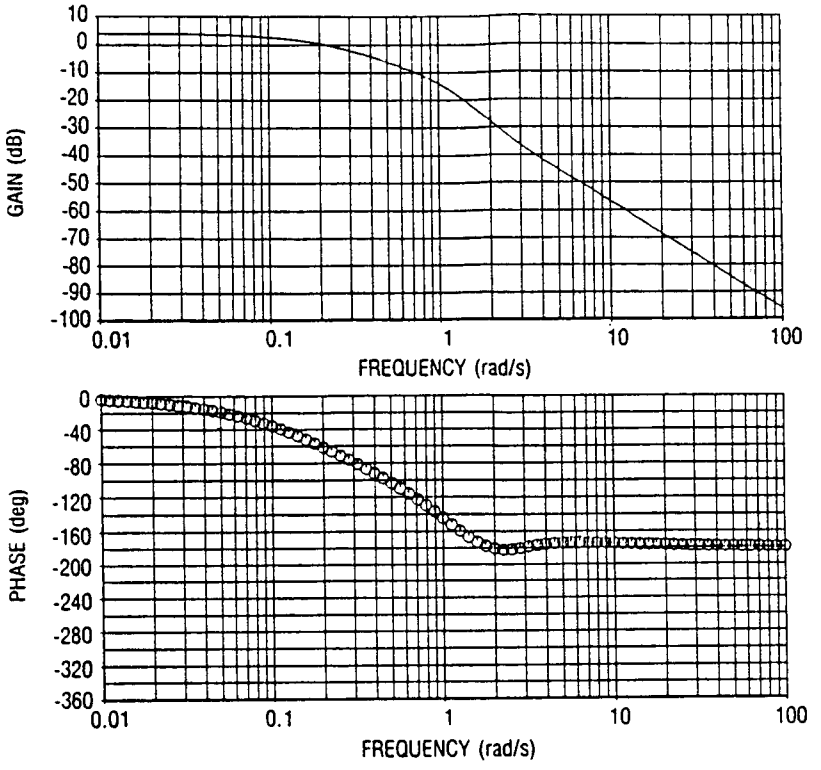

Figure 51. δ_{plac} Control Loop Frequency Response Optimal Gain Schedule Output Feedback Design, Mach .60, Altitude 5000 ft

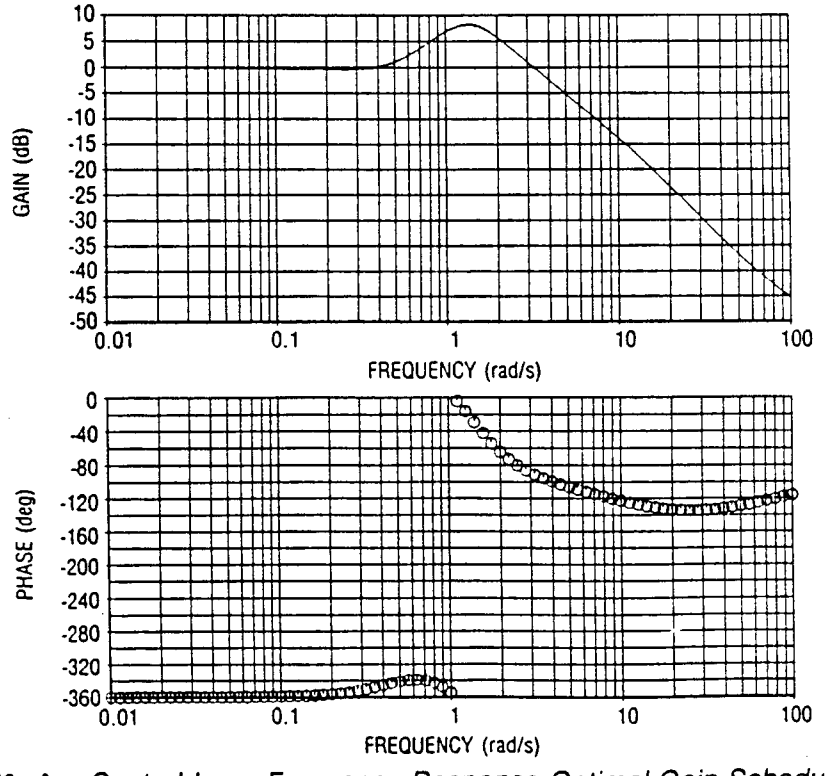

Figure 52. δ_{vcc} Control Loop Frequency Response Optimal Gain Schedule Output Feedback Design, Mach .60, Altitude 5000 ft

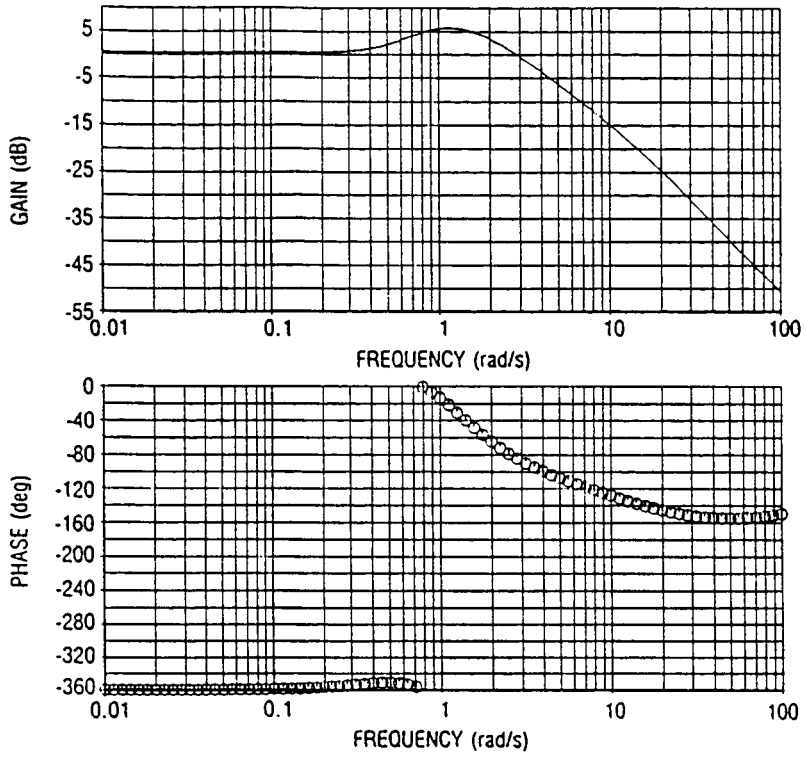

Figure 53. δ_{htc} Control Loop Frequency Response Optimal Gain Schedule Output Feedback Design, Mach .60, Altitude 5000 ft

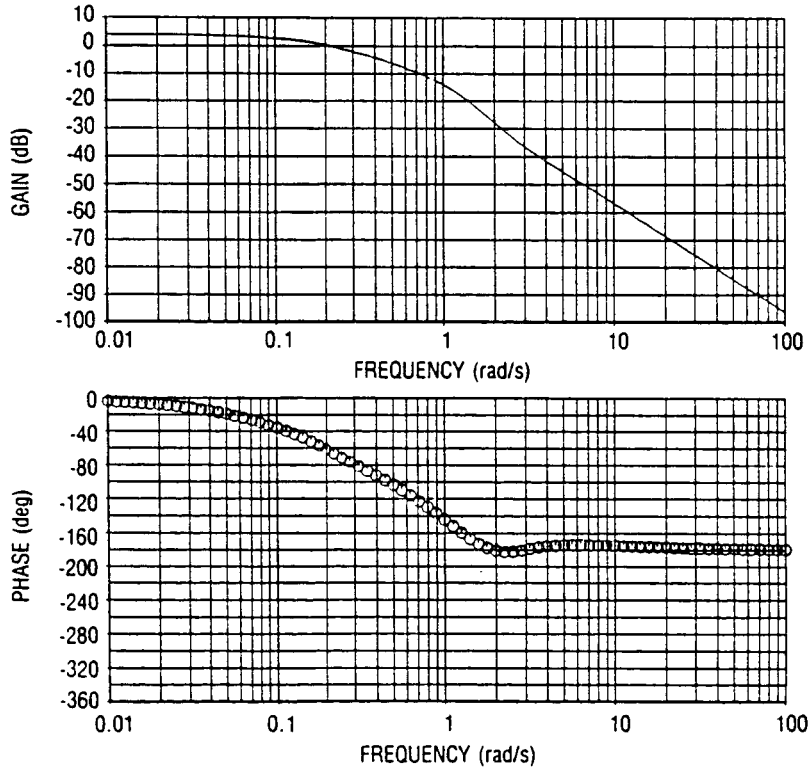

Figure 54. δ_{plac} Control Loop Frequency Response With δ_{ht} Failed Optimal Gain Schedule Output Feedback Design, Mach .60, Altitude 5000 ft

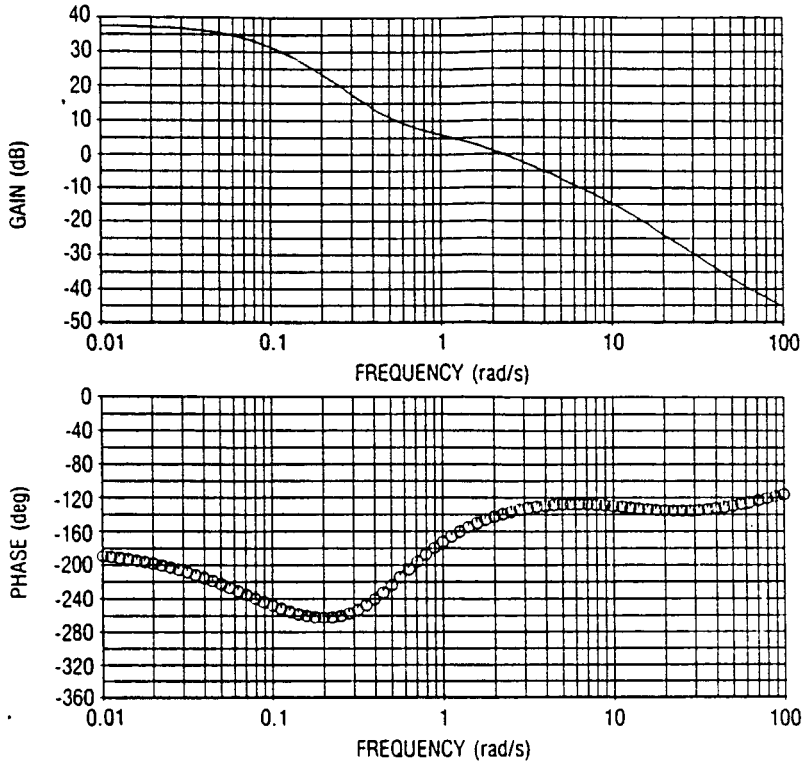

Figure 55. δ_{vcc} Control Loop Frequency Response With δ_{ht} Failed Optimal Gain Schedule Output Feedback Design, Mach .60, Altitude 5000 ft

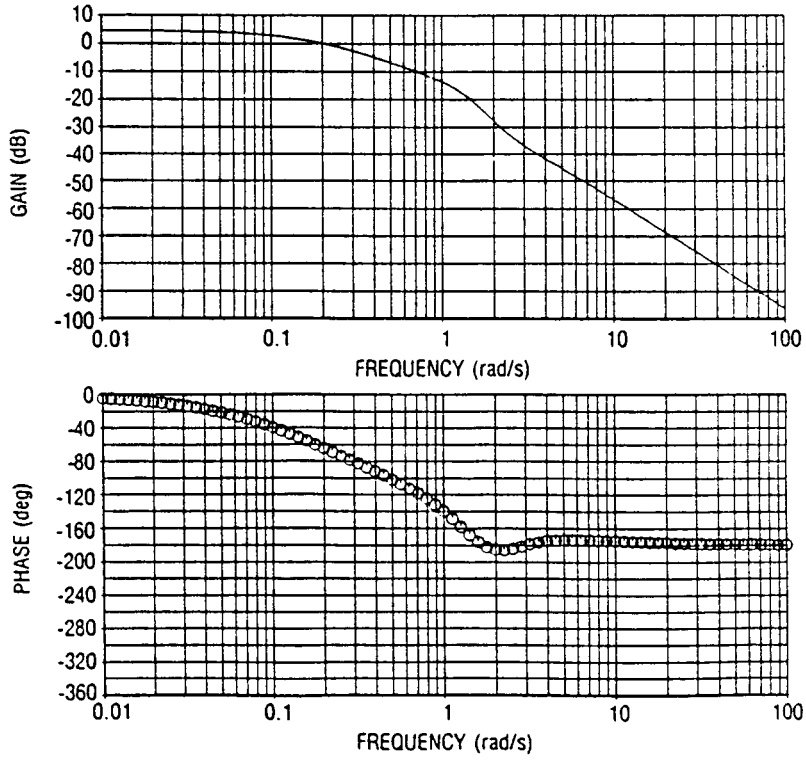

Figure 56. δ_{plac} Control Loop Frequency Response With δ_{vc} Failed Optimal Gain Schedule Output Feedback Design, Mach .60, Altitude 5000 ft

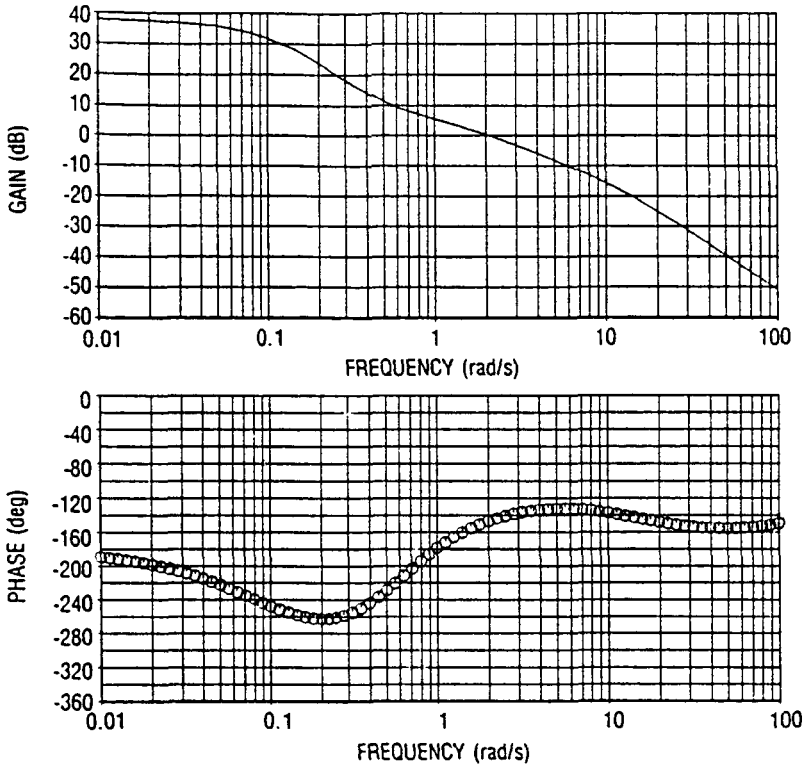

Figure 57. δ_{htc} Control Loop Frequency Response With δ_{vc} Failed Optimal Gain Schedule Output Feedback Design, Mach .60, Altitude 5000 ft

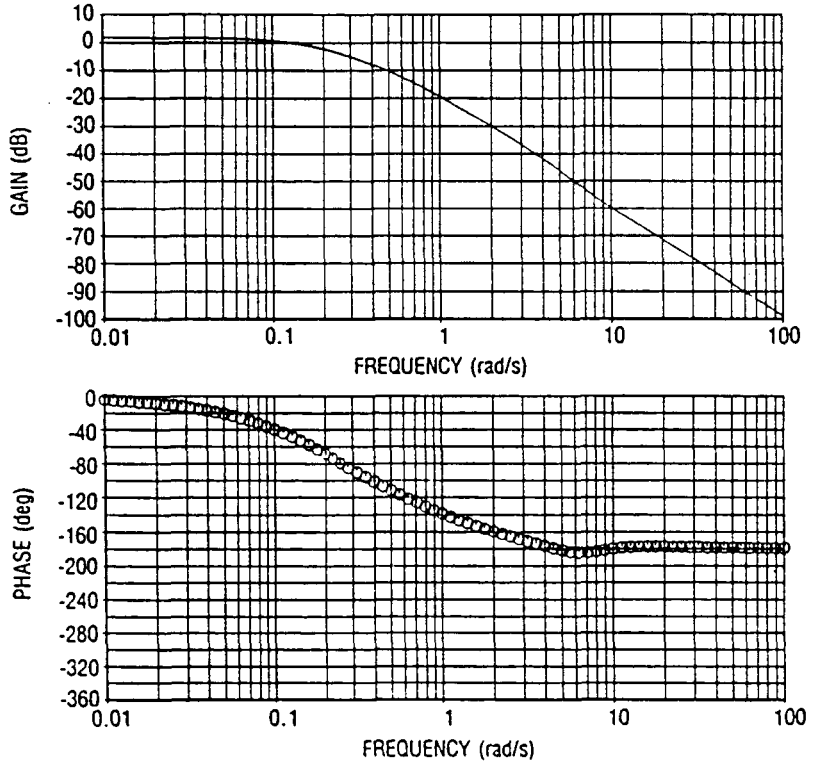

Figure 58. δ_{plac} Control Loop Frequency Response Optimal Gain Schedule Output Feedback Design, Mach .90, Altitude 20,000 ft

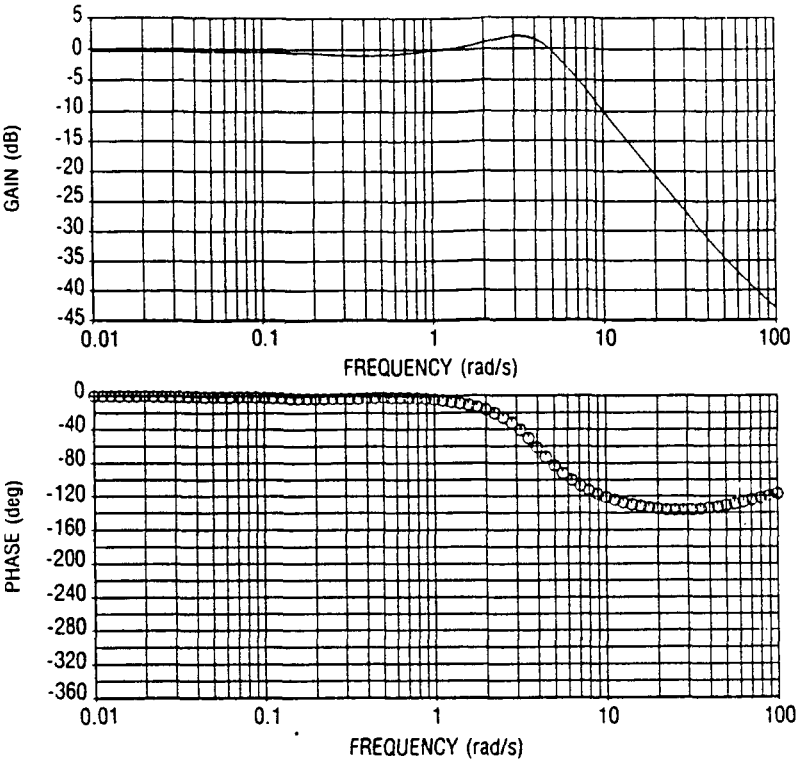

Figure 59. δ_{vcc} Control Loop Frequency Response Optimal Gain Schedule Output Feedback Design, Mach .90, Altitude 20,000 ft

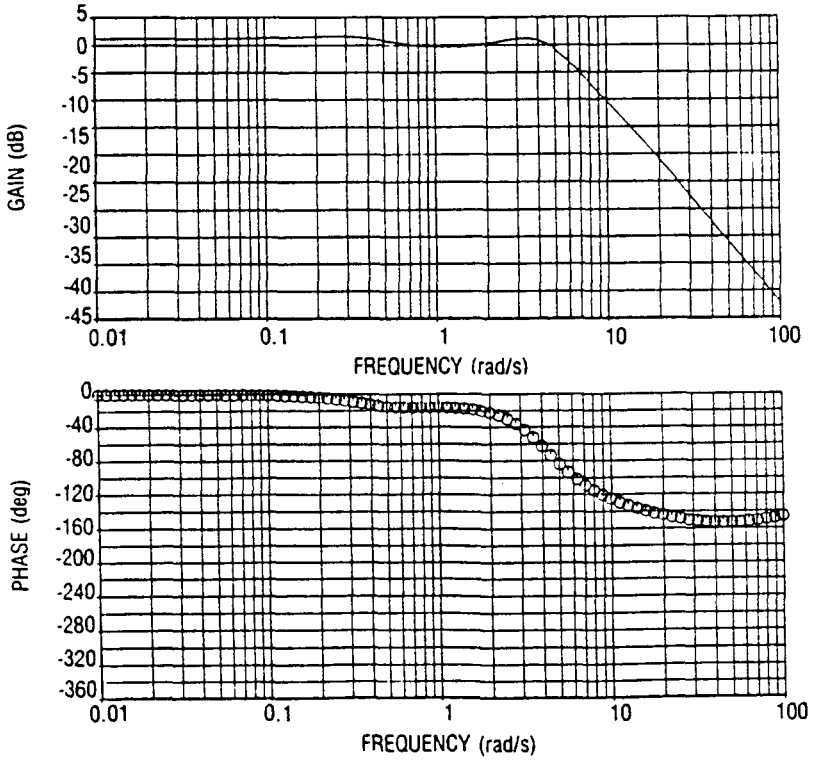

Figure 60. δ_{htc} Control Loop Frequency Response Optimal Gain Schedule Output Feedback Design, Mach .90, Altitude 20,000 ft

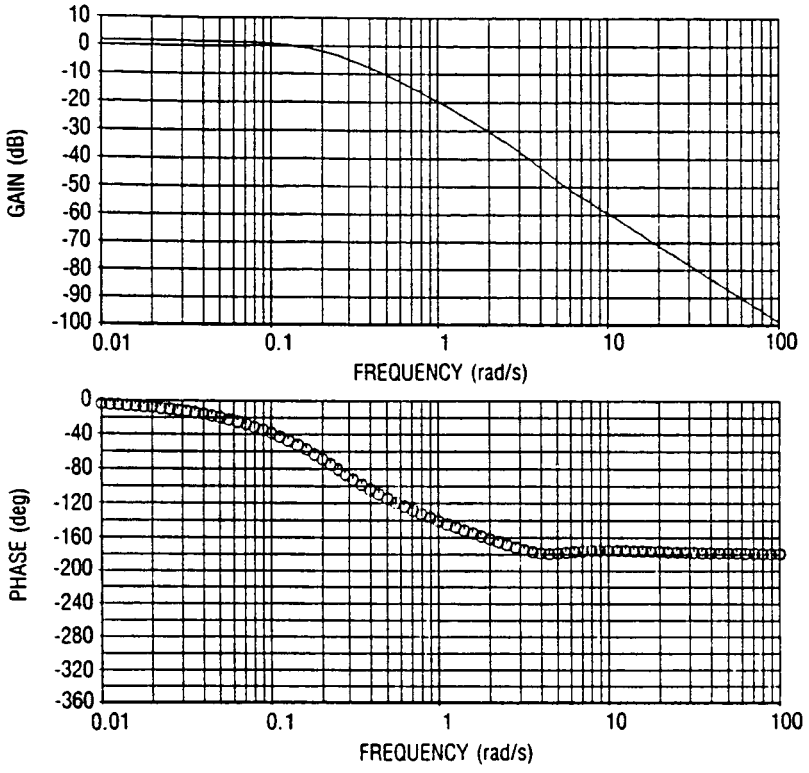

Figure 61. δ_{plac} Control Loop Frequency Response With δ_{ht} Failed Optimal Gain Schedule Output Feedback Design, Mach .90, Altitude 20,000 ft

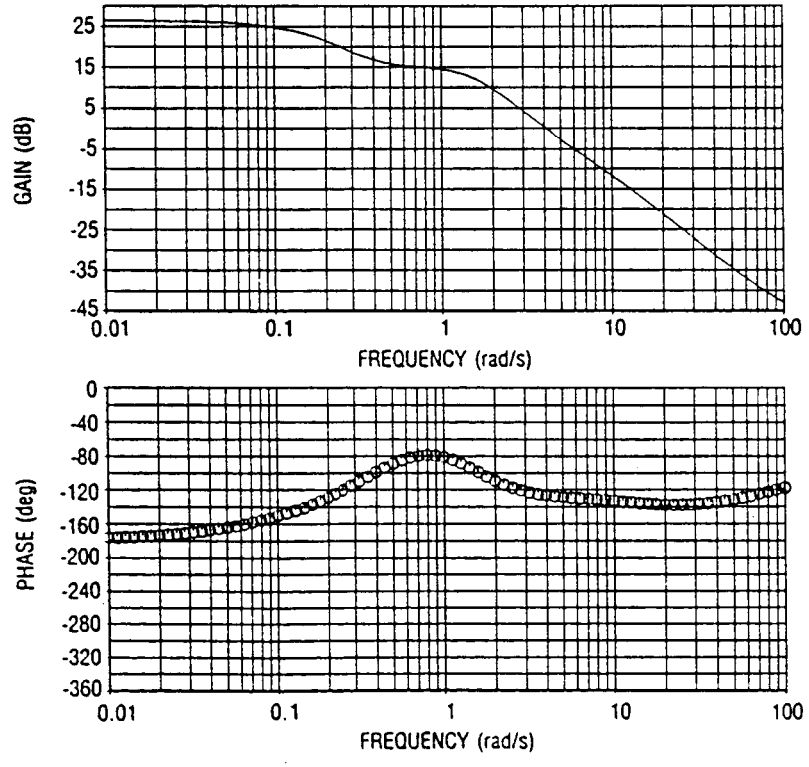

Figure 62. δ_{vcc} Control Loop Frequency Response With δ_{ht} Failed Optimal Gain Schedule Output Feedback Design, Mach .90, Altitude 20,000 ft

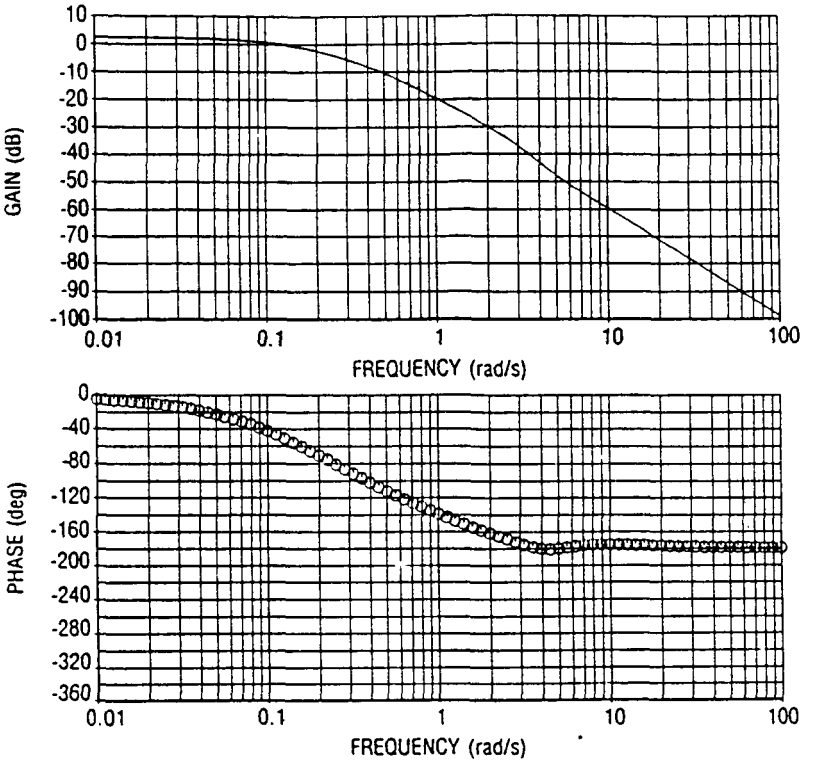

Figure 63. δ_{plac} Control Loop Frequency Response With δ_{vc} Failed Optimal Gain Schedule Output Feedback Design, Mach .90, Altitude 20,000 ft

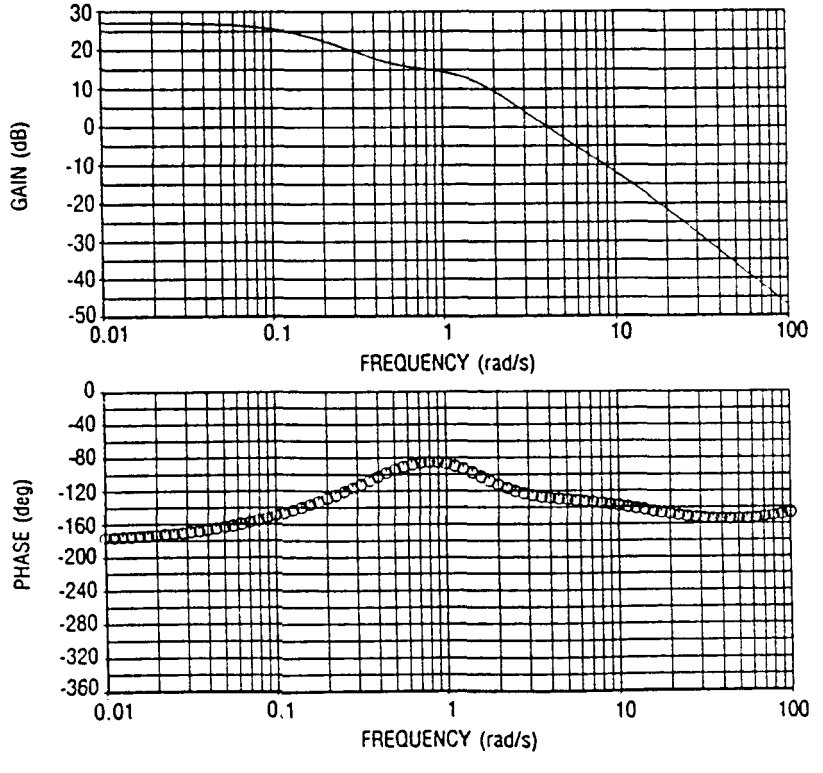

Figure 64. δ_{htc} Control Loop Frequency Response With δ_{vc} Failed Optimal Gain Schedule Output Feedback Design, Mach .90, Altitude 20,000 ft

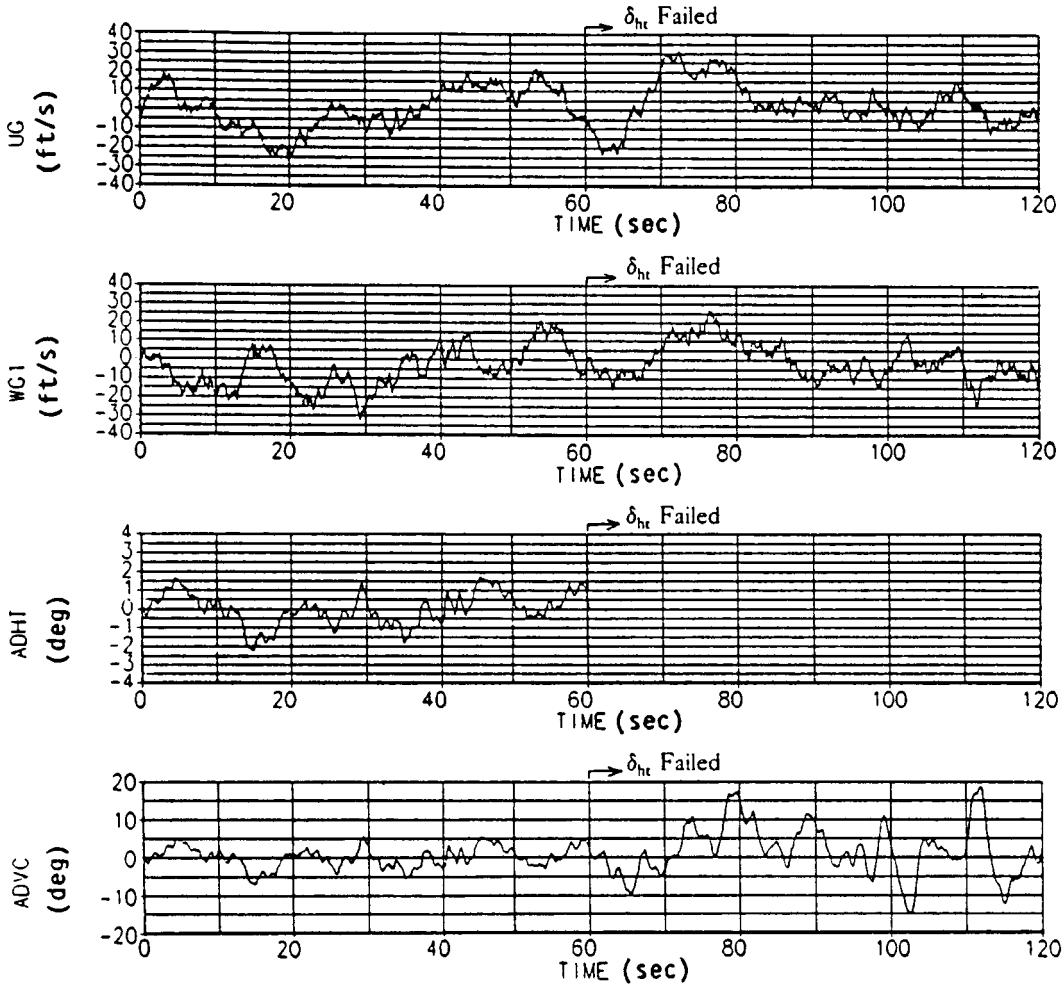

Figure 65. Time Responses Due to 10 ft/s Vertical and Longitudinal Turbulences, Optimal Gain Schedule Output Feedback Design, δ_{ht} Failed, Mach .25, Altitude 5000 ft

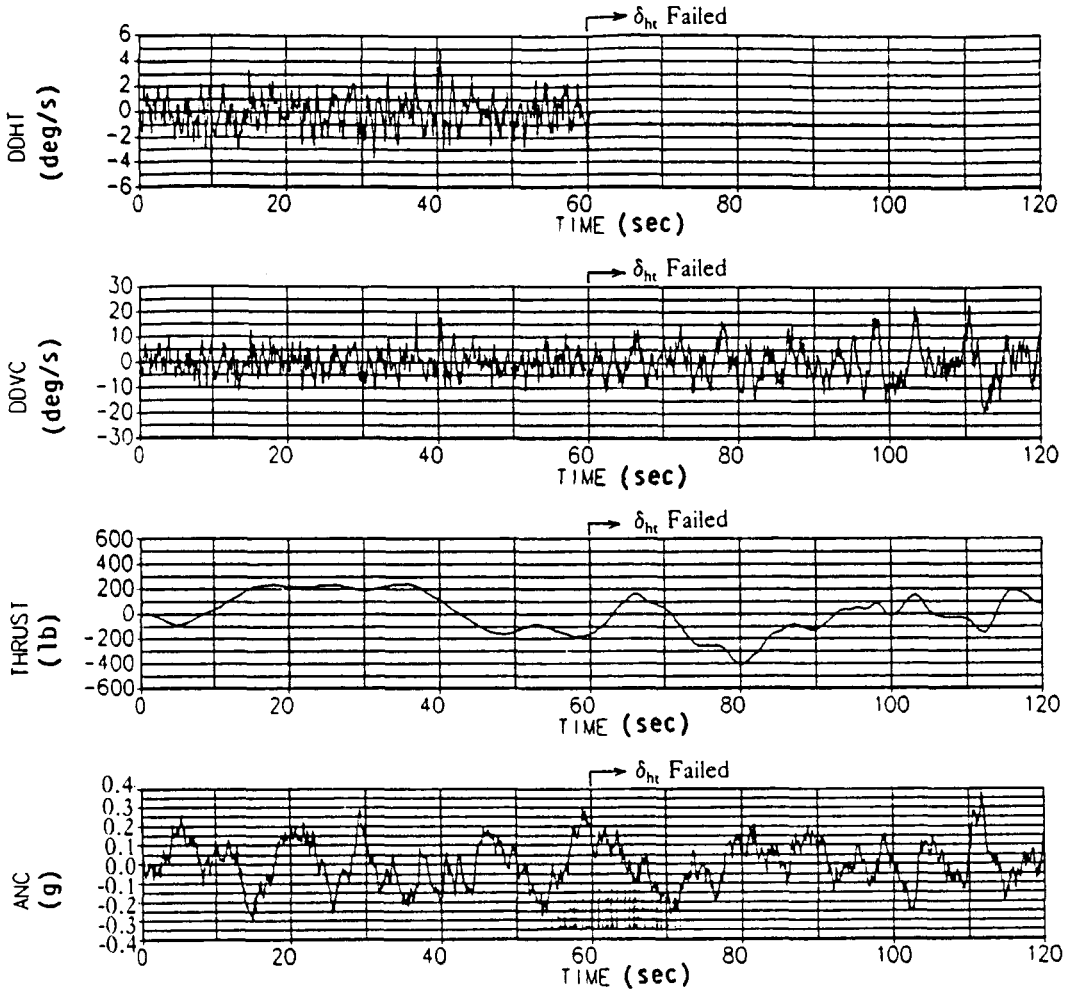

Figure 65. Time Responses Due to 10 ft/s Vertical and Longitudinal Turbulences, Optimal Gain Schedule Output Feedback Design, δ_{ht} Failed, Mach .25, Altitude 5000 ft (Continued)

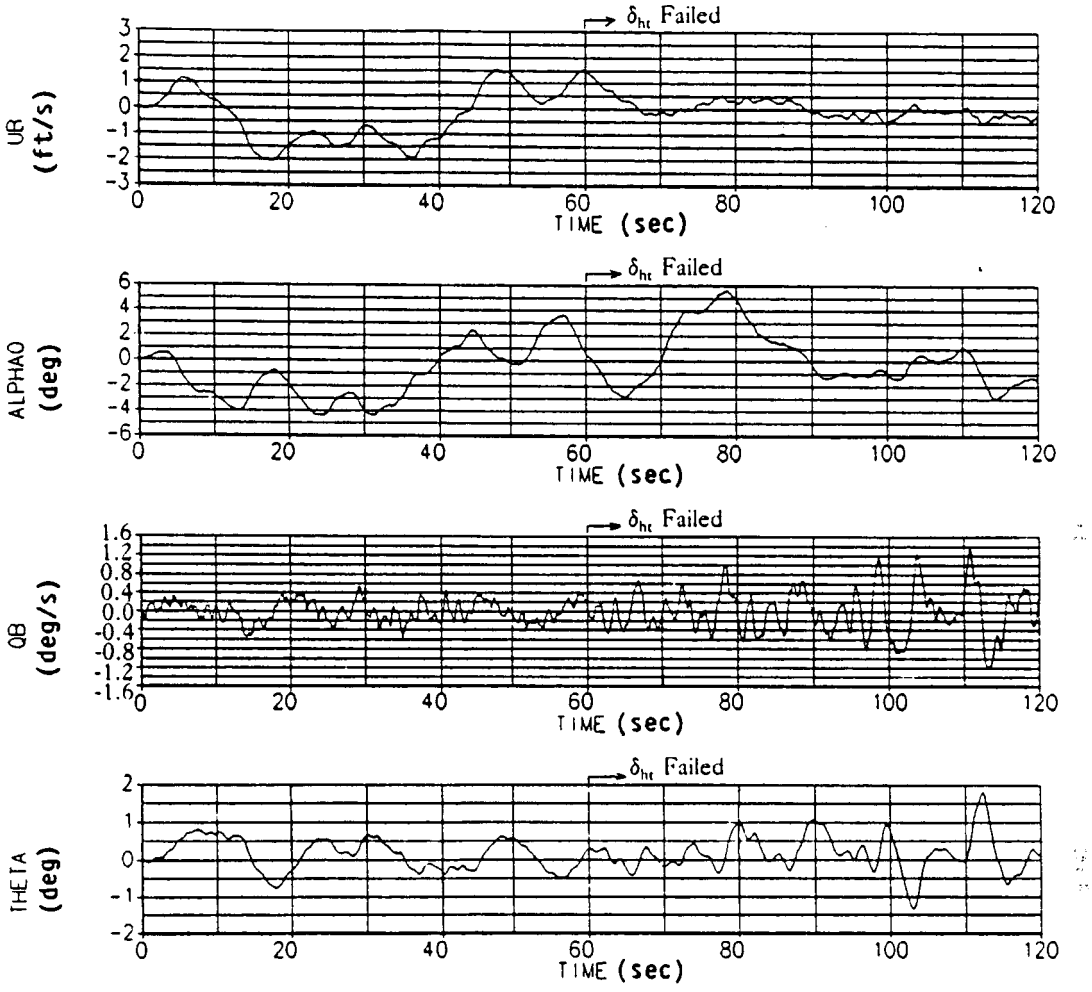

Figure 65. Time Responses Due to 10 ft/s Vertical and Longitudinal Turbulences, Optimal Gain Schedule Output Feedback Design, δ_{ht} Failed, Mach .25, Altitude 5000 ft (Concluded)

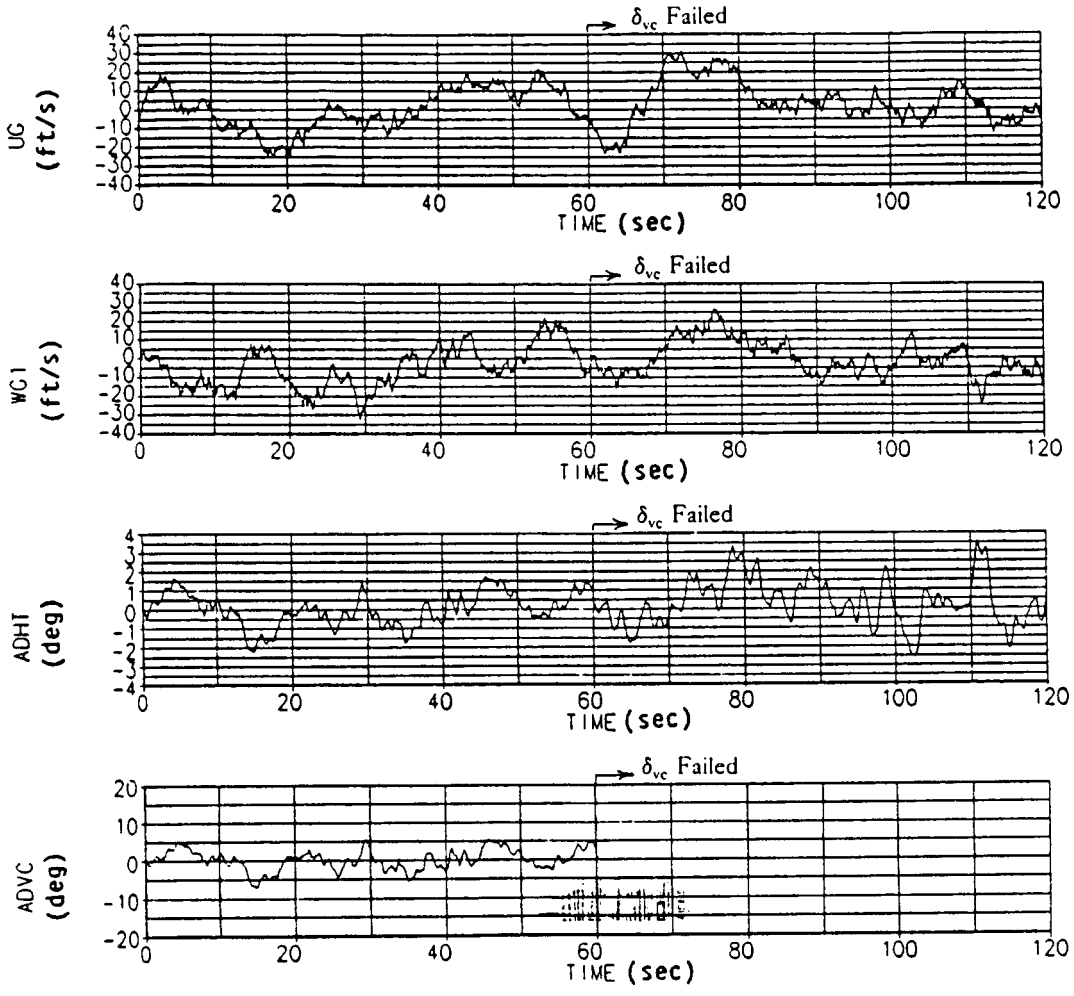

Figure 66. Time Responses Due to 10 ft/s Vertical and Longitudinal Turbulences, Optimal Gain Schedule Output Feedback Design, δ_{vc} Failed, Mach .25, Altitude 5000 ft

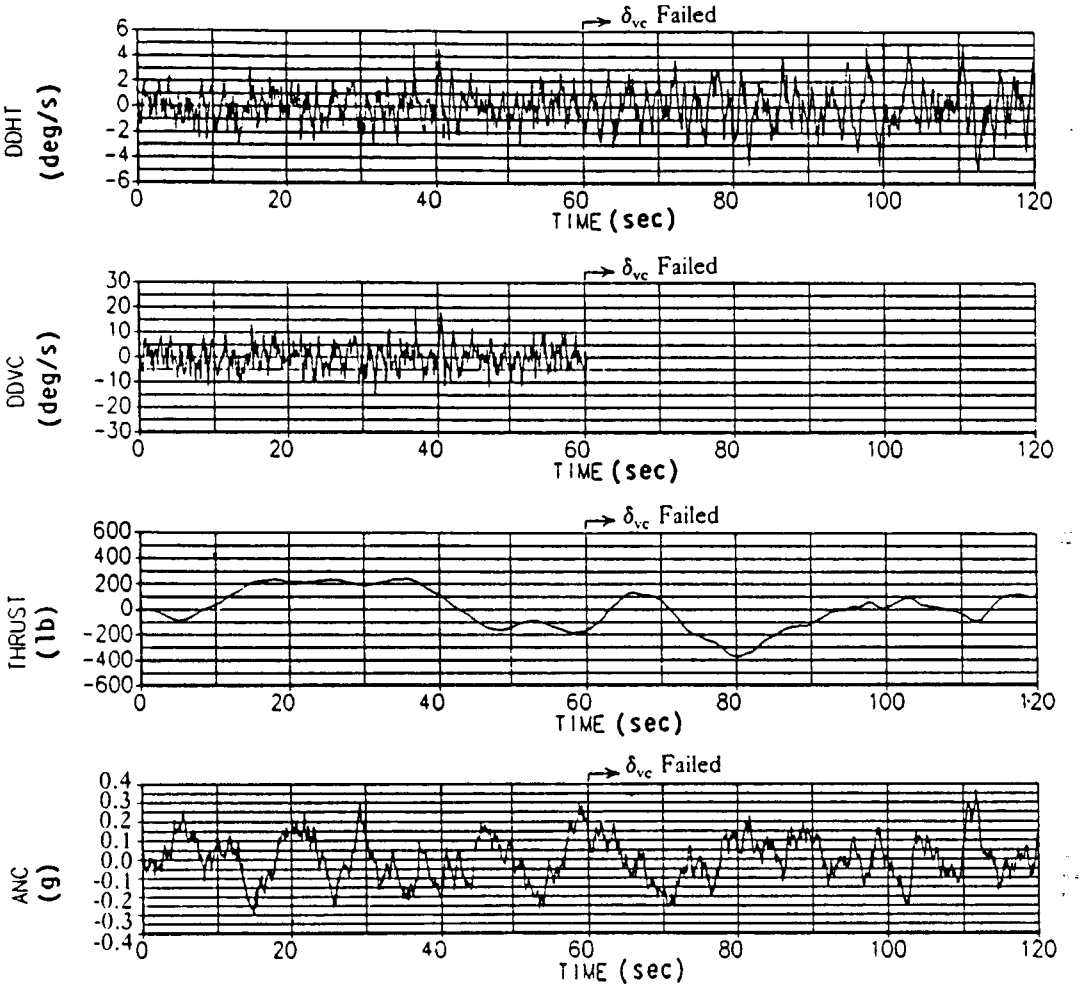

Figure 66. Time Responses Due to 10 ft/s Vertical and Longitudinal Turbulences, Optimal Gain Schedule Output Feedback Design, δ_{vc} Failed, Mach .25, Altitude 5000 ft (Continued)

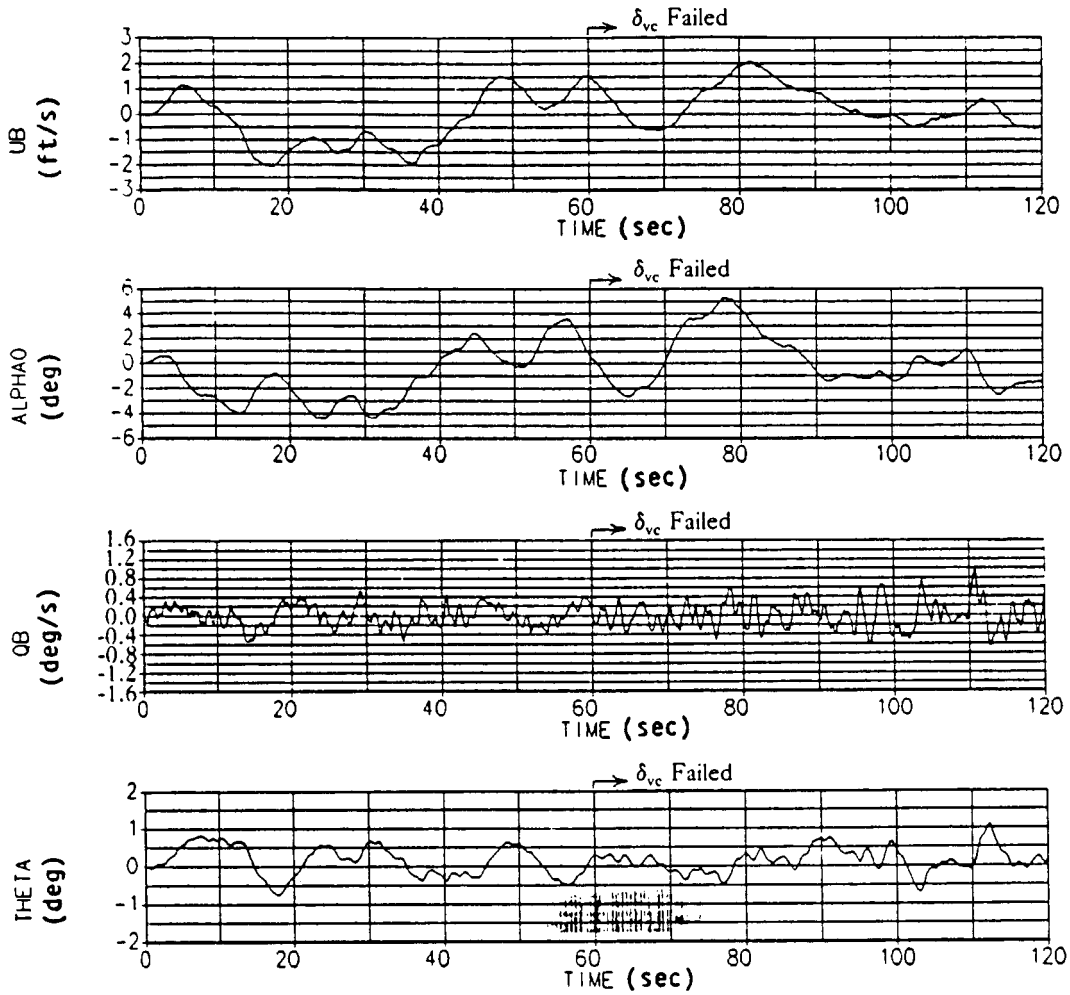

Figure 66. Time Responses Due to 10 ft/s Vertical and Longitudinal Turbulences, Optimal Gain Schedule Output Feedback Design, δ_{vc} Failed, Mach .25, Altitude 5000 ft (Concluded)

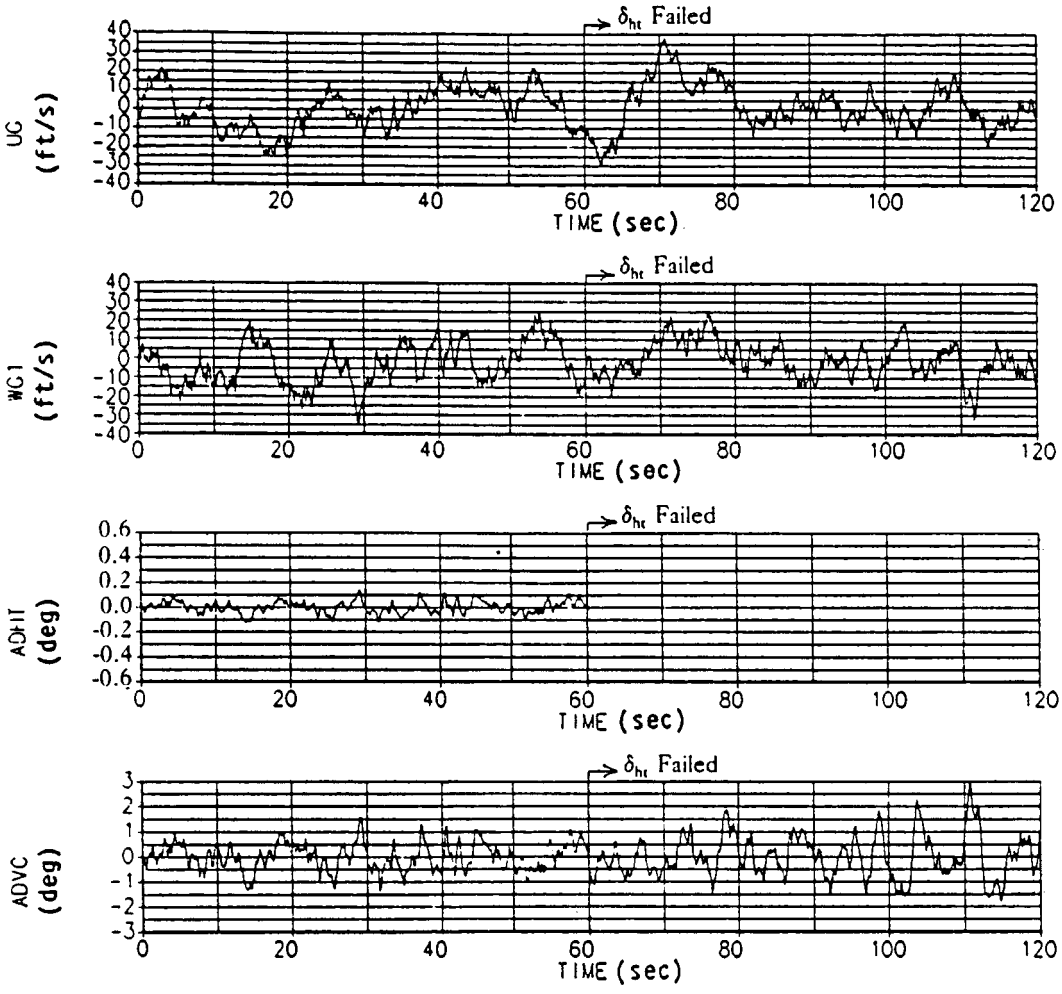

Figure 67. Time Responses Due to 10 ft/s Vertical and Longitudinal Turbulences, Optimal Gain Schedule Output Feedback Design, δ_{ht} Failed, Mach .60, Altitude 5000 ft

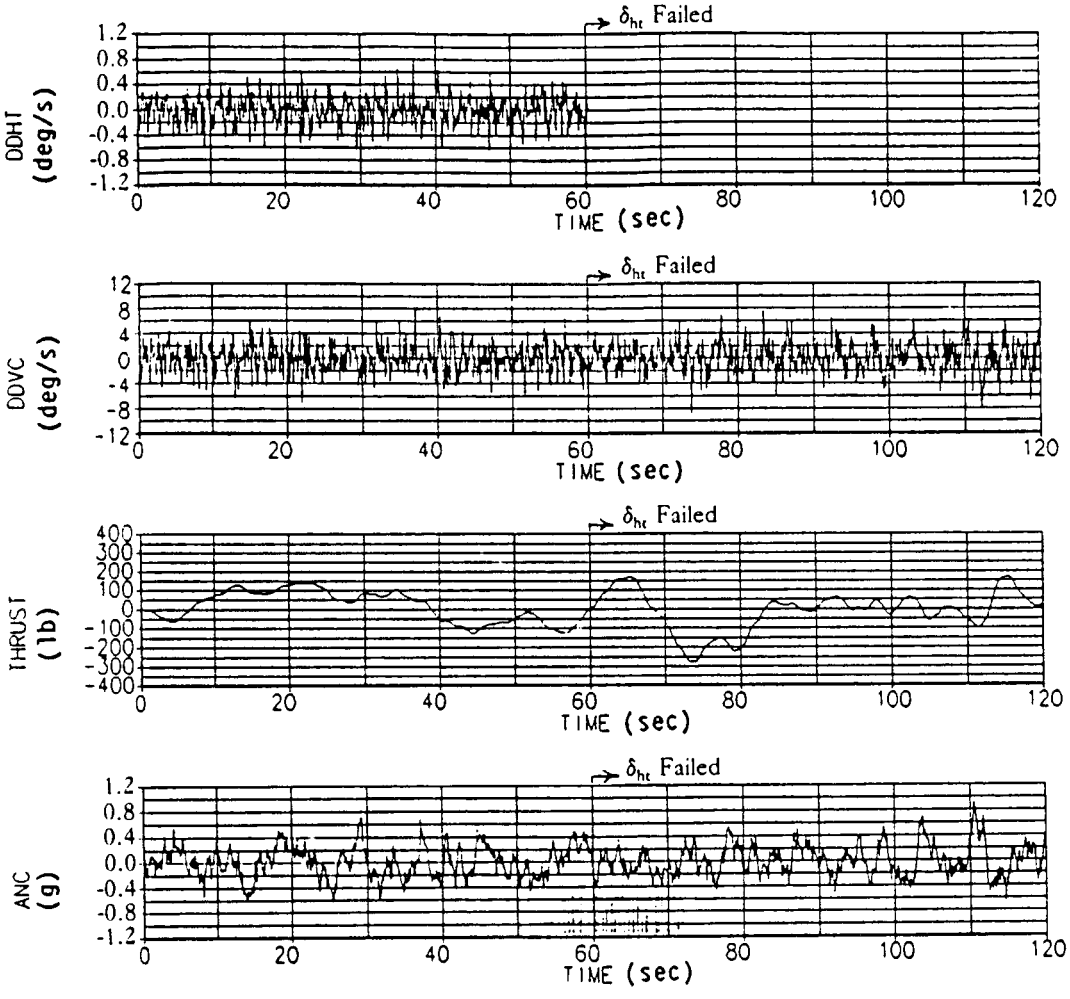

Figure 67. Time Responses Due to 10 ft/s Vertical and Longitudinal Turbulences, Optimal Gain Schedule Output Feedback Design, δ_{ht} Failed, Mach .60, Altitude 5000 ft (Continued) .

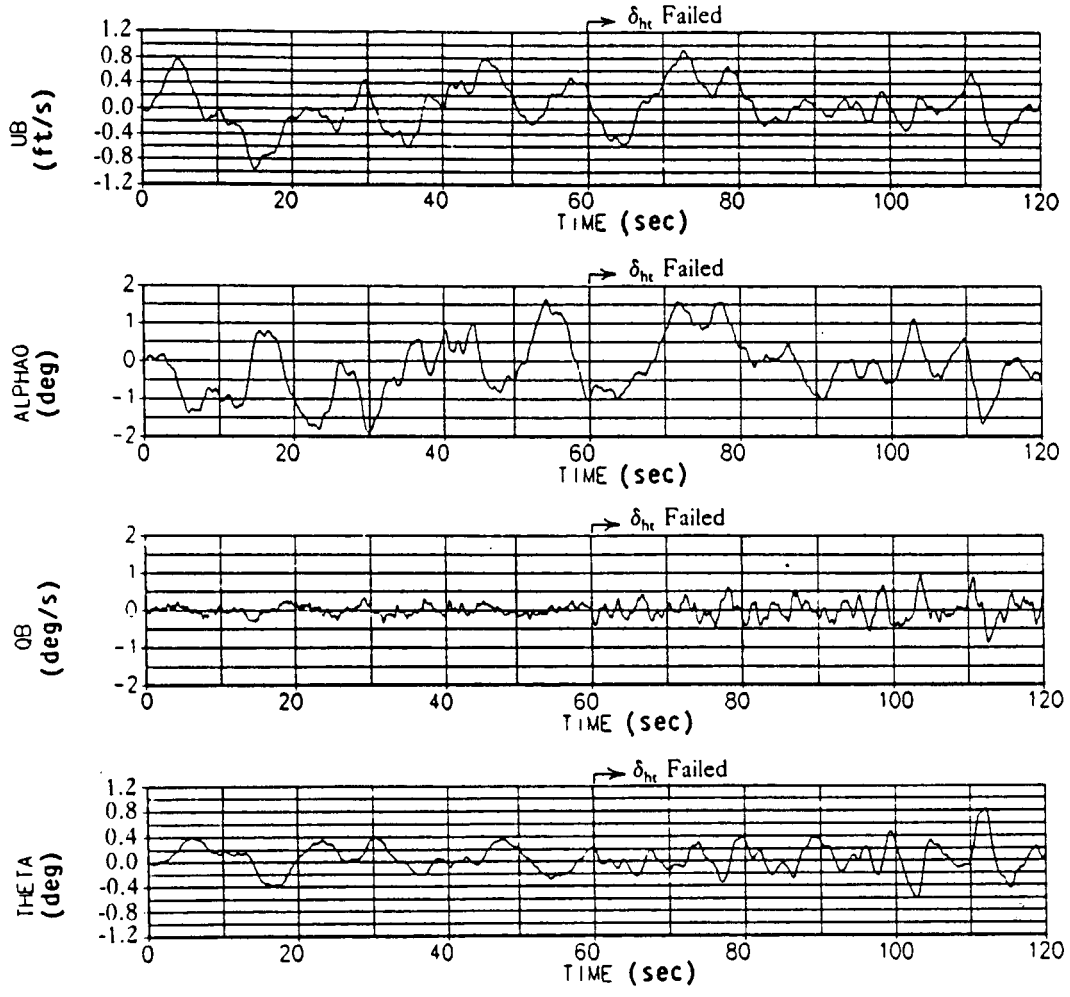

Figure 67. Time Responses Due to 10 ft/s Vertical and Longitudinal Turbulences, Optimal Gain Schedule Output Feedback Design, δ_{ht} Failed, Mach .60, Altitude 5000 ft (Concluded)

C-2

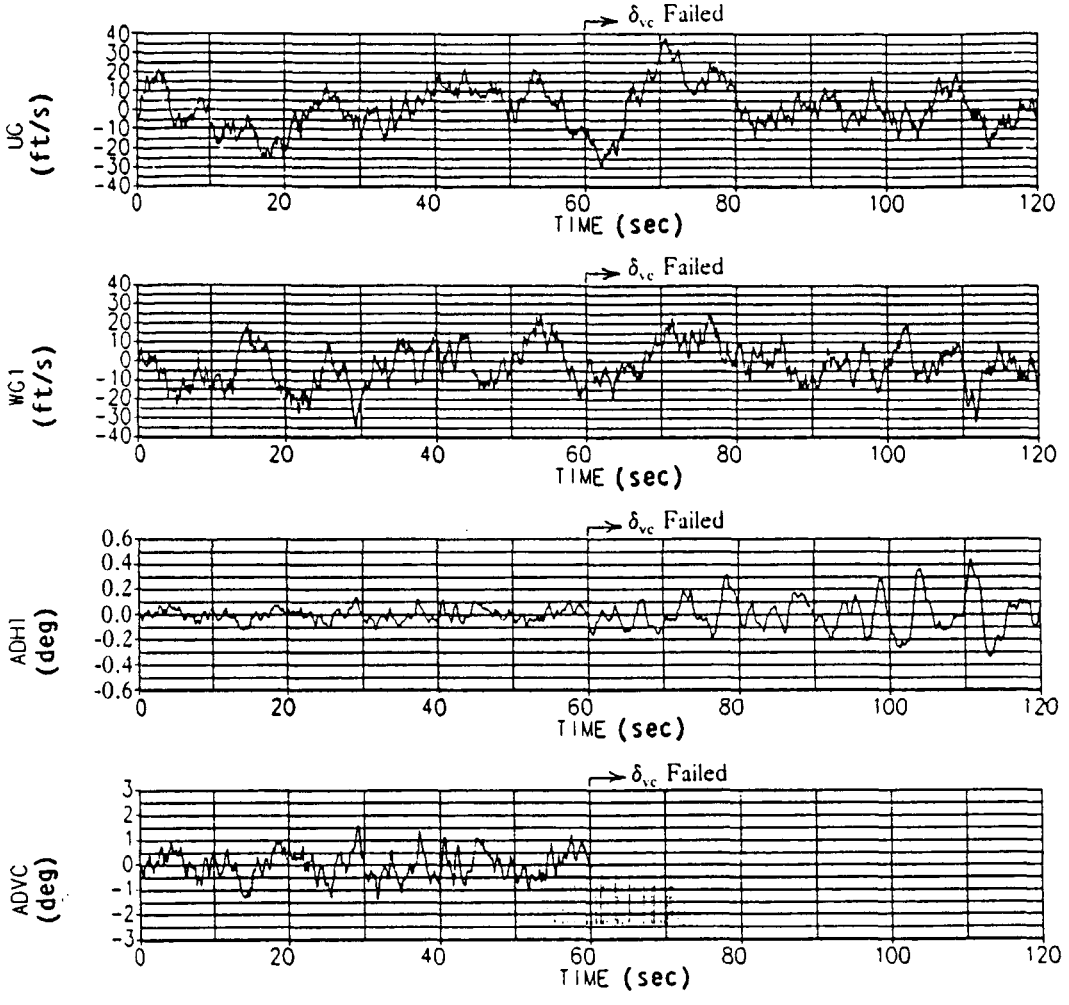

Figure 68. Time Responses Due to 10 ft/s Vertical and Longitudinal Turbulences, Optimal Gain Schedule Output Feedback Design, δ_{vc} Failed, Mach .60, Altitude 5000 ft

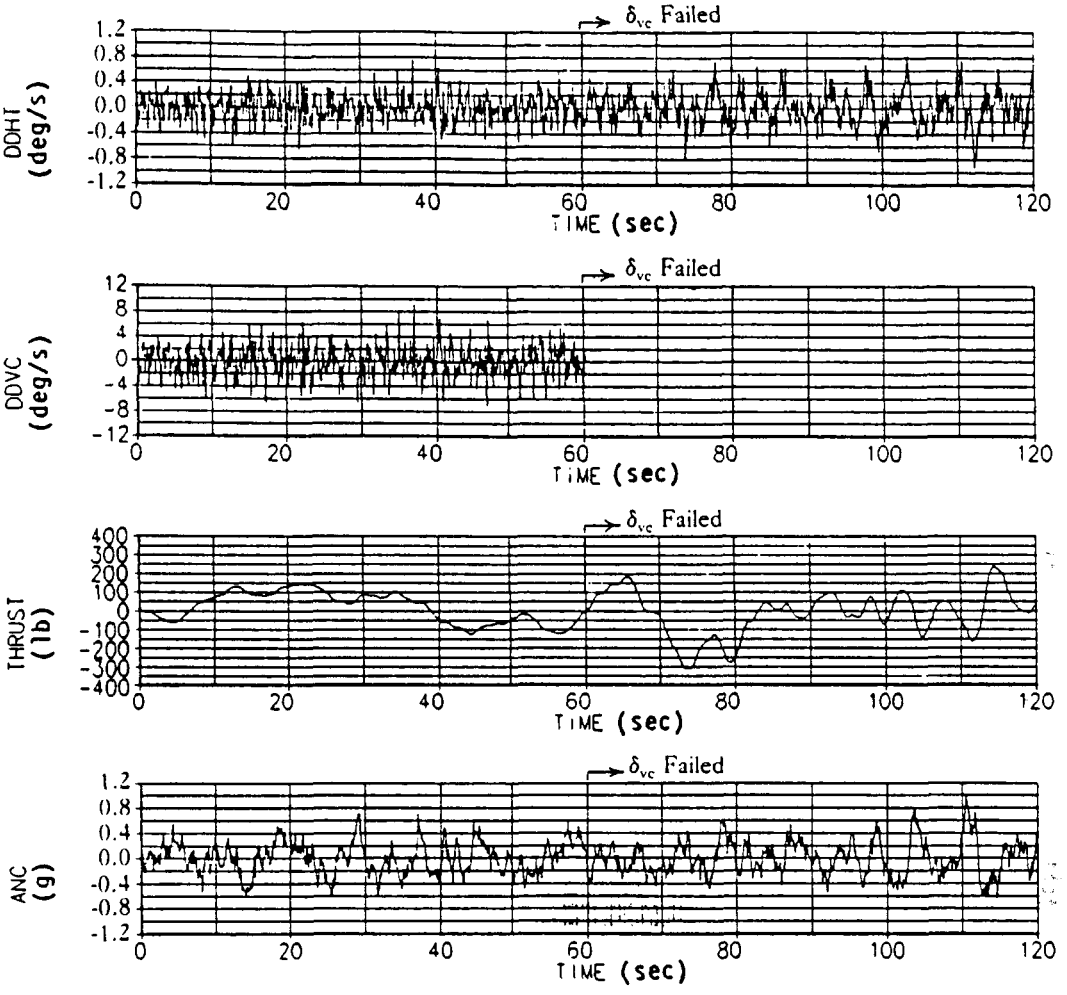

Figure 68. Time Responses Due to 10 ft/s Vertical and Longitudinal Turbulences, Optimal Gain Schedule Output Feedback Design, δ_{vc} Failed, Mach .60, Altitude 5000 ft (Continued)

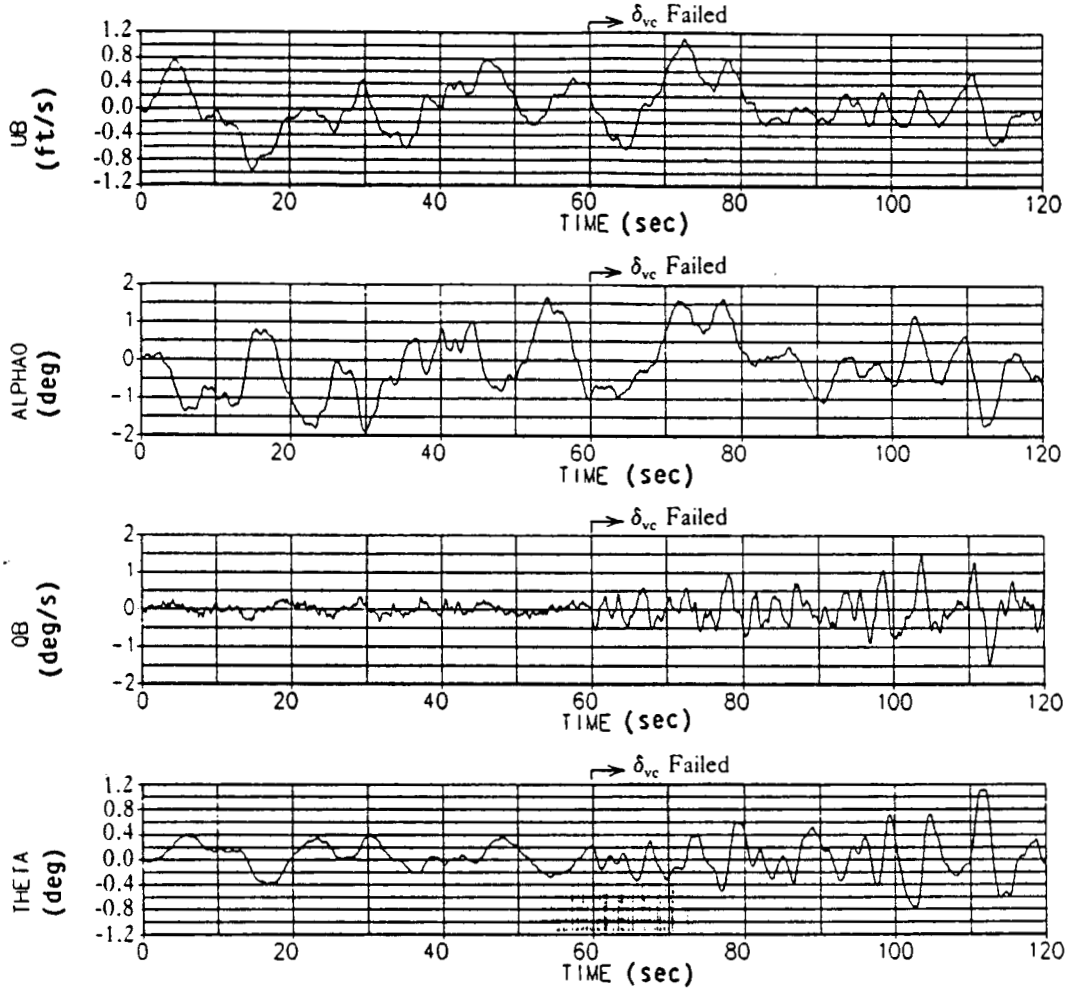

Figure 68. Time Responses Due to 10 ft/s Vertical and Longitudinal Turbulences, Optimal Gain Schedule Output Feedback Design, δ_{vc} Failed, Mach .60, Altitude 5000 ft (Concluded)

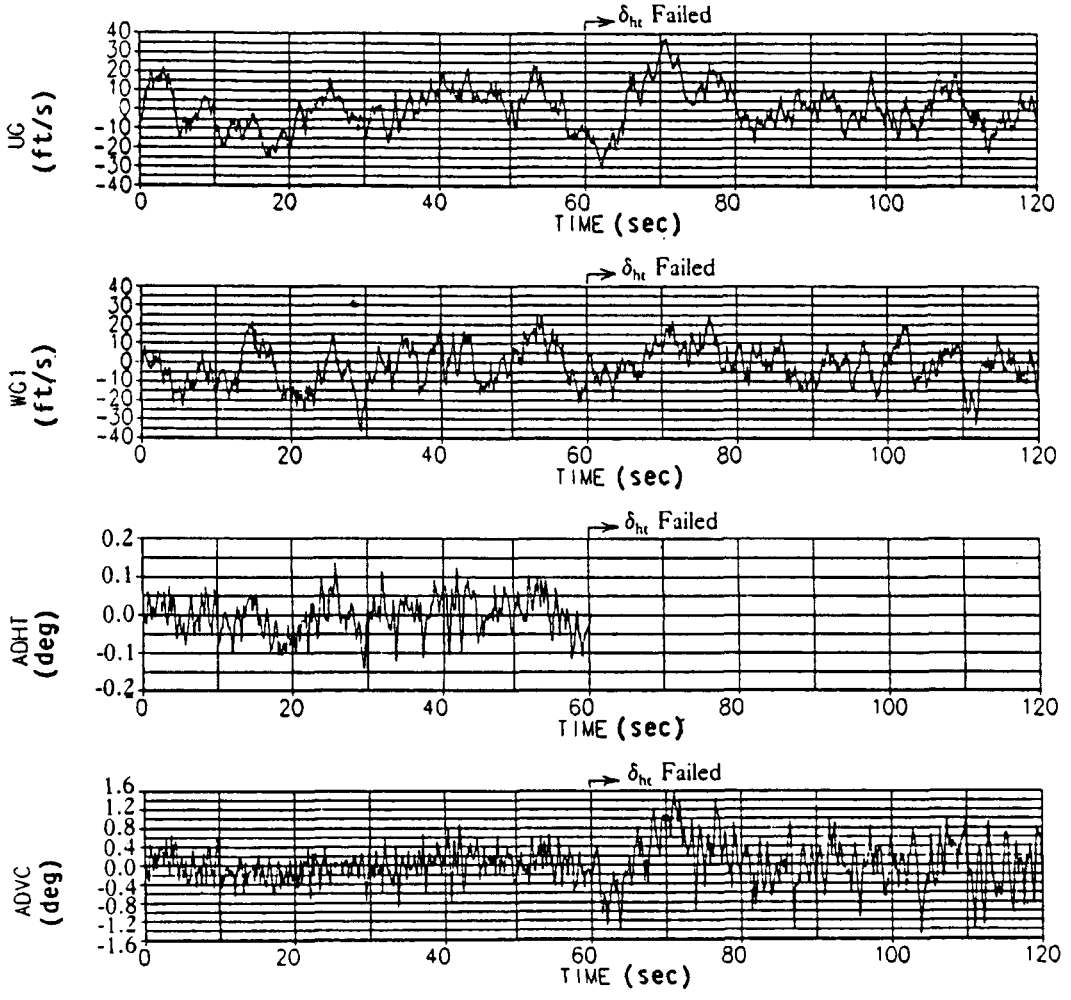

Figure 69. Time Responses Due to 10 ft/s Vertical and Longitudinal Turbulences, Optimal Gain Schedule Output Feedback Design, δ_{ht} Failed, Mach .90, Altitude 20,000 ft

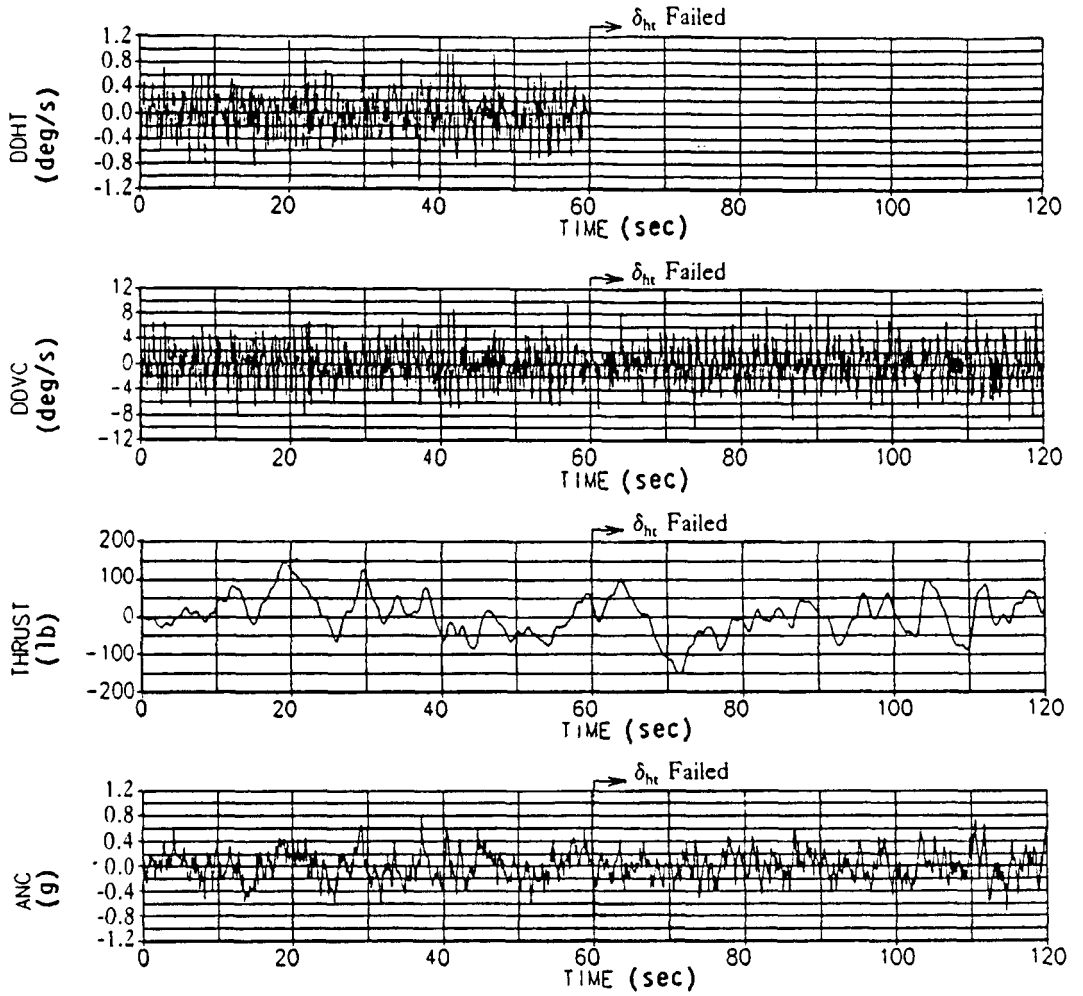

Figure 69. Time Responses Due to 10 ft/s Vertical and Longitudinal Turbulences, Optimal Gain Schedule Output Feedback Design, δ_{ht} Failed, Mach .90, Altitude 20,000 ft (Continued)

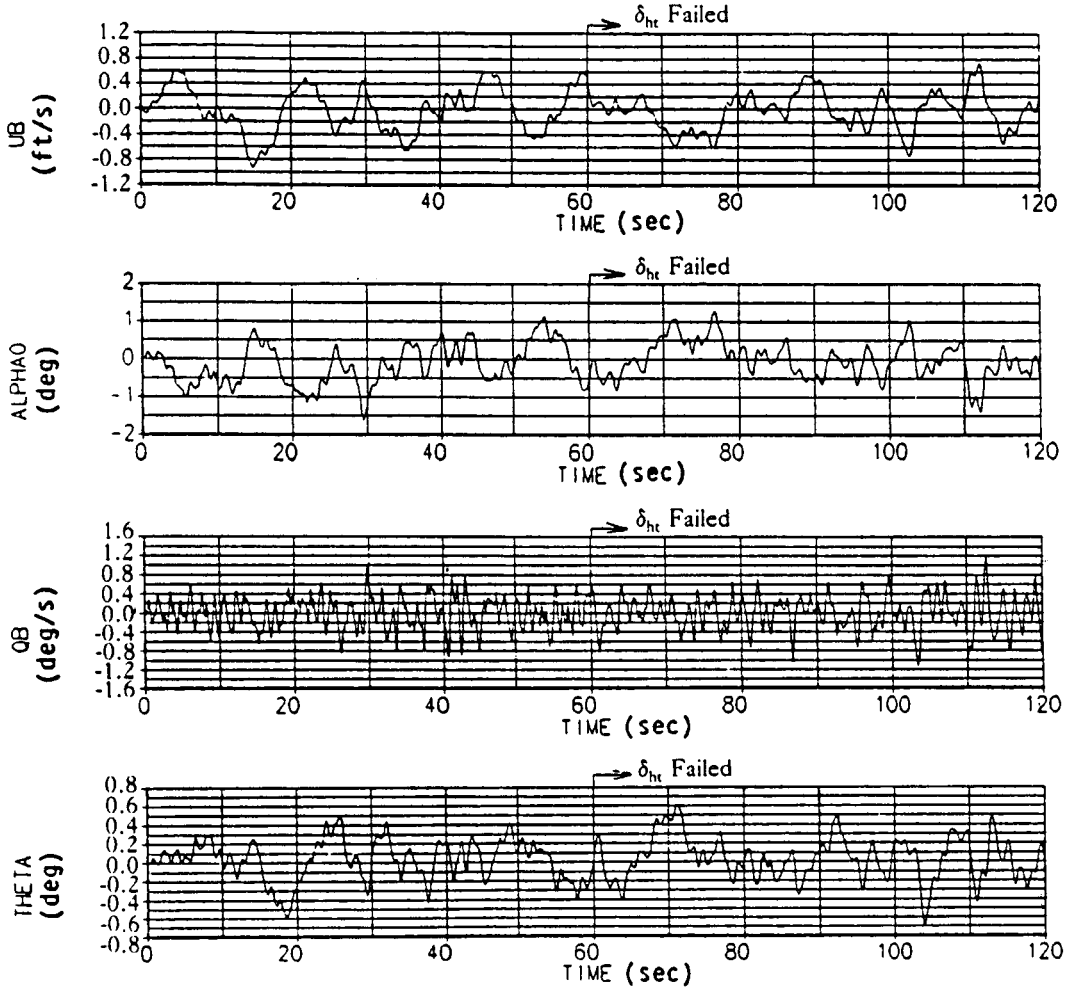

Figure 69. Time Responses Due to 10 ft/s Vertical and Longitudinal Turbulences, Optimal Gain Schedule Output Feedback Design, δ_{ht} Failed, Mach .90, Altitude 20,000 ft (Concluded)

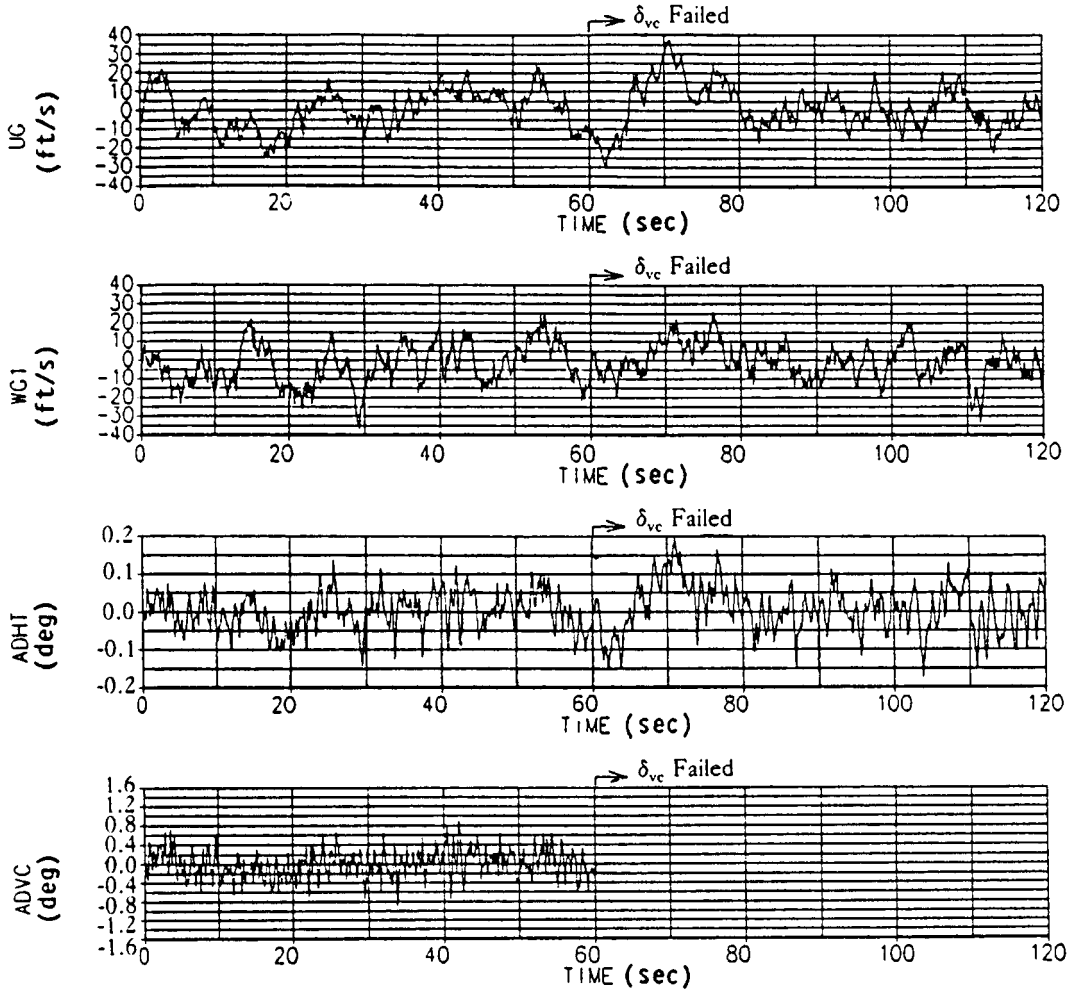

Figure 70. Time Responses Due to 10 ft/s Vertical and Longitudinal Turbulences, Optimal Gain Schedule Output Feedback Design, δ_{vc} Failed, Mach .90, Altitude 20,000 ft

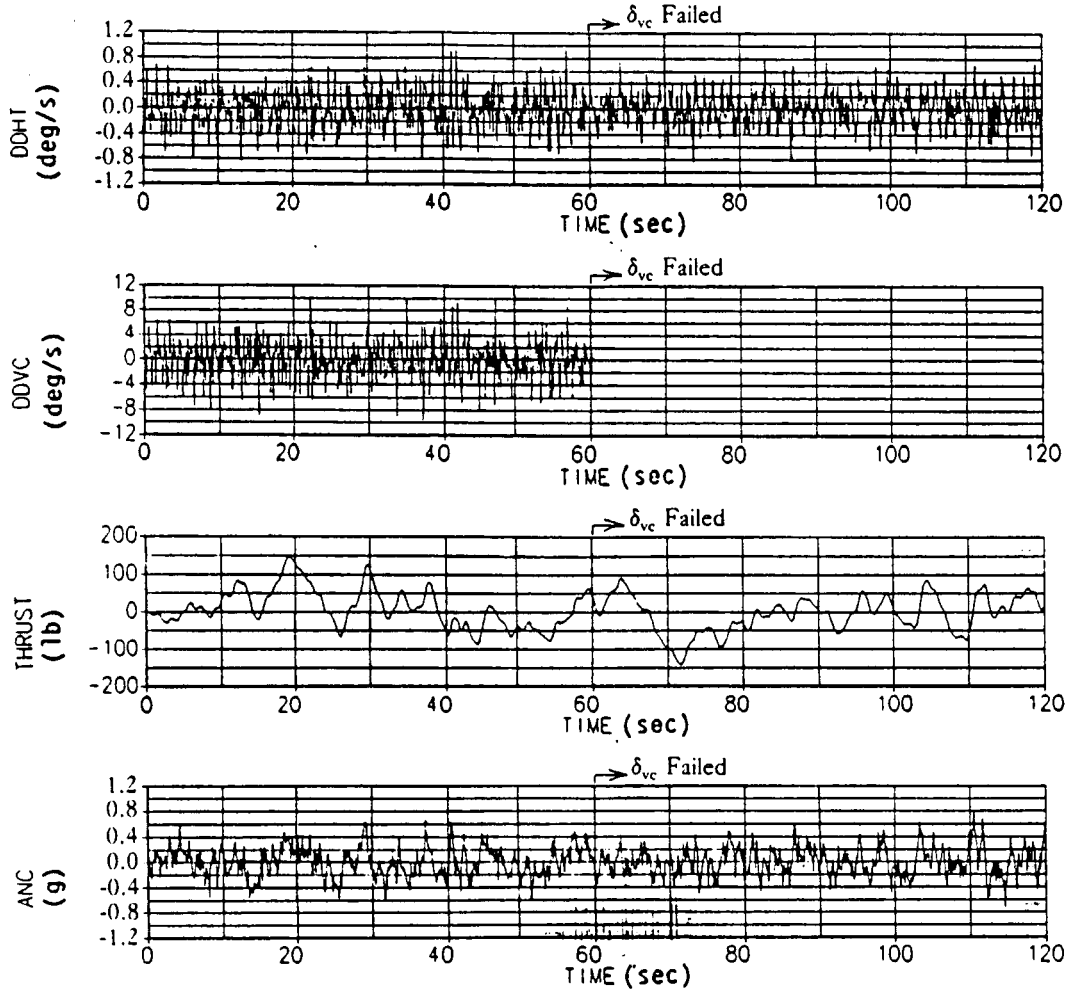

Figure 70. Time Responses Due to 10 ft/s Vertical and Longitudinal Turbulences, Optimal Gain Schedule Output Feedback Design, δ_{vc} Failed, Mach .90, Altitude 20,000 ft (Continued)

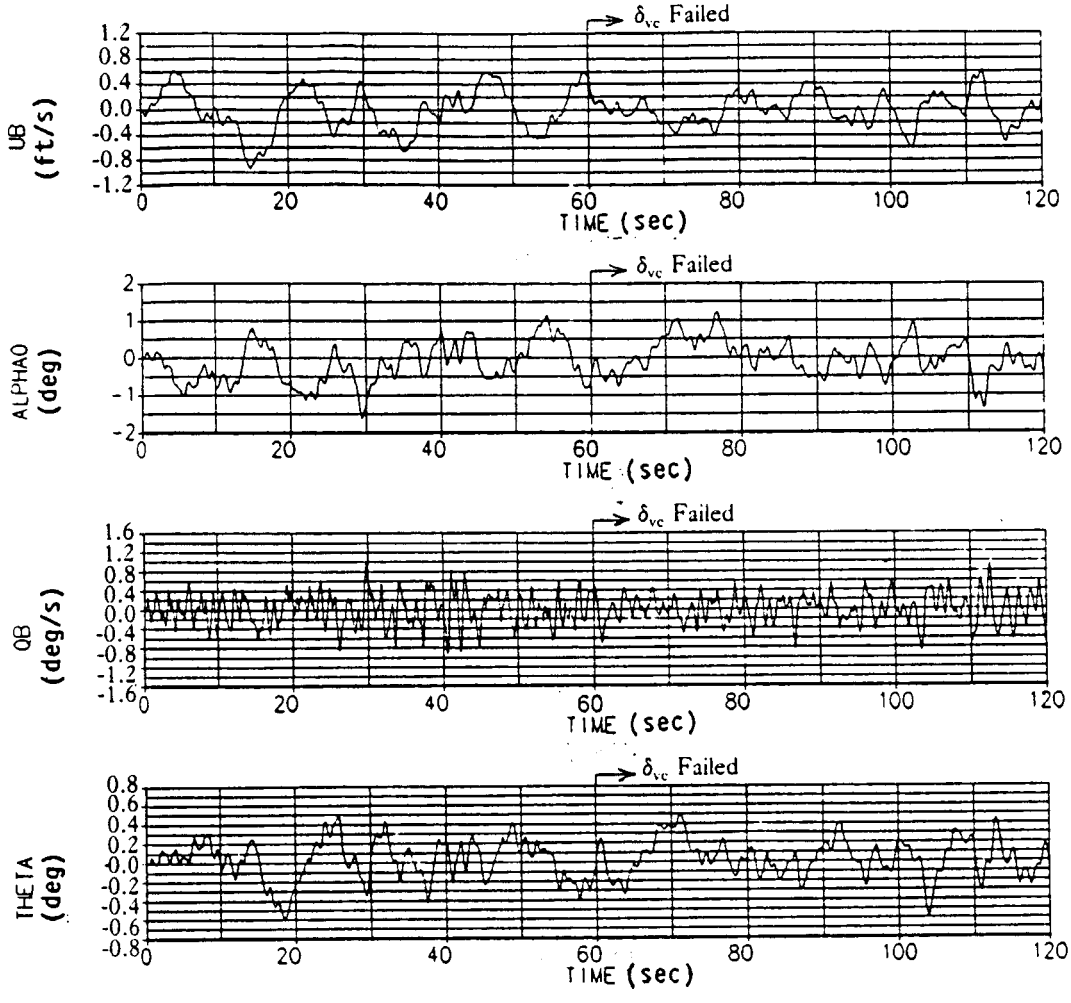

Figure 70. Time Responses Due to 10 ft/s Vertical and Longitudinal Turbulences, Optimal Gain Schedule Output Feedback Design, δ_{vc} Failed, Mach .90, Altitude 20,000 ft (Concluded)

APPENDIX A

AIRCRAFT STATE MODEL MATRICES

1. Flight Condition Mach .25, Altitude 5000 ft

```
==============
===== A =====
==============
```

	UB	WB	QB	THETA	DHT	DVC	DPLA	UG	WG1	WG2
UB	-1.2472E-02	6.6315E-02	-0.8458	-0.5523	4.6340E-03	3.1650E-04	1.4970E-03	1.2472E-02	-6.6315E-02	0.0000E+00
WB	-0.1529	-0.4791	4.692	-9.9578E-02	-0.1515	-1.7550E-03	-2.6530E-07	0.1529	0.4791	0.0000E+00
QB	-6.0073E-02	0.3298	-0.4393	0.0000E+00	-0.9369	-0.1943	2.4135E-06	6.0073E-02	-0.3298	0.0000E+00
THETA	0.0000E+00	0.0000E+00	1.000	0.0000E+00	0.0000E+00	0.0000E+00	0.0000E+00	0.0000E+00	0.0000E+00	0.0000E+00
DHT	0.0000E+00	0.0000E+00	0.0000E+00	0.0000E+00	-13.00	0.0000E+00	0.0000E+00	0.0000E+00	0.0000E+00	0.0000E+00
DVC	0.0000E+00	0.0000E+00	0.0000E+00	0.0000E+00	0.0000E+00	-13.00	0.0000E+00	0.0000E+00	0.0000E+00	0.0000E+00
DPLA	0.0000E+00	0.0000E+00	0.0000E+00	0.0000E+00	0.0000E+00	0.0000E+00	-1.000	0.0000E+00	0.0000E+00	0.0000E+00
UG	0.0000E+00	0.0000E+00	0.0000E+00	0.0000E+00	0.0000E+00	0.0000E+00	0.0000E+00	-0.1567	0.0000E+00	0.0000E+00
WG1	0.0000E+00	0.0000E+00	0.0000E+00	0.0000E+00	0.0000E+00	0.0000E+00	0.0000E+00	0.0000E+00	-0.1567	1.5670E-03
WG2	0.0000E+00	0.0000E+00	0.0000E+00	0.0000E+00	0.0000E+00	0.0000E+00	0.0000E+00	0.0000E+00	-1.5670E-03	-0.1567

```
==============
===== B =====
==============
```

	DHTC	DVCC	DPLAC	UNOISE	WNOISE
UB	0.0000E+00	0.0000E+00	0.0000E+00	0.0000E+00	0.0000E+00
WB	0.0000E+00	0.0000E+00	0.0000E+00	0.0000E+00	0.0000E+00
QB	0.0000E+00	0.0000E+00	0.0000E+00	0.0000E+00	0.0000E+00
THETA	0.0000E+00	0.0000E+00	0.0000E+00	0.0000E+00	0.0000E+00
DHT	26.00	0.0000E+00	0.0000E+00	0.0000E+00	0.0000E+00
DVC	0.0000E+00	26.00	0.0000E+00	0.0000E+00	0.0000E+00
DPLA	0.0000E+00	0.0000E+00	113.1	0.0000E+00	0.0000E+00
UG	0.0000E+00	0.0000E+00	0.0000E+00	0.5599	0.0000E+00
WG1	0.0000E+00	0.0000E+00	0.0000E+00	0.0000E+00	0.6857
WG2	0.0000E+00	0.0000E+00	0.0000E+00	0.0000E+00	-28.98


```
==============
===== C =====
==============
```

	UB	WB	QB	THETA	DHT	DVC	DPLA	UG	WG1	WG2
UBO	1.000	0.0000E+00	0.0000E+00	0.0000E+00	0.0000E+00	0.0000E+00	0.0000E+00	0.0000E+00	0.0000E+00	0.0000E+00
QBO	0.0000E+00	0.0000E+00	1.000	0.0000E+00	0.0000E+00	0.0000E+00	0.0000E+00	0.0000E+00	0.0000E+00	0.0000E+00
THETAO	0.0000E+00	0.0000E+00	0.0000E+00	1.000	0.0000E+00	0.0000E+00	0.0000E+00	0.0000E+00	0.0000E+00	0.0000E+00
ALPHAO	0.0000E+00	0.2089	0.0000E+00	0.0000E+00	0.0000E+00	0.0000E+00	0.0000E+00	0.0000E+00	0.0000E+00	0.0000E+00
ANC	4.3074E-03	1.7330E-02	-2.8755E-04	-1.7866E-05	-2.2177E-03	-1.3820E-03	2.6089E-08	-4.3074E-03	-1.7330E-02	0.0000E+00

```
==============
===== D =====
==============
```

	DHTC	DVCC	DPLAC	UNOISE	WNOISE
UBO	0.0000E+00	0.0000E+00	0.0000E+00	0.0000E+00	0.0000E+00
QBO	0.0000E+00	0.0000E+00	0.0000E+00	0.0000E+00	0.0000E+00
THETAO	0.0000E+00	0.0000E+00	0.0000E+00	0.0000E+00	0.0000E+00
ALPHAO	0.0000E+00	0.0000E+00	0.0000E+00	0.0000E+00	0.0000E+00
ANC	0.0000E+00	0.0000E+00	0.0000E+00	0.0000E+00	0.0000E+00

2. *Flight Condition Mach .60, Altitude 5000 ft*

```
==========
===== A =====
==========
```

	UB	WB	QB	THETA	DHT	DVC	DPLA	UG	WG1	WG2
UB	-1.3682E-02	4.1490E-02	-0.3791	-0.5609	7.2530E-02	-1.0350E-03	1.4960E-03	1.3682E-02	-4.1490E-02	0.0000E+00
WB	-6.6683E-02	-1.246	11.34	-1.8743E-02	-0.8979	3.0980E-02	-1.2410E-07	6.6683E-02	1.246	0.0000E+00
QB	-2.7934E-03	0.3186	-0.7379	0.0000E+00	-7.277	-1.061	7.2026E-07	2.7934E-03	-0.3186	0.0000E+00
THETA	0.0000E+00	0.0000E+00	1.000	0.0000E+00	0.0000E+00	0.0000E+00	0.0000E+00	0.0000E+00	0.0000E+00	0.0000E+00
DHT	0.0000E+00	0.0000E+00	0.0000E+00	0.0000E+00	-13.00	0.0000E+00	0.0000E+00	0.0000E+00	0.0000E+00	0.0000E+00
DVC	0.0000E+00	0.0000E+00	0.0000E+00	0.0000E+00	0.0000E+00	-13.00	0.0000E+00	0.0000E+00	0.0000E+00	0.0000E+00
DPLA	0.0000E+00	0.0000E+00	0.0000E+00	0.0000E+00	0.0000E+00	0.0000E+00	-1.000	0.0000E+00	0.0000E+00	0.0000E+00
UG	0.0000E+00	0.0000E+00	0.0000E+00	0.0000E+00	0.0000E+00	0.0000E+00	0.0000E+00	-0.3730	0.0000E+00	0.0000E+00
WG1	0.0000E+00	0.0000E+00	0.0000E+00	0.0000E+00	0.0000E+00	0.0000E+00	0.0000E+00	0.0000E+00	-0.3730	3.7300E-03
WG2	0.0000E+00	0.0000E+00	0.0000E+00	0.0000E+00	0.0000E+00	0.0000E+00	0.0000E+00	0.0000E+00	-3.7300E-03	-0.3730

```
==========
===== B =====
==========
```

	DHTC	DVCC	DPLAC	UNOISE	WNOISE
UB	0.0000E+00	0.0000E+00	0.0000E+00	0.0000E+00	0.0000E+00
WB	0.0000E+00	0.0000E+00	0.0000E+00	0.0000E+00	0.0000E+00
QB	0.0000E+00	0.0000E+00	0.0000E+00	0.0000E+00	0.0000E+00
THETA	0.0000E+00	0.0000E+00	0.0000E+00	0.0000E+00	0.0000E+00
DHT	26.00	0.0000E+00	0.0000E+00	0.0000E+00	0.0000E+00
DVC	0.0000E+00	26.00	0.0000E+00	0.0000E+00	0.0000E+00
DPLA	0.0000E+00	0.0000E+00	134.9	0.0000E+00	0.0000E+00
UG	0.0000E+00	0.0000E+00	0.0000E+00	0.8637	0.0000E+00
WG1	0.0000E+00	0.0000E+00	0.0000E+00	0.0000E+00	1.058
WG2	0.0000E+00	0.0000E+00	0.0000E+00	0.0000E+00	-44.72

```
==========
===== C =====
==========
```

	UB	WB	QB	THETA	DHT	DVC	DPLA	UG	WG1	WG2
UBO	1.000	0.0000E+00	0.0000E+00	0.0000E+00	0.0000E+00	0.0000E+00	0.0000E+00	0.0000E+00	0.0000E+00	0.0000E+00
QBO	0.0000E+00	0.0000E+00	1.000	0.0000E+00	0.0000E+00	0.0000E+00	0.0000E+00	0.0000E+00	0.0000E+00	0.0000E+00
THETAO	0.0000E+00	0.0000E+00	0.0000E+00	1.000	0.0000E+00	0.0000E+00	0.0000E+00	0.0000E+00	0.0000E+00	0.0000E+00
ALPHAO	0.0000E+00	8.7770E-02	0.0000E+00	0.0000E+00	0.0000E+00	0.0000E+00	0.0000E+00	0.0000E+00	0.0000E+00	0.0000E+00
ANC	2.0519E-03	4.1069E-02	-3.9487E-03	-3.5044E-07	-2.5894E-02	-8.8085E-03	9.1821E-09	-2.0519E-03	-4.1069E-02	0.0000E+00

```
==========
===== D =====
==========
```

	DHTC	DVCC	DPLAC	UNOISE	WNOISE
UBO	0.0000E+00	0.0000E+00	0.0000E+00	0.0000E+00	0.0000E+00
QBO	0.0000E+00	0.0000E+00	0.0000E+00	0.0000E+00	0.0000E+00
THETAO	0.0000E+00	0.0000E+00	0.0000E+00	0.0000E+00	0.0000E+00
ALPHAO	0.0000E+00	0.0000E+00	0.0000E+00	0.0000E+00	0.0000E+00
ANC	0.0000E+00	0.0000E+00	0.0000E+00	0.0000E+00	0.0000E+00

3. Flight Condition Mach .90, Altitude 20,000 ft

```
=============
===== A =====
=============
```

	UB	WB	QB	THETA	DHT	DVC	DPLA	UG	WG1	WG2
UB	-1.1669E-02	2.4753E-02	-0.5271	-0.5601	8.5560E-03	-7.1910E-04	1.4960E-03	1.1669E-02	-2.4753E-02	0.0000E+00
WB	-4.4669E-02	-1.437	16.14	-1.8286E-02	-1.152	2.2030E-02	-1.0650E-07	4.4669E-02	1.437	0.0000E+00
QB	-8.8168E-02	-8.0495E-02	-0.7046	0.0000E+00	-10.85	-1.420	7.2141E-07	8.8168E-02	8.0495E-02	0.0000E+00
THETA	0.0000E+00	0.0000E+00	1.000	0.0000E+00	0.0000E+00	0.0000E+00	0.0000E+00	0.0000E+00	0.0000E+00	0.0000E+00
DHT	0.0000E+00	0.0000E+00	0.0000E+00	0.0000E+00	-13.00	0.0000E+00	0.0000E+00	0.0000E+00	0.0000E+00	0.0000E+00
DVC	0.0000E+00	0.0000E+00	0.0000E+00	0.0000E+00	0.0000E+00	-13.00	0.0000E+00	0.0000E+00	0.0000E+00	0.0000E+00
DPLA	0.0000E+00	0.0000E+00	0.0000E+00	0.0000E+00	0.0000E+00	0.0000E+00	-1.000	0.0000E+00	0.0000E+00	0.0000E+00
UG	0.0000E+00	0.0000E+00	0.0000E+00	0.0000E+00	0.0000E+00	0.0000E+00	0.0000E+00	-0.5303	0.0000E+00	0.0000E+00
WG1	0.0000E+00	0.0000E+00	0.0000E+00	0.0000E+00	0.0000E+00	0.0000E+00	0.0000E+00	0.0000E+00	-0.5303	5.3030E-03
WG2	0.0000E+00	0.0000E+00	0.0000E+00	0.0000E+00	0.0000E+00	0.0000E+00	0.0000E+00	0.0000E+00	-5.3030E-03	-0.5303

```
=============
===== B =====
=============
```

	DHTC	DVCC	DPLAC	UNOISE	WNOISE
UB	0.0000E+00	0.0000E+00	0.0000E+00	0.0000E+00	0.0000E+00
WB	0.0000E+00	0.0000E+00	0.0000E+00	0.0000E+00	0.0000E+00
QB	0.0000E+00	0.0000E+00	0.0000E+00	0.0000E+00	0.0000E+00
THETA	0.0000E+00	0.0000E+00	0.0000E+00	0.0000E+00	0.0000E+00
DHT	26.00	0.0000E+00	0.0000E+00	0.0000E+00	0.0000E+00
DVC	0.0000E+00	26.00	0.0000E+00	0.0000E+00	0.0000E+00
DPLA	0.0000E+00	0.0000E+00	99.06	0.0000E+00	0.0000E+00
UG	0.0000E+00	0.0000E+00	0.0000E+00	1.030	0.0000E+00
WG1	0.0000E+00	0.0000E+00	0.0000E+00	0.0000E+00	1.261
WG2	0.0000E+00	0.0000E+00	0.0000E+00	0.0000E+00	-53.32

```
=============
===== C =====
=============
```

	UB	WB	QB	THETA	DHT	DVC	DPLA	UG	WG1	WG2
UBO	1.000	0.0000E+00	0.0000E+00	0.0000E+00	0.0000E+00	0.0000E+00	0.0000E+00	0.0000E+00	0.0000E+00	0.0000E+00
QBO	0.0000E+00	0.0000E+00	1.000	0.0000E+00	0.0000E+00	0.0000E+00	0.0000E+00	0.0000E+00	0.0000E+00	0.0000E+00
THETAO	0.0000E+00	0.0000E+00	0.0000E+00	1.000	0.0000E+00	0.0000E+00	0.0000E+00	0.0000E+00	0.0000E+00	0.0000E+00
ALPHAO	0.0000E+00	6.1730E-02	0.0000E+00	0.0000E+00	0.0000E+00	0.0000E+00	0.0000E+00	0.0000E+00	0.0000E+00	0.0000E+00
ANC	7.3647E-04	4.4067E-02	-3.4630E-03	-1.2980E-06	-4.4389E-02	-1.1186E-02	8.6435E-09	-7.3647E-04	-4.4067E-02	0.0000E+00

```
=============
===== D =====
=============
```

	DHTC	DVCC	DPLAC	UNOISE	WNOISE
UBO	0.0000E+00	0.0000E+00	0.0000E+00	0.0000E+00	0.0000E+00
QBO	0.0000E+00	0.0000E+00	0.0000E+00	0.0000E+00	0.0000E+00
THETAO	0.0000E+00	0.0000E+00	0.0000E+00	0.0000E+00	0.0000E+00
ALPHAO	0.0000E+00	0.0000E+00	0.0000E+00	0.0000E+00	0.0000E+00
ANC	0.0000E+00	0.0000E+00	0.0000E+00	0.0000E+00	0.0000E+00

REFERENCES

1. Howell, W. E., et al., "Workshop on Restructurable Controls," NASA CP-2277, September 1982.

2. Howell, W. E., Bundick, W. T., Hueschen, R. M., and Ostroff, A. J., "Restructurable Controls for Aircraft," AIAA Guidance and Control Conference, Gatlinburg, Tennessee, August 15-17, 1983.

3. Ostroff, A. J., Hueschen, R. M., and Richard, M., "Reconfigurable Multivariable Control Law for Commercial Airplane Using a Direct Digital Output Feedback Design," NASA TM-85759, February 1984.

4. Ostroff, A. J., "Techniques for Accommodating Control Effector Failures on a Mildly Statically Unstable Airplane," 1985 American Control Conference, Boston, Massachusetts, June 19-21, 1985.

5. Ly, U. and Gangsaas, D., "Application of a Modified LQG Design to Active Control of a Transport Airplane," presented at the AIAA Guidance and Control Conference, Boulder, Colorado, August 6-9, 1979.

6. Kwakernaak, K. and Sivan, R., "Linear Optimal Control Systems," Wiley-Interscience, New York, 1972.

7. Ly, U., "A Design Algorithm for Robust Low Order Controllers," Stanford University, Department of Aeronautics and Astronautics, Report No. 536, November 1982.

8. Gill, P. E., Murray, W., Saunders, M. A., and Wright, M. H., "User's Guide for NPSOL (Version 2.1)," Technical Report SOL-84-7, September 1984.

9. Mukhopadhaya, V., Newsom, J. R., and Abel, I., "A Method for Obtaining Reduced-Order Control Laws for High Order Systems Using Optimization Techniques," NASA, TP-1876, August 1981.

10. Davison, E. J. and Ferguson, I. J., "The Design of Controllers for the Multivariable Robust Servomechanism Problem Using Parameter Optimization Methods," IEEE Transactions on Automatic Control, Vol. AC-26, No.1, February 1981.

1. Report No.	2. Government Accession No.	3. Recipient's Catalog No.
NASA CR-178094		

4. Title and Subtitle	5. Report Date
Fault Tolerant Control Laws	July 1986
	6. Performing Organization Code

7. Author(s)	8. Performing Organization Report No.
Uy-Loi Ly and John K. Ho	

9. Performing Organization Name and Address	10. Work Unit No.
Boeing Commercial Airplane Company P.O. Box 3707 Seattle, WA 98124	11. Contract or Grant No. NAS1-17635 Task No. 10
	13. Type of Report and Period Covered Final Report
12. Sponsoring Agency Name and Address National Aeronautics and Space Administration Washington, DC 20546	14. Sponsoring Agency Code

15. Supplementary Notes

Langley Contracting Officer: Mary L. Harwood

16. Abstract

A systematic procedure for the synthesis of fault tolerant control laws to actuator failure has been presented. Two design methods were used to synthesize fault tolerant controllers: the conventional LQ design method and a direct feedback controller design method SANDY. The latter method is used primarily to streamline the full-state LQ feedback design into a practical implementable output feedback controller structure.

To achieve robustness to control actuator failure, the redundant surfaces are properly balanced according to their control effectiveness. A simple gain schedule based on the landing gear up/down logic involving only three gains was developed to handle three design flight conditions: Mach .25 and Mach .60 at 5000 ft and Mach 90 at 20,000 ft. The fault tolerant control law developed in this study provides good stability augmentation and performance for the relaxed static stability aircraft. The augmented aircraft responses are found to be invariant to the presence of a failure.

Furthermore, single-loop stability margins of +6 dB in gain and +30 deg in phase were achieved along with -40 dB/decade rolloff at high frequency.

17. Key Words (Suggested by Author(s))	18. Distribution Statement
Fault Tolerant Stability Augmentation System Robustness Reconfigurable Restructurable Output Feedback SANDY	Unclassified—Unlimited

19. Security Classif. (of this report)	20. Security Classif. (of this page)	21. No. of Pages	22. Price
Unclassified	Unclassified		

For sale by the National Technical Information Service, Springfield, Virginia 22151